MINISTRY OF HIGHER EDUCATION AND SCIENTIFIC RESEARCH

وزارة التعليم العالي والبحث العلمي

UNIVERSITY OF BLIDA
FACULTY OF TECHNOLOGY
DEPARTEMENT OF AUTOMATIC
AND
ELECTRICAL ENGINEERING



جامعة البليدة كلية التكنولوجيا قسم الالية والهندسة الكهربائية

A THESIS PRESENTED IN FULFILMENT OF THE REQUIREMENT FOR THE DEGREE OF

DOCTOR LMD IN ELECTRICAL ENGINEERING

Specialty: Renewable Energy

PRESENTED BY

ABID MOKHTAR

THESIS TITLE:

PLANNING OF RENEWABLE ENERGY RESOURCES AND CONNECTION TO POWER GRIDS: OPTIMIZATION AND STABILITY

Approved: October 9th, 2025

Bradai Rafik	Professor	Univ. of Blida 1	Chair of committee
Ferdjouni Abdelaziz	Professor	Univ. of Blida 1	Examiner
Mellah Hacene	MCA	Univ. of Bouira	Examiner
Yahiou Abdelghani	MCA	Univ. of Bouira	Examiner
Belazzoug Messaoud	MCA	Univ. of Blida 1	Supervisor
Chanane Abdallah	MCA	Univ. of Blida 1	Co-Supervisor
Mouassa Souhil	MCA	Univ. of Bouira	Invited

ACKNOWLEDGEMENTS

I would like to begin by expressing our deepest gratitude to Allah, the source of all inspiration and guidance, for granting us the strength and perseverance to successfully complete this Doctoral thesis.

My gratitude also extends to all my family, who have been an unwavering source of support throughout this experience. Their love, encouragement, and constant support have been sources of inspiration and motivation that have contributed to my success.

I would also like to express my appreciation to my supervisors Dr. Messaoud Belazzoug and Dr. Abdallah Chanane, for their invaluable guidance, expertise, and support throughout this research, their insightful advice, availability, and dedication have been instrumental in the completion of this thesis.

I would like to extend my gratitude to Dr. Souhil Mouassa for his contributions, both direct and indirect, to this research and my academic development. His ideas, suggestions, and collaboration have enriched my work and significantly contributed to its improvement.

my thanks also go to those who have shared their knowledge, experience, and support during this journey.

Their contribution has been invaluable and has greatly contributed to my growth as researchers.

In conclusion, this Doctoral thesis would not have been possible without the benevolent presence of God, the unwavering support of my family, and the attentive guidance of my supervisors. Their contribution has been of utmost importance.

Abstract

In the current century, electrical networks have witnessed great developments and continuous increases in the demand for fossil-fuel-based energy, leading to excessive rise in the total production cost and the pollutant gases emitted by thermal plants. Under these circumstances, energy supply from different resources became necessary, such as renewable energy sources (RES) as an alternative solution. These sources, however, are characterized by uncertainty in their operational principle, especially when the system operator needs to define the optimal contribution of each resource to ensure economic efficiency and enhanced grid reliability. However, even with the huge demand met, networks still face other problems such as power loss and voltage instability. Therefore, FACTS devices appear as an effective solution, but they remain expensive. This thesis addresses the growing complexity of modern power systems as they incorporate high shares of variable renewable energy. A unified framework is developed that couples probabilistic modelling of wind, solar, and hydro output using Monte Carlo simulation and specific probability density functions (Weibull distribution for wind speeds, lognormal distribution for solar irradiance, and Gumbel distribution for river flow) with an enhanced metaheuristic optimizer tailored for large-scale optimal power flow. Key developments in the Kepler Optimization Algorithm include a novel exploratory-exploitative search operator for deeper solution-space exploration and a non-dominated sorting scheme to support efficient multi-objective trade-offs. Additionally, the framework incorporates SVC and TCSC devices by determining their optimal sizing and placement to reinforce the transmission lines and buses that demand the most reactive-power support, thereby achieving a cost-effective trade-off between capital investment and operational performance. When validated on a large scale test system, this integrated solution enhances economic efficiency, reduces environmental impact, and bolsters reliability under uncertainty. By combining advanced uncertainty quantification, customized metaheuristics, and targeted network reinforcement, this work provides a versatile, scalable methodology for planning and operating resilient, low-carbon electrical grids.

Keywords: Renewable Energy Sources, Metaheuristic Optimization Techniques, Kepler Optimization Algorithm, Optimal Power Flow, FACTS, Voltage Stability

ملخص

شهدت الشبكات الكهربائية في هذا القرن تطورات كبيرة وزيادات مستمرة في الطلب على الطاقة المعتمدة على الوقود الأحفوري، مما أدى إلى ارتفاع مغرط في التكلفة الإجمالية للإنتاج، بالإضافة إلى الغازات الملوثة المنبعثة من المحطات الحرارية. في ظل هذه الظروف، أصبح من الضروري توفير الطاقة من مصادر متنوعة، مثل مصادر الطاقة المتجددة كحل بديل. إلا أن هذه المصادر تتسم بعدم اليقين في مبدأ تشغيلها، لا سيما عندما يحتاج مشغل النظام إلى تحديد المساهمة المثلى لكل مصدر لضمان الكفاءة الاقتصادية وتحسين موثوقية الشبكة. ولكن حتى مع تلبية الطلب الكبير، لا تزال الشبكات تواجه مشكلات أخرى مثل فقدان الطاقة وعدم استقرار الجهد. لذا، تظهر أجهزة التحكم المرنة في نقل الطاقة الكهربائية كحل فقل، لكنها تظل باهظة التكلفة تعالج هذه الرسلة التعقيد المتزايد في أنظمة الطاقة الحديثة نتيجة دمج نصب عالية من الطاقة المتجددة المتغيرة. تم تطوير إطار موحد يجمع بين النمذجة الاحتمالية لطاقة الرياح والطاقة المسلمية والطاقة المائية باستخدام محاكاة مونت كارلو ودوال الكثاقة الاحتمالية المحددة (توزيع ويبل لسرعة الرياح، وتوزيع لوغاريتمي طبيعي للإشعاع الشمسي، وتوزيع غومبل انتفق الأنهار)، مع مُحسن ميتاهيوريستيكي مُعزز مصمم خصيصًا انتفق الطاقة الأمثل على نطاق واسع. تتضمن التطويرات الأسلول في خوارزمية كبلر للتحسين مشغلاً جديدًا للبحث الاستكشافي-الاستغلالي لتعميق استكشاف فضاء الحلول، ونظام فرز غير مهيمن لدعم المفاضلات متعددة والتحكم عبر الثاير ستور (Static VAR Compensator - SVC) وجهاز تعويض السعة المتسلسل في خوارزمية كبلر للطاقة التفاعلية، مما يحقق توازئا فعالاً من خلال تحديد الحجم الأمثل والموقع المناسب لها لتعزيز خطوط التبار بط الكهربائية التي تحتاج إلى دعم أكبر للطاقة التفاعلية، مما يحقق توازئا فعالاً من حيث التكلفة بين الاستثمار الرأسمالي والأداء التشغيلي. وعند التكلفة بين الاستثمار الرأسمالي والأداء التشغيلي. وعند عنظا طروف وتعزيز الشبكة الموجهة، تقدم هذه الدراسة منهجية مرنة وقابلة للتوسعة التخطيط وتشغيل شبكات كبر بائية مرنة ومذفضة الكربون.

الكلمات المفتاحية: مصادر الطاقة المتجددة، تقنيات التحسين الميتاهوريستيكية، خوارزمية كبلر للتحسين، التدفق الأمثل للطاقة، أجهزة FACTS، استقرار الجهد

ACKN(OWLEDGEMENTS	i
ABSTR	RACT	ii
TABLI	E OF CONTENTS	iii
LIST C	OF FIGURES	viii
LIST C	OF TABLES	X
LIST C	OF ABBREVIATIONS	xi
Chapte	r 1: GENERAL INTRODUCTION	1
1.1	Introduction	2
1.1.1	Background	2
1.1.2	The Research Gap:	3
1.1.3	Thesis Objectives & Scope:	4
Chapte	r 2: RENEWABLE ENERGY SOURCES AND UNCERTAINTIES MODELING.	5
2.1	Introduction	6
2.2	Renewable Energy Sources	6
2.2.1	Wind Power Plants	7
2.2.1.1	Operating Principle	8
2.2.1.2	Key Variables	8
2.2.2	Solar Power Plants	9
2.2.2.1	Operating Principle	9
2.2.2.2	Key Variables	9
2.2.3	Hydro Power Plants	10
2.2.3.1	Operating Principle	10
2.2.3.2	Key Variables	11
2.3	Uncertainty Modeling Methods	11
2.3.1	Markov Chains:	11
2.3.2	Time Series Analysis (ARIMA)	12
2.3.3	Machine Learning (ML) Models	12
2.3.4	Interval Optimization	13
2.3.5	Robust Optimization	13
2.4	Monte Carlo Simulation (MCS)	14
2.4.1	Monte Carlo Simulation Methodology and Application in Uncertainty Modeling	14
2.4.1.1	System Definition and Identification of Uncertainties	14

2.4.1.2	Assignment of Probability Distributions	14
2.4.1.3	Analysis of Simulation Results	15
2.4.1.4	Advantages of Using MCS	15
2.5	Probability Density Functions for RES	15
2.5.1	Wind Power Modeling Using Weibull Probability Density Function	16
2.5.1.1	Power Model For Wind	16
2.5.1.2	Calculation of Wind Power Probabilities	17
2.5.2	Solar Photovoltaic Power Modeling Using Lognormal Probability Density Function	17
2.5.2.1	Generated Power Modeling in Solar Power Plant	19
2.5.3	Hydropower Modeling Using Gumbel Probability Density Function	19
2.5.3.1	Generated Power Modeling in Hydro Power Plant	20
2.6	Cost Evaluation Based on Scenarios Outcomes	20
2.6.1	Cost generation for renewable sources:	20
2.6.2	Direct Cost of RES Generators (DCost):	20
2.6.2.1	Direct Cost of Wind Power Units	21
2.6.2.2	Direct Cost of Solar Power Units:	21
2.6.2.3	Direct Cost of Hydro Power Units:	21
2.6.3	The Evaluation of Cost Uncertainties in RES Generators	22
2.6.3.1	Uncertain Wind Power Cost Evaluation	22
2.6.3.2	Uncertain Solar Photovoltaic Power Cost Evaluation	23
2.6.3.3	Cost Evaluation of Uncertain Combined Solar Photovoltaic And Small-Hydro Power	23
2.7	Conclusion	24
Chapte	r 3: POWER SYSTEM AND POWER FLOW MODELING	25
3.1	Introduction	26
3.2	Power Flow Definition and Objectives	26
3.2.1	Definition of Power Flow	26
3.2.2	Objective	27
3.2.3	Classification of Bus Bars According to Their Specifications	27
3.2.4	Formulation of Power Flow Equations	28
3.2.5	Power Flow Problem Solution Methods	
3.3	Optimal Power Flow	
3.3.1	Problem Formulation Optimal Power Flow Model	
3.3.2	Optimal Power Flow Variables Classification	
3.3.3	Constraints Formulation	
	1 Equality Constraints	

3.3.3.1.	2 Inequality Constraints	33
3.3.4	Constraint Handling (CH) Methods	34
3.3.4.1	Penalty Function Method (PF)	34
3.4	Objective Function	35
3.4.1	Classical Methods Applied to The Optimal Power Flow Problem	36
3.5	Conclusion	37
Chapte	er 4: METAHEURISTIC OPTIMIZATION TECHNIQUES	38
4.1	Introduction	39
4.2	Classification of Metaheuristic Algorithms	40
4.2.1	Evolutionary Techniques:	40
4.2.2	Swarm-intelligence (SI):	41
4.2.3	Physics-Based Techniques	42
4.2.4	Human-related Techniques	42
4.2.5	Differences Between Classes:	43
4.3	Kepler Optimization Algorithm (KOA):	44
4.3.1	Inspiration	44
4.3.2	Mathematical model of Kepler optimization algorithm (KOA):	46
4.4	Enhanced Kepler Optimization Algorithm	54
4.5	Non-Dominated Sorting Kepler Optimization Algorithm (NSKOA)	55
4.5.1	Non-Dominated Sorting Principle	55
4.5.2	Concept of Dominance	55
4.5.3	The classification of the population	55
4.5.4	Crowding Distance (CD)	56
4.5.5	Elitism and Population Combination	56
4.5.6	Best Compromise Solution (BCS)	57
4.6	Conclusion	58
_	er 5: POWER FLOW ANALYSES IN PRESENCE OF RENEWABLE ENERGY	50
5.1	Introduction:	
5.2	Optimal Power Flow Problem Formulation:	
5.2.15.2.1.1	Optimization Problems: Cost of Generation for Thermal Units:	
5.2.1.1	Emission and Carbon Tax:	
5.2.1.2		
	Voltage Deviation:	

5.2.2	Objective Functions	63
5.2.2.1	Minimization of Total Generation Cost	63
5.2.2.2	Minimization of Emission Gases with Carbon Tax	63
5.2.2.3	Minimization of The Real Power Losses	63
5.2.2.4	Minimization of The Voltage Deviation	63
5.2.3	System Constrains	64
5.2.3.1	Equality-Constraints	64
5.2.3.2	Security Constraints	64
5.3	Simulation Results	65
5.3.1	Test System 1: Modified IEEE 30 Bus Power System	66
5.3.1.1	Case 1: Total Generation Cost Minimization	69
5.3.1.2	Case 2 Minimizing the Total Cost with Emission-Carbon Tax	72
5.3.1.3	Case 3: Optimized Cost Vs The Reserve Cost	73
5.3.1.4	Case 4: Optimized Cost vs the Penalty Cost	76
5.3.1.5	Case 5: Minimization of the Real Power Losses	78
5.3.1.6	Case 6: Minimization of Voltage Deviation	79
5.3.2	Test-system 2: The Modified Algerian DZA 114-BUS Power System	81
5.4	Conclusion	85
_	er 6: VOLTAGE STABILITY IMPROVEMENT IN PRESENCE OF RENE	
6.1	Introduction:	87
6.2	Problem Formulation	87
6.2.1	Optimization Problem	88
6.2.1.1	Cost of Generation for Thermal Units	88
6.2.1.2	The Investment Cost of FACTS Modeling	88
6.2.1.2.	1 SVC Modeling	88
6.2.1.2.	2 TCSC Modeling	89
6.2.2	Objective Functions	90
6.2.2.1	Minimization of Power Production Cost	90
6.2.2.2	Real Power Losses (RPLs)	90
6.2.2.3	Total Voltage Deviation (TVD)	90
6.2.2.4	Voltage Stability Index (VSI)	90
6.2.3	Constraints	91
6.2.3.1	Equality Constraints	91
6.2.3.2	Security Constraints	92

6.3.1	Test-System: Conventional and Modified IEEE 57 BUS Network	94
6.3.1.1	Case 1: Total Generation Cost and the Investment Cost of FACTS Optimization	99
6.3.1.2	Case 2: Real Power Loses and the Investment Cost of FACTS Optimization	102
6.3.1.3	Case 3: Total Voltage Deviation and the Investment Cost of FACTS Optimization	105
6.3.1.4	Case 4: Voltage Stability Index and the Investment Cost of FACTS Optimization	108
6.4	Conclusion	112
GENEF	RAL CONCLUSION	115
BIBLIC	OGRAPHY	115

LIST OF FIGURES

Figure 2-1: Modern Power System	7
Figure 2-2:Wind Power System	8
Figure 2-3: Solar Power System	9
Figure 2-4:Hydro Power System	10
Figure 2-5:Wind Speed Frequency For Wind Generator	16
Figure 2-6:Solar Irradiance Frequency For The Site	18
Figure 2-7:River Flow Frequency For The Site	20
Figure 4-1: The trajectory of planets motion	45
Figure 4-2:Different Ellipse Shapes	45
Figure 4-3:2D Dimension Of Planets Motion	46
Figure 4-4:3D Dimension Of Planets Motion.	46
Figure 4-5: Exploration And Exploitation Regions In The Search Space	50
Figure 4-6:Flowchart of (KOA)	53
Figure 4-7: ψ variation with iteration	54
Figure 4-8: Concept Of Dominance	55
Figure 4-9: Crowding Distance	56
Figure 4-10:Non-Dominated Selection	57
Figure 4-11: Crowding Distance	57
Figure 5-1: Modified IEEE 30 Bus System Configuration	66
Figure 5-2:Speed Of Wind Frequency For Wind Generator At Bus 5	67
Figure 5-3:Wind Speed Frequency For Wind Plant At Bus 11	68
Figure 5-4:Lognormal PDF Of Solar Irradiance For SPV Bus 13	68
Figure 5-5: Aviable Real Power From Solar PV Unit	69
Figure 5-6:Voltage Profile Of 30 BUSS With And Without RES	70
Figure 5-7:Convergence Curve For Case 1 30-Bus System	72
Figure 5-8: Variation Of The Scheduled Active Power Vs The Reserve Cost	74
Figure 5-9: Variation Of The Scheduled Reactive Power Vs The Reserve Cost Coefficients	75
Figure 5-10: Variation Of Production Cost Against Reserve Cost Coefficients	75
Figure 5-11: Variation Of The Scheduled Active Power Vs The Penalty Cost Coefficients	76
Figure 5-12: Variation Of The Scheduled Reactive Power Vs The Penalty Cost Coefficients	77
Figure 5-13: Variation Of Production Cost Against Penalty Cost Coefficients	77
Figure 5-14: Algerian Electricity Grid Topology- DZA 114-Bus	81

Figure 5-15: Convergence Curve For Case 1 DZA 114-Bus System	82
Figure 5-16: Voltage Profile Of DZA 114- Load Buses For Case 1	82
Figure 5-17: Generators Reactive Power For Case 1	83
Figure 6-1:SVC Model And Configuration.	89
Figure 6-2:TCSC Configuration	89
Figure 6-3:Schematic Diagram Of TCSC	89
Figure 6-4:Distribution of wind speed at bus 12	95
Figure 6-5: Rate Of River Flow For The Site	95
Figure 6-6:Solar Irradiance For The Site	96
Figure 6-7: Solar Irradiance For Solar PV Generator	96
Figure 6-8: Available Real Power At Bus 9	97
Figure 6-9: Available Real Power For Combined Solar-Hydro Power	97
Figure 6-10: Available Real Power For Solar PV Unit	98
Figure 6-11: Available Real Power For Hydro Unit	98
Figure 6-12:Pareto Front Of Case 1	100
Figure 6-13:Load Bus Voltage Profile For Case 1	101
Figure 6-14: Generator's Reactive Power For Case 1	102
Figure 6-15: Pareto Front of case 2	103
Figure 6-16:Load Bus Voltage Profile For Case 2	104
Figure 6-17: Pareto Front Of Case 3	106
Figure 6-18:Load Bus Voltage Profile For Case 3	106
Figure 6-19: Generator's Reactive Power For Case 3	108
Figure 6-20: Pareto Front Of Case 4	109
Figure 6-21:Load Bus Voltage Profile For Case 4	110
Figure 6-22: Generator's Reactive Power For Case 4	110

LIST OF TABLES

Table 3-1:Classification of bus bars according to their specifications	27
Table 4-1: Metaheuristic Algorithms Classification	43
Table 5-1: EKOA Process Dealing With OPF	65
Table 5-2: Emission And Cost Coefficients Of Thermal Generators Of IEEE 30 Bus Netv	vork 67
Table 5-3:PDF Parameter Of Wind And Solar Pv Units	67
Table 5-4:Optimal results for variables and objective function in Case 1	71
Table 5-5: Statistical Analysis For Case 1 Of EKOA With Other Algorithms	72
Table 5-6:Optimal Results For Variables And Objective Function In Case 2	73
Table 5-7:Optimal Results For Variables And Objective Function In Case 5	79
Table 5-8: Optimal Results For Variables And Objective Function In Case 6	80
Table 5-9: Objective Function Of Test System 2 For 4 Case	84
Table 6-1: Control Variables Of The Test System.	94
Table 6-2:PDF parameters of renewable generators	95
Table 6-3:Optimal Result And Control Variables Of Case	100
Table 6-4: Statistical Comparison Of Case 1 And Case 2 For The First Scenario	102
Table 6-5:Optimal Result And Control Variables For Case 2	104
Table 6-6:Optimal result and control variables for case 3	107
Table 6-7:Optimal Result And Control Variables For Case 4	111

LIST OF ABBREVIATIONS

TGcost Total Generation cost

KOA

FACTS Flexible AC Transmission System
TFcost Total investment cost of FACTs
RES Renewable Energy Sources
OPF Optimal Power Flow
PDF Probability Density Function

 \mathcal{S}_{ij} voltage angle change between i and bus j Vg_i Amplitude of Voltage for Generator at bus I N_{PO} The number of PQ buses (Load buses)

 Ngb/N_{lb} stands for the number of generator and load buses

Kepler Optimization Algorithm

 \mathcal{E}_k Conductance of kth branch linked into i & j V_i, V_i Voltage amplitude in the specified bus i or j

 N_{TG} , N_{WG} , N_{SG} N_{ShG} represent the number of thermal, wind, solar pv, solar-hydro generators

 $G_{q(ij)}$ the conductance of the branch i-j $\delta_{_{ii}}=\delta_{_{i}}-\delta_{_{i}}$ the difference in voltage angles

 $PK_{W,j}$ penalty cost coefficients of jth wind unit $PK_{S,L}$ penalty cost coefficients of kth solar unit

 PK_{SH} penalty cost coefficients of i^{th} solar-hydro unit $RK_{W,j}$ reserve cost coefficients of jth wind unit $RK_{S,k}$ reserve cost coefficients kth solar unit

 $RK_{SH,i}$ reserve cost coefficients i^{th} solar-hydro unit $WP_{r,i}$ rated output power of the wind farm

 G_{std} Solar irradiante Under environnemental conditions

 $WP_{A,i}$ available power from the corresponding wind power plants

 $SP_{Av,k}$ power output available from PV generator

 ShP_{tv} power output available from PV-hydro generator

 $m{h}_k$ coefficients of direct cost related to kth solar power unit $m{g}_j$ coefficients of direct cost related to wind power unit $m{H}_i$ coefficients of direct cost related to hydro power unit

 $SP_{Sc.k}$ scheduled power of PV units

 $\begin{array}{ll} \mathit{WP}_{Sc,j} & \text{scheduled power of wind power units} \\ \mathit{hP}_{sc,i} & \text{scheduled power of PV-hydro unit} \\ \mathit{Q}_{\mathit{TCSC}_i} & \text{reactive power generated by i-th TCSC} \\ \mathit{C}_{\mathit{TCSC}} & \text{total investment cost of TCSC devices} \end{array}$

 N_{TCSC} total number of TCSC devices

 Q_{SVC} reactive power generated by i-th SVC

 C_{SVCi} associated SVC cost

 N_{SVC} total number of SVC devices

Chapter 1: GENERAL INTRODUCTION

1.1 Introduction

1.1.1 **Background**

Electrical power systems are in a state of continuous expansion and evolution, driven by rising electricity demand and the quest for economic, reliable, and environmentally sustainable energy supply. To meet these challenges, utilities and system operators must extend and reinforce existing transmission and distribution networks, while also commissioning new generation units. However, increasing reliance on conventional thermal plants such as coal- and gas-fired units to satisfy peak loads leads to higher fuel costs, greater operational expenditures, and elevated greenhouse-gas emissions [1]. These factors require substantial capital investments in network infrastructure along with strategic planning to balance immediate demand requirements against long-term sustainability goals.

The global transition to sustainable energy systems is crucial for mitigating climate change, enhancing energy security, and reducing reliance on fossil fuels [2]. (RES) including wind, solar photovoltaic (PV), and hydropower play a central role in this paradigm shift by lowering fuel expenses, cutting carbon emissions, and diversifying generation portfolios. However, their inherent variability and uncertainty resulting from fluctuating wind speeds, solar irradiance, and river flows pose significant challenges for power system stability, economic dispatch, and operational planning. Effectively integrating large-scale RES into existing grids demands advanced uncertainty modeling techniques and constrained optimization frameworks. Methods such as Monte Carlo simulation, scenario-based stochastic programming, and probabilistic load flow studies enable accurate quantification of generation variability and system risk, while comprehensive cost analyses must account for capital investment, integration-related balancing expenses, and long-term operational impacts [2].

Flexible AC Transmission Systems (FACTS) devices have emerged as vital components for augmenting grid performance in this changing landscape. Based on high-speed power-electronic converters, FACTS modules dynamically control line impedance, voltage magnitude, and phase angle to regulate power flow and maintain system stability. Shunt compensators such as Static Var Compensators (SVCs) utilizing Thyristor-switched capacitors/reactors, and Static Synchronous Compensators (STATCOMs) based on voltage-source converters inject or absorb reactive power to manage voltage profiles and support transient stability [3]. Series compensators, like the Thyristor-Controlled Series Capacitor (TCSC), insert a controllable reactance into transmission lines to adjust power transfer capability and damp oscillations. By rapidly modulating reactive-power injection and series impedance, these devices reduce losses, relieve congestion, and enhance voltage regulation [4]. To fully harness FACTS benefits and ensure cost-effectiveness, precise determination of each device's optimal location and sizing is essential; misplacement or improper rating can compromise voltage support and even increase overall system losses [5].

The Optimal Power Flow (OPF) problem is the foundational tool for optimizing generation dispatch and network-control settings to minimize an objective commonly fuel cost, generation cost, or system losses while satisfying operational constraints [6]. A full AC-OPF formulation captures both active and reactive power balances at each bus, voltage magnitude limits, generator capability curves, and thermal line-flow restrictions, resulting in a large-scale, nonlinear, and nonconvex

optimization problem. Typical variables include generator real/reactive outputs, bus voltages, and transformer tap ratios, with equality constraints enforcing Kirchhoff's laws and inequalities representing equipment and security limits. Classical solution methods ranging from gradient-based techniques and sequential quadratic programming to interior-point and successive linear programming often struggle with convergence guarantees and computational tractability as network size grows [7]. The advent of high renewable energy source (RES) penetration introduces additional layers of complexity: stochastic, time-coupled constraints for forecasting error margins; reserve and ramping requirements; and multi-period coupling for energy storage [8]. Addressing these requires robust solution strategies, such as stochastic programming, chance-constrained OPF, and decomposition-based algorithms, to ensure reliable and economical operation under uncertainty.

In recent years, metaheuristic optimization algorithms including Genetic Algorithms (GAs), Particle Swarm Optimization (PSO), Differential Evolution (DE), and Ant Colony Optimization (ACO) have gained widespread acceptance for tackling large-scale, nonlinear, and stochastic OPF problems. These population-based methods leverage mechanisms inspired by natural and social phenomena to navigate complex search spaces without gradient information. The exploration phase promotes global search by diversifying candidate solutions, while the exploitation phase intensifies local search around promising regions. Effective balancing of these phases is crucial: excessive exploration delays convergence, whereas premature exploitation risks entrapment in local optima. To further enhance performance, researchers increasingly employ hybrid metaheuristics that combine complementary strengths for instance, integrating GA's crossover operators with PSO's velocitydriven update rules or embedding local search heuristics within DE frameworks. Such hybrids often incorporate adaptive control strategies that dynamically adjust exploration-exploitation trade-offs based on convergence metrics or population diversity measures. Moreover, multi-objective metaheuristic extensions address conflicting goals such as minimizing cost, emissions, and voltage deviations by generating Pareto-optimal solution sets, using techniques like the Non-Dominated Sorting Genetic Algorithm II (NSGA-II) and multi-objective PSO (MOPSO) [9].

The application of these advanced metaheuristics to stochastic OPF involves novel formulations that explicitly model RES uncertainty via scenario sampling, probabilistic constraints, or chanceconstraint programming. Parallel and GPU-accelerated implementations further enable real-time or near-real-time optimization, making metaheuristics a viable option for modern grid operation and planning with high renewable penetration and FACTS device coordination [10].

This thesis investigates the coordinated planning and operation of modern power systems with high levels of renewable penetration. It focuses on optimal placement and sizing of FACTS devices, development of stochastic OPF formulations, and the design of advanced metaheuristic solvers to efficiently handle the resulting large-scale, multi-objective optimization problems.

The Research Gap: 1.1.2

Despite advances in uncertainty-modeling techniques (e.g., Monte Carlo simulation), the increasing complexity of OPF with high renewable penetration, and the need to optimally size and site FACTS devices, there remains a critical need for:

Robust frameworks: integrating high-fidelity RES uncertainty models (Weibull, Lognormal, Gumbel PDFs) with security-constrained OPF for large-scale practical systems.

Efficient metaheuristic algorithms capable of handling the high-dimensional, multi-objective, nonconvex optimization problems arising from RES integration, particularly when combined with optimal size and location of FACTS devices.

Comprehensive assessment quantifying the joint benefits of RES and FACTS on production costs, emissions reduction (including carbon tax impacts), voltage stability, and power losses under uncertainty.

1.1.3 **Thesis Objectives & Scope:**

In chapter 2, we provide a comprehensive overview of RES technologies, detailing the operating principles of wind turbines, photovoltaic arrays, and hydroelectric plants. We highlight the key stochastic parameters wind speed, solar irradiance, and river flow and discuss their impacts on power output and grid integration benefits. Various uncertainty-handling methods, including Monte Carlo simulation (MCS), machine learning, fuzzy logic, robust optimization, and interval optimization, are surveyed, with an emphasis on the choice of MCS in our work. We delve into probability density functions (Weibull for wind, lognormal for solar, and Gumbel for hydro) and outline the process of scenario generation and cost quantification (direct, reserve, and penalty costs).

In chapter 3, we introduce the classical power flow and (OPF) problems, formulating the objective functions, decision variables, and both equality and inequality constraints. We review traditional solution methods, their strengths, and limitations when faced with nonconvex, stochastic OPF formulations. This sets the stage for employing metaheuristic approaches.

An extensive classification of metaheuristic algorithms is then presented covering evolutionary, swarm intelligence, physics-based, and human-inspired methods before focusing on the Kepler Optimization Algorithm (KOA) In chapter 4. Two enhancements are proposed: (1) a novel exploration exploitation operator φ that accelerates convergence by deeper neighbor searches, and (2) integration of a Non-dominated sorting scheme for multi-objective optimization.

The enhanced EKOA is applied to two test systems. In Chapter 5, we optimize generation dispatch for a 114-bus Algerian system under renewable uncertainty, minimizing total production cost and carbon taxation, and compare the performance of our enhanced version EKOA to original KOA. Chapter 6 extends this work by incorporating FACTS devices (SVC and TCSC), optimizing their siting and sizing to bolster voltage stability and reduce losses, subject to investment cost constraints.

Together, these contributions advance the state of the art in stochastic OPF by blending rigorous uncertainty modeling with powerful, tailored metaheuristic optimization, demonstrating tangible benefits in cost savings, emissions reduction, and system stability.

Chapter 2: RENEWABLE ENERGY SOURCES AND UNCERTAINTIES MODELING

2.1 Introduction

The global transition toward renewable energy systems (RES) has revolutionized power systems, replacing traditional deterministic generation with inherently variable sources such as wind, solar, and hydro [11]. While RES offer unparalleled environmental benefits, their integration introduces significant operational challenges. Environmental factors including fluctuating irradiance, stochastic wind speeds, and seasonal hydro inflows create uncertainty that propagates through power system planning and real-time energy markets [12]. Measurement errors and forecasting limitations further compound these challenges, often leading to mismatches between predicted and actual generation [13]. To address this, modern power systems increasingly rely on multi-source modeling frameworks that combine wind, solar, and hydro resources into cohesive operational strategies. These frameworks are critical for balancing supply-demand mismatches, mitigating curtailment risks, and ensuring grid stability in real-time markets [14].

Uncertainty in RES is not merely a technical hurdle; it directly impacts the economic and operational efficiency of power systems. Deterministic approaches to (OPF) and economic dispatch, which assume fixed generation profiles, fall short in accounting for the probabilistic nature of RES. This gap underscores the need for probabilistic modeling to quantify risks, optimize reserve margins, and enhance decision-making under uncertainty. Monte Carlo simulation (MCS) and probability density functions (PDFs) emerge as indispensable tools in this context [15]. By generating thousands of plausible scenarios based on RES variability, MCS enables system operators to evaluate the likelihood of extreme events, such as wind droughts or solar curtailment, while PDFs like the Weibull (wind speed), lognormal (solar irradiance), and Gumbel (hydro inflows) provide statistically rigorous representations of resource-specific uncertainties [16].

The chapter focuses on detailed information of the probabilistic modeling for RES uncertainty representation (Probability Density Functions) with computational scenario-based methods (Mont Carlo Simulation). This approach is structured as follows:

- Parametric Distributions & Historical Data: Parametric PDFs (e.g., Weibull for wind speed, lognormal for solar irradiance, Gumbel for hydro inflow) are combined with historical weather records to synthesize time-correlated RES profiles
- Monte Carlo Sampling: A large ensemble of scenarios is generated by randomly sampling each PDF across thousands of iterations, capturing the temporal variability of RES inputs
- Parameter Calibration: Key PDF parameters shape, scale, and location are calibrated against site-specific climate data (e.g., local wind and irradiance measurements) to ensure that generated profiles reflect actual operating conditions

2.2 **Renewable Energy Sources**

RES such as wind, solar, hydroelectric, and bioenergy generate electricity with minimal greenhouse gas emissions, playing a critical role in mitigating climate change and reducing atmospheric CO2 levels [17]. According to the International Renewable Energy Agency IRENA, up to 90 percent of global electricity could and should be supplied by renewables by 2050, underscoring their transformative potential [18]. Unlike fossil fuels, renewable technologies emit virtually no pollutants during operation, significantly lowering air and water contamination over their lifecycle [19]. The renewable energy sector also drives significant job creation, with IRENA reporting steady

global growth in clean energy employment across manufacturing, installation, and operations. By replacing coal and gas plants, renewables contribute to improved public health, preventing thousands of premature deaths each year through reductions in air pollution, particulate matter, and smog formation. Beyond environmental benefits, the expansion of clean energy industries supports economic resilience and fosters innovation in sustainable technologies. Enhanced local generation from wind and solar bolsters energy security by diversifying supply and reducing reliance on imported fuels. Cost trends reported by the International Energy Agency IEA show that solar and wind power are now among the cheapest sources of new electricity in many regions, making them economically competitive with existing fossil-fired plants. Projections indicate that renewables will supply nearly 46 % of global electricity by 2030, driven by policy support and technological advances. Community-led renewable projects further offer social benefits, enhancing local resilience and delivering energy access to underserved areas. Finally, transitioning to renewable systems reduces geopolitical and supply-chain risks associated with fossil fuel extraction, trade, and price volatility [18].

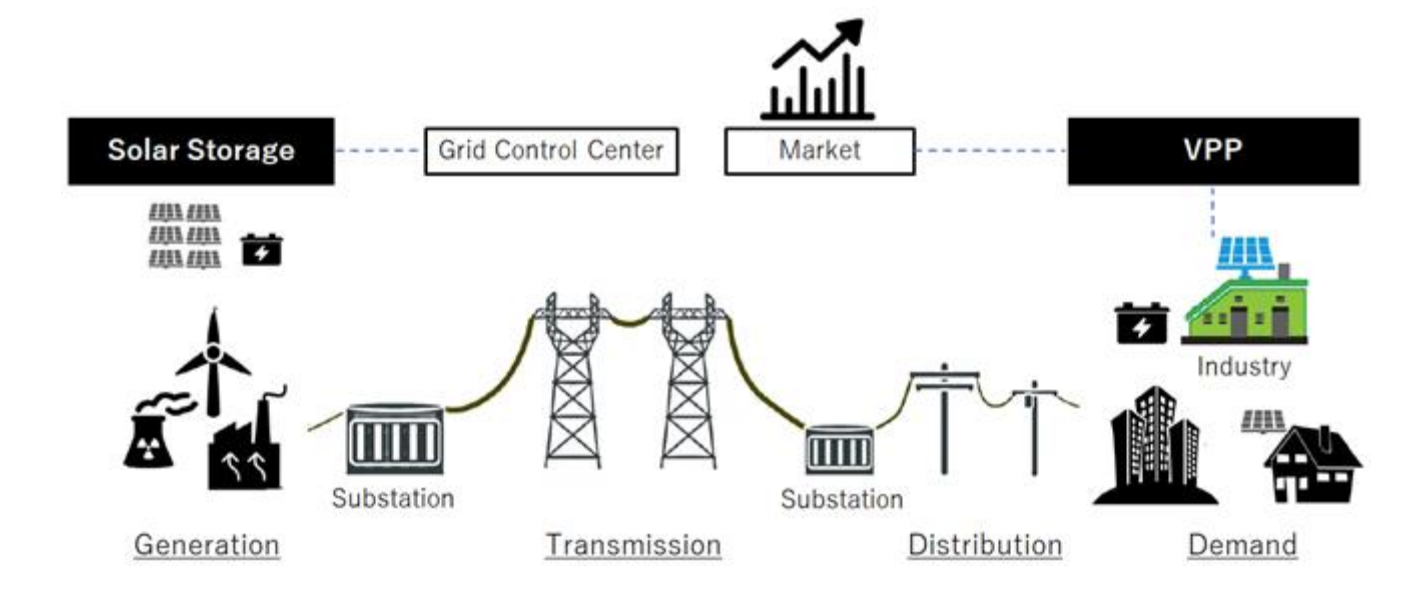


Figure 2-1: Modern Power System

2.2.1 Wind Power Plants

A grid-connected wind power plant converts kinetic energy from the wind into electrical energy through wind turbines coupled with generators and power electronic interfaces, delivering power directly to the utility network while maintaining voltage and frequency standards [20]. Key operational variables include wind speed and direction, air density, turbine rotor dynamics, generator characteristics, and power-electronic control settings. Major challenges encompass the inherent variability and intermittency of wind, grid stability and power quality concerns, reactive power support, fault ride-through capability, low system inertia, accurate forecasting, and compliance with stringent grid codes [21]. Addressing these issues requires advanced control strategies, robust power electronics, energy storage integration, and coordinated grid management to ensure reliable and efficient operation.

WIND Rotating generator converts wind energy to electricity Substation increases voltage for transmission over long distances Transmission to the grid Transformer increases voltage for transmission to substation 1 All Other Generation Source

Figure 2-2: Wind Power System

2.2.1.1 Operating Principle

A grid-connected wind farm comprises one or more wind turbines, each equipped with a rotor, gearbox (in most designs), and generator either an induction machine or a permanent magnet synchronous generator (PMSG) that converts mechanical shaft power into alternating current (AC) [20]. Modern turbines often use variable-speed operation with power electronics back-to-back converters or doubly fed induction generator (DFIG) systems to decouple rotor speed from grid frequency, optimizing energy capture across a wide wind speed range and allowing dynamic control of active and reactive power [22]. The generated AC is typically stepped up via a transformer to medium or high voltage and synchronized to the grid, where grid-side converters regulate voltage, frequency, and power factor to meet utility requirements.

2.2.1.2 Key Variables

a) Wind Speed and Direction

Wind power output follows a cubic relation with wind speed within the turbine's operational window, making accurate measurement and control of rotor orientation critical.

b) Air Density

Variations in temperature, pressure, and humidity alter air density, affecting the mass flow through the rotor and thus the available power.

c) Rotor and Generator Dynamics

Blade pitch angle, rotor inertia, and generator torque control determine the mechanicalelectrical energy conversion efficiency and transient response during gusts or grid events.

2.2.2 Solar Power Plants

A grid-connected solar power plant converts sunlight into electrical energy using photovoltaic (PV) modules that generate DC power, which is then inverted to AC and synchronized with the utility grid for direct injection or local consumption. It relies on power electronics (inverters) to match voltage, frequency, and phase with grid requirements, and often includes transformers to step up voltage to medium or high-voltage levels for efficient transmission [23]. Advanced systems incorporate Maximum Power Point Tracking (MPPT) algorithms to optimize DC output under varying irradiance and temperature conditions, ensuring maximal energy harvest throughout the day [24].

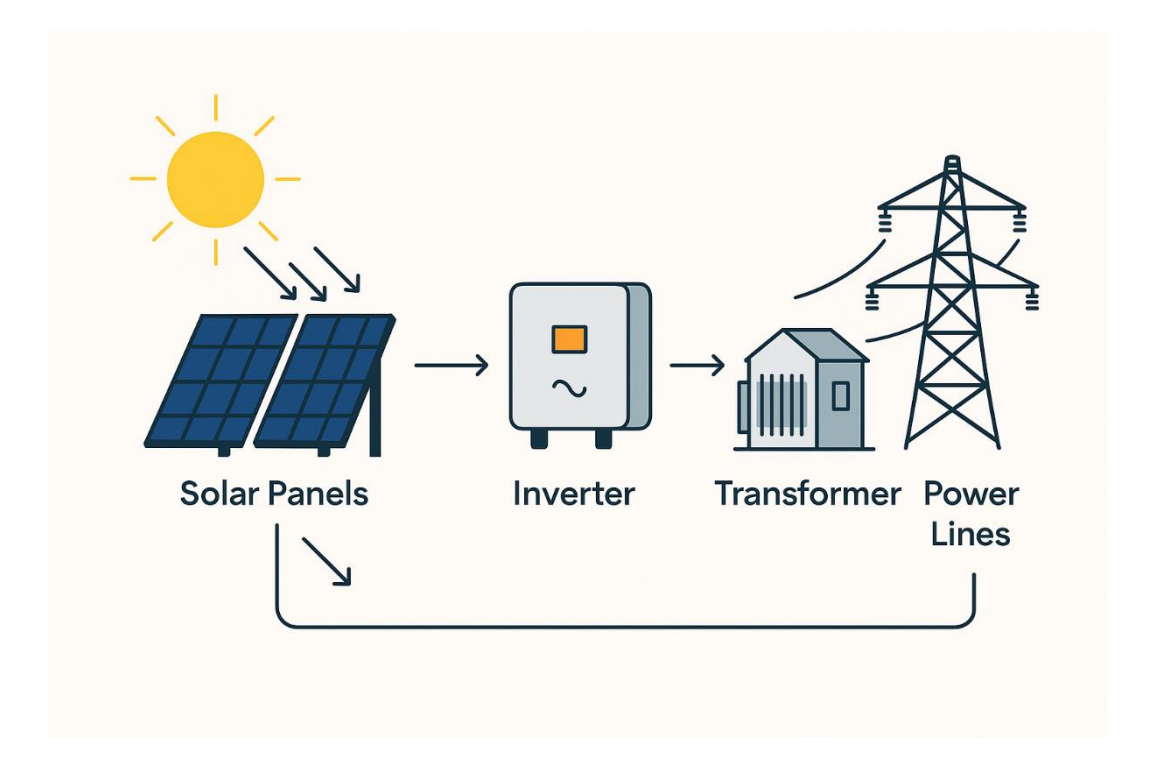


Figure 2-3: Solar Power System

2.2.2.1 Operating Principle

A PV array absorbs solar irradiance and converts photon energy into DC electricity via the photovoltaic effect. This DC power is fed into an inverter typically a central, string, or module-level unit that employs pulse-width modulation (PWM) to synthesize grid-compatible AC voltage and frequency. The inverter's control system continuously adjusts switching to maintain synchronization and power factor requirements, and may provide ancillary services such as reactive power support and low-voltage ride-through during grid disturbances. A transformer then steps the inverter's AC output to the grid voltage level, and power is dispatched onto transmission or distribution lines to meet load demand or feedback excess energy [25].

2.2.2.2 Key Variables

Solar Irradiance: Instantaneous solar insolation (W/m²) drives PV output, with short-term fluctuations due to cloud cover and atmospheric conditions.

- a) Module Temperature: Cell temperature inversely affects efficiency; higher temperatures reduce voltage and thus power output, making thermal management critical.
- **b) Tilt and Orientation**: Panel tilt angle and azimuth orientation relative to sun path determine daily and seasonal energy capture profiles.
- c) Inverter Performance: Conversion efficiency, MPPT accuracy, and control response dictate how effectively DC is converted to grid-quality AC under dynamic conditions.
- **d) Grid Interface Characteristics**: Grid impedance, voltage level, and short-circuit ratio at the point of interconnection influence stability margins and reactive power needs.

2.2.3 Hydro Power Plants

A grid-connected hydroelectric plant converts the potential energy of water stored at elevation into electrical energy via turbines and generators, then synchronizes this power with the utility network to meet demand. Key variables include the hydraulic head, flow rate, turbine-generator efficiency, penstock dynamics, and reservoir storage levels [26]. Major challenges span hydrological variability intensified by climate change, environmental and regulatory constraints, sedimentation impacts on hydraulic components, and grid-integration issues such as low inertia and frequency support [27].

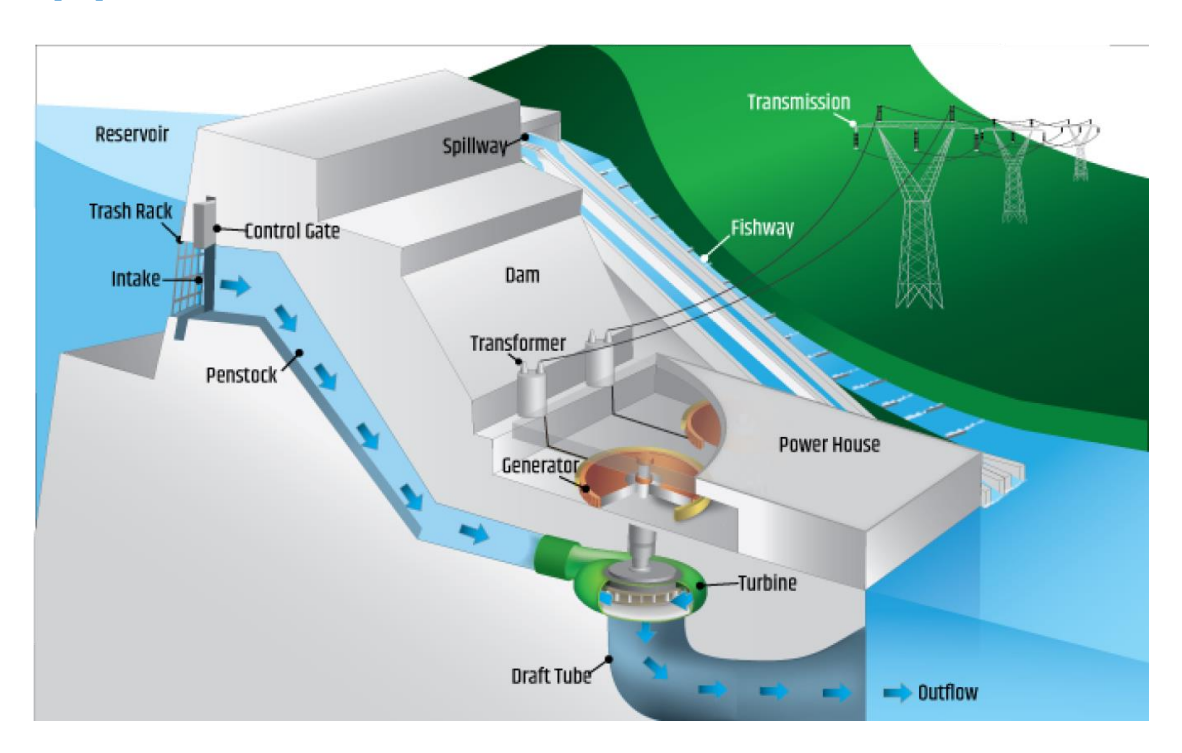


Figure 2-4:Hydro Power System

2.2.3.1 Operating Principle

Hydroelectric plants harness gravitational potential energy: water collected in a reservoir or diverted in a run-of-river scheme descends through a penstock, gaining kinetic energy that drives a turbine coupled to an electrical generator. The turbine's mechanical power is converted to AC electricity, which is stepped up in voltage via transformers and synchronized to the grid through excitation and governor control systems that regulate frequency and voltage Modern installations often include power-electronic converters or variable-speed units that provide synthetic (virtual)

inertia and enhanced grid-support capabilities, improving fast frequency response and flexibility in low-inertia systems heavily penetrated by renewables [27].

2.2.3.2 Key Variables

- a) Hydraulic Head: The vertical distance between the reservoir surface and turbine, determining the potential energy per unit volume of water.
- **b)** Flow Rate: Volume of water flowing through the turbine per second, directly proportional to output power.
- c) Turbine-Generator Efficiency: Conversion losses in the hydraulic-to-mechanical and mechanical-to-electrical stages, typically 85–95 % under optimal conditions.
- **d)** Penstock Dynamics: Fluid inertia and head losses due to friction, characterized by parameters of the penstock PVM (penstock-varying model) to capture transient response.
- e) Reservoir Storage: Active volume available for power generation and seasonal flow regulation, influencing dispatch flexibility and peaking capability.
- f) Control Systems: Governor response, excitation control, and any added power-electronic interfaces that adjust output to maintain grid frequency and voltage within limits

2.3 Uncertainty Modeling Methods

Uncertainty in modeling arises whenever inputs, parameters, or system behaviors cannot be determined with absolute precision, requiring a structured framework to characterize and manage its effects on model outputs. Broadly, uncertainties are classified into aleatoric inherent randomness such as wind speed fluctuations and epistemic stemming from limited knowledge or model form errors [28]. Probabilistic methods represent uncertain variables with parametric probability distributions (e.g., normal, Weibull, lognormal, Gumbel) calibrated from historical or experimental data. Monte Carlo Simulation then propagates these distributions through the model via random sampling to build statistical output distributions, estimating metrics like mean, variance, and confidence intervals [29]– [31]. Bayesian inference offers a dynamic approach by updating prior distributions with new data to reduce epistemic uncertainty over time. When data are insufficient for full probabilistic treatment, non-probabilistic methods such as interval analysis and convex models use bounds on parameters to guarantee output ranges without assuming specific distributions. Fuzzy logic and Dumpster Shafer evidence theory further extend non-probabilistic frameworks to model vagueness or partial belief, assigning membership or belief masses to sets of outcomes. Standards like the NIST Guide to the Expression of Uncertainty in Measurement provide formal procedures to combine and report uncertainty components in a consistent manner Finally, software tools such as the NIST Uncertainty Machine automate uncertainty propagation often via Monte Carlo facilitating robust quantification and decision-making under uncertainty across engineering, environmental, and financial applications.

2.3.1 Markov Chains:

Markov chains are stochastic models that describe systems transitioning from one state to another within a state space in a memoryless manner; that is, the probability of moving to the next state depends solely on the current state rather than on the sequence of preceding events. This mathematical framework handles uncertainty by representing transitions through a probability matrix, enabling analysts to predict the long-term behavior of complex systems by assessing the steady-state

distribution of outcomes. Over the decades, Markov Chains have been utilized in fields ranging from economics and genetics to engineering and reliability studies [32], [33]

In renewable energy systems (RES), Markov Chains can be applied to model uncertainties such as weather conditions that affect solar irradiance or wind speeds. For example, in a solar power installation, different weather states (e.g., sunny, partly cloudy, and cloudy) can be defined as distinct states in a Markov model with transition probabilities estimated from historical weather data. By simulating the transitions between these states over time, engineers can generate probabilistic forecasts of solar irradiance, helping to assess the likelihood of power production levels and optimize the system's design and operational strategies. This approach provides valuable insights into performance reliability and risk management under inherently variable environmental conditions [34].

2.3.2 Time Series Analysis (ARIMA)

Time Series Analysis, particularly methods like ARIMA (Auto Regressive Integrated Moving Average), originated from the work of Box and Jenkins in the 1970s and has since become a cornerstone in forecasting and uncertainty quantification across numerous engineering and econometric fields. ARIMA models work by analyzing historical time-dependent data to capture underlying patterns such as trends, seasonality, and cycles, while also modeling random fluctuations through autoregressive and moving average components. By differencing the data to achieve stationarity, these models effectively handle non-stationary behavior, and the resulting residuals quantify the inherent uncertainty, enabling predictions with statistically derived confidence intervals [35].

In renewable energy systems (RES), ARIMA can be used to forecast critical variables like solar irradiance or wind speeds, which directly impact power generation. For instance, by fitting an ARIMA model to historical solar irradiance data, engineers can generate forecasts that predict daily or hourly solar output along with uncertainty bounds [36]. These forecasts inform system design and operational strategies by revealing potential periods of underperformance, aiding in the planning of energy storage, load management, or backup generation [37]. The ability to quantify and incorporate forecast uncertainty allows stakeholders to make more informed decisions, ultimately enhancing the reliability and resilience of RES installations.

2.3.3 Machine Learning (ML) Models

Machine Learning (ML) models have evolved over several decades from early statistical pattern recognition techniques to modern deep learning architectures, profoundly transforming various engineering fields. These models learn complex relationships from data through training processes that adjust internal parameters. Uncertainty is handled in ML by employing approaches such as probabilistic modeling, ensemble methods, or Bayesian inference, which allow the generation of prediction intervals or confidence estimates alongside point predictions. This ability to quantify uncertainty helps in understanding the reliability of the predictions and in making risk-aware decisions[38].

In renewable energy systems (RES), ML models can be used to manage uncertainty in forecasting energy generation. For example, a solar power plant can leverage historical irradiance data, weather forecasts, and operational sensor data to train an ML model that predicts daily or hourly power output. By integrating techniques like ensemble learning or Bayesian neural networks, the model not only forecasts the expected energy output but also provides uncertainty bounds that indicate potential variability due to changing environmental conditions. This information is crucial for optimizing energy storage strategies, grid integration plans, and ensuring the overall reliability and resilience of the renewable energy infrastructure [38].

2.3.4 **Interval Optimization**

Interval optimization is extensively utilized in engineering disciplines where uncertainties are inherent. In mechanical and structural engineering, it aids in tolerance analysis and ensures safety margins by accounting for variability in material properties and manufacturing processes. Electrical engineers employ interval methods to design circuits that remain functional despite component tolerances. Moreover, in control systems engineering, interval optimization helps in designing controllers that maintain performance despite model uncertainties and external disturbances [39], [40].

Handling Uncertainty in Renewable Energy Systems (RES): In the realm of renewable energy, interval optimization plays a pivotal role in addressing the inherent uncertainties of RES outputs, such as fluctuations in solar irradiance and wind speeds. By representing uncertain parameters as intervals rather than fixed values, this method allows for the development of operational strategies that are robust against variability. For instance, in integrated energy systems, interval optimization can be used to devise operation schedules that ensure reliability and efficiency even when actual RES outputs deviate within expected bounds. This approach is particularly beneficial in planning and managing energy systems where precise predictions are challenging, ensuring that systems can adapt to a range of possible scenarios [41].

2.3.5 **Robust Optimization**

Robust Optimization (RO) emerged in the 1950s, rooted in decision theory and the concept of worst-case analysis, notably Wald's maximin model. It evolved into a distinct discipline in the 1970s, with developments across various scientific and technological fields. Over the years, RO has been applied in statistics, operations research, electrical engineering, control theory, finance, logistics, manufacturing, chemical engineering, medicine, and computer science [42], [43].

In the context of RES, RO addresses the inherent variability of sources like wind and solar power. By considering uncertainty sets that encompass potential deviations in generation, RO develops strategies that ensure system performance under worst-case scenarios [44]. For example, in energy management, RO can optimize the operation of integrated energy systems to reduce trading costs while accommodating renewable generation uncertainties. Additionally, RO has been applied to large-scale wind-solar storage systems, considering hybrid storage and multi-energy synergy, to enhance system robustness. These applications demonstrate RO's critical role in ensuring the reliability and efficiency of renewable energy systems amidst uncertainty [45].

2.4 **Monte Carlo Simulation (MCS)**

Monte Carlo Simulation (MCS) is extensively utilized to address uncertainties in renewable energy systems (RES) by modeling variables such as solar irradiance, wind speed, and river flow as probabilistic variables [46]. These variables are characterized using probability distributions derived from historical and empirical data. For instance, solar irradiance data collected at one minute intervals can be modeled using a Beta probability density function (PDF) to capture its variability. Similarly, wind speed and river flow data are analyzed to establish appropriate statistical models that reflect their stochastic nature.

Once the probability distributions are established, MCS involves generating thousands of random samples for each uncertain parameter. These samples are then propagated through the deterministic models of the RES to simulate a wide range of possible outcomes. This process results in a spectrum of potential energy outputs, enabling engineers to assess the probabilities of underperformance or over performance under various environmental conditions [47]. Such probabilistic analysis is crucial for designing resilient and reliable renewable energy installations, as it accounts for the inherent variability and uncertainty in environmental factors, leading to optimized system performance and risk-informed decision-making.

Monte Carlo Simulation Methodology and Application in Uncertainty Modeling

2.4.1.1 System Definition and Identification of Uncertainties

The first step in applying a Monte Carlo Simulation (MCS) is to define the system or model of interest and identify the input parameters that exhibit uncertainty. These uncertain parameters may stem from environmental factors, operational variability, physical properties, or market dynamics. Instead of assigning fixed values, MCS treats these variables as random inputs described by probability distributions [48].

Example: In renewable energy systems, key parameters such as solar irradiance, ambient temperature, and wind speed are inherently uncertain. Their variability can be effectively captured using probability distributions developed from historical or empirical data [49].

2.4.1.2 Assignment of Probability Distributions

Each identified uncertain parameter is assigned an appropriate probability distribution that reflects its statistical behavior. Common choices include normal, uniform, lognormal, and Weibull distributions. The selection depends on the nature of the variable and the availability of reliable data [48].

Example:

- Solar irradiance is often modeled using a lognormal distribution to account for its skewed nature and daily variability.
- Wind speed is typically characterized using the Weibull distribution, a well-established model in wind energy analysis.

Random Sampling Process

At the heart of MCS lies the process of random sampling from the assigned distributions. The simulation performs a large number of iterations, each time selecting random values for the input variables based on their respective probability distributions [49].

- Iterations: For every simulation run, a new set of input values is generated.
- Propagation: These values are then fed into the model to compute the corresponding output.
- Repeating this process thousands (or even millions) of times builds a statistical profile of the system's performance.

2.4.1.3 Analysis of Simulation Results

Once the simulation is complete, the resulting output data provides insights into how the system behaves under uncertainty. Several statistical measures can be derived from this output:

- Probability Distributions: Assess the likelihood of various outcomes.
- Mean and Variance: Determine the average result and the degree of variability.
- Confidence Intervals: Define the range within which the true output is likely to fall, with a specified level of confidence.
- Risk and Reliability Metrics: Quantify the likelihood of the system meeting (or failing to meet) performance thresholds.

2.4.1.4 Advantages of Using MCS

- Comprehensive Uncertainty Quantification: MCS does not just provide a single expected outcome but a full probability distribution, allowing for detailed risk analysis.
- Flexibility: It can incorporate various types of uncertainties and complex system interactions that might be difficult to model analytically.
- **Data-Driven:** The simulation directly uses historical and empirical data to characterize uncertainties, resulting in a model that closely reflects real-world conditions.

2.5 Probability Density Functions for RES

Probability density functions (PDFs) are mathematical functions describing the likelihood that a continuous random variable such as wind speed or solar irradiance will assume a particular value within its domain, enabling probabilistic forecasts that quantify uncertainty in renewable generation rather than merely point estimates [50]. Commonly utilized PDFs in renewable energy modeling include the Normal distribution for symmetric variables with low skewness, the Lognormal for positively skewed data, the Weibull distribution to accurately capture wind speed variability, and the Beta distribution for bounded parameters like solar irradiance. Selection of an appropriate PDF for a specific renewable resource relies on empirical data quality and quantity, the resource's physical and temporal variability, and goodness-of-fit metrics. The stochastic power output of RES is derived by convolving the resource's PDF with its power conversion curve, producing a probabilistic representation of generation profiles that informs risk-aware planning and dispatch decisions [50].

2.5.1 Wind Power Modeling Using Weibull Probability Density Function

The Weibull probability density function (PDF) is widely used to model wind speed distributions. The probability that wind speed in (m/s) follows a Weibull distribution is given in Ref[51]. as:

$$f_{\mathcal{U}}(S) = \left(\frac{\beta}{\alpha}\right) \left(\frac{S}{\alpha}\right)^{(\beta-1)} \times \exp\left(\frac{S}{\alpha}\right)^{\beta} \quad \text{for } 0 < S < \infty$$
 (2.1)

Here, β and α represent the scale and shape parameters of the Weibull PDF, respectively. In the present study, the selected values of the Weibull scale β and shape α parameters are listed in Table 3. These parameters have been realistically chosen based on the installed capacities of the power generation sources, with many values closely matching those used in Ref [51]. Figure 2-5 illustrates the Weibull fit alongside the wind speed frequency distributions, obtained through 8,000 Monte Carlo simulation scenarios [51].

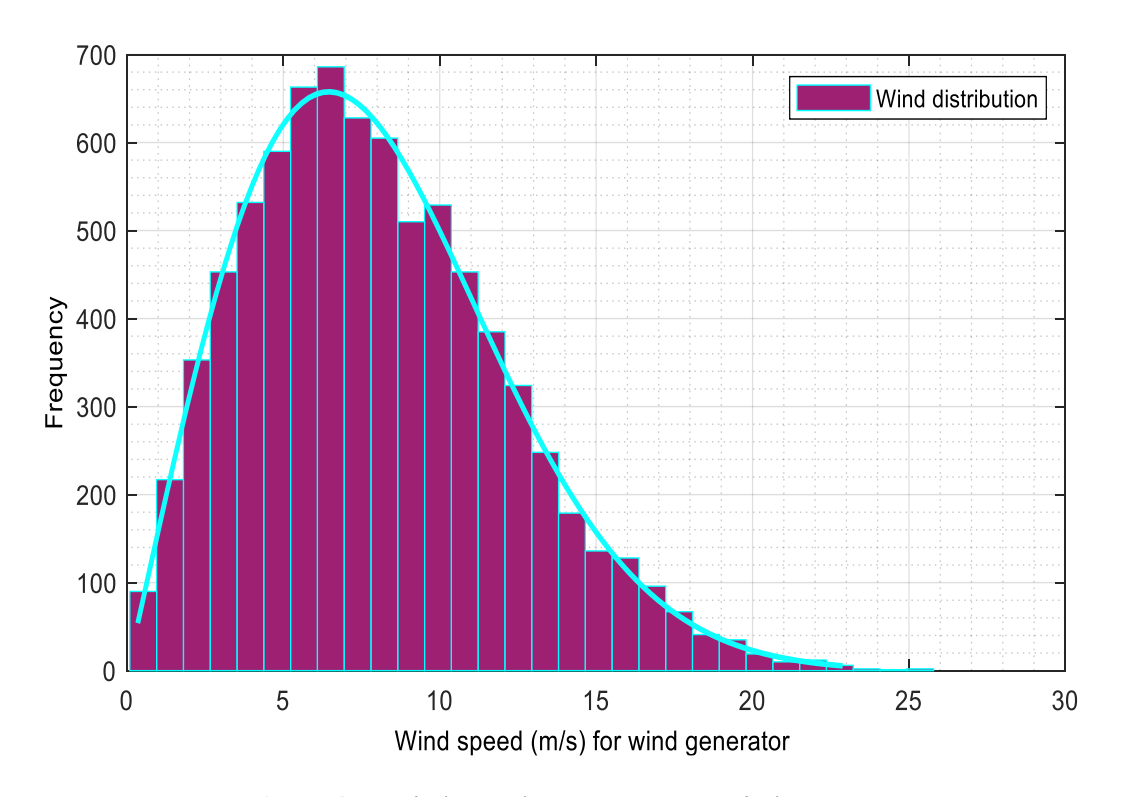


Figure 2-5: Wind Speed Frequency For Wind Generator

2.5.1.1 Power Model For Wind

In this study the wind farm connected is assumed to consist of 25 identical turbines, each with a rated capacity of 3 MW, resulting in a total farm capacity of 75 MW. The output power from each wind turbine varies based on the wind speed it encounters. The relationship between the output power and wind speed is expressed as follows [52]:

$$P_{w}(v) = \begin{cases} 0, & \text{for } v \langle v_{in} \text{ and } v \rangle v_{out} \\ P_{wr}\left(\frac{v - v_{in}}{v_{r} - v_{in}}\right) & \text{for } v_{in} \leq v \leq v_{r} \\ P_{wr} & \text{for } v_{r} \leq v \leq v_{out} \end{cases}$$

$$(2.2)$$

Here, P_{wr} represents the rated output power of a single wind turbine. The variables V_{in} , V_r and V_{out} correspond to the cut-in, rated, and cut-out wind speeds of the turbine, respectively. In this study, the wind speed parameters are selected as $V_{in} = 3$ m/s, $V_r = 16$ m/s, and $V_{out} = 25$ m/s, which are consistent with the specifications of the Enercon E82-E4 turbine [53].

2.5.1.2 Calculation of Wind Power Probabilities

The output power from a wind turbine is discrete at certain wind speed ranges, as shown in Equation (34). Specifically, the power output is zero when the wind speed v is below the cut-in speed V_{in} or above the cut-out speed V_{out} . Between the rated wind V_r and the cut-out speed V_{out} , the turbine delivers its rated power output P_{wr} . The probabilities of wind power generation within these discrete operational zones are calculated using the methods described in [54].

$$f_{w}(P_{w})\{P_{w}=0\} = 1 - \exp\left[-\left(\frac{v_{in}}{\alpha}\right)^{\beta}\right] + \exp\left[-\left(\frac{v_{out}}{\alpha}\right)^{\beta}\right]$$

$$f_{w}(p_{w})\{p_{w}=p_{wr}\} = 1 - \exp\left[-\left(\frac{v_{r}}{\alpha}\right)^{\beta}\right] + \exp\left[-\left(\frac{v_{out}}{\alpha}\right)^{\beta}\right]$$
(2.3)

In contrast to the discrete zones, the power output of wind turbine varies continuously in the bounds of a specific range $V_{in} \le V \le V_r$. Thus, the probability for this region can be modelled as follows [54]:

$$f_{w}(p_{w}) = \frac{\beta(v_{r} - v_{in})}{\alpha^{\beta} * P_{wr}} \left[v_{in} + \frac{P_{w}}{P_{wr}} (v_{r} - v_{in}) \right]^{\beta - 1} \exp \left[-\left(\frac{v_{in} + \frac{P_{w}}{P_{wr}} (v_{r} - v_{in})}{\alpha} \right)^{\beta} \right]$$
(2.5)

2.5.2 Solar Photovoltaic Power Modeling Using Lognormal Probability Density Function

In real-world scenarios, solar irradiance is influenced by a wide range of environmental factors including cloud cover, atmospheric conditions, geographic location, and time of day. These factors introduce randomness and variability that are effectively captured by the lognormal model. Additionally, the lognormal distribution provides mathematical convenience when integrating it into power system simulations and optimization models, especially when dealing with stochastic or probabilistic methods in renewable energy analysis.

The lognormal probability density function (PDF) is widely regarded as a reliable statistical model for representing the distribution of solar irradiance G_s , which is the measure of solar power received per unit area on a surface. This preference for the lognormal distribution arises from the nature of solar irradiance data itself it is strictly non-negative and tends to exhibit positive skewness, meaning that while most values cluster around a typical range, higher values occur less frequently but are still possible. This behavior makes the lognormal distribution more appropriate than the normal (Gaussian) distribution, which assumes symmetry and allows for negative values something physically impossible for irradiance [51].

$$f(G_S) = \frac{1}{G_S \sigma \sqrt{2\pi}} \exp\left\{ \frac{-(\ln G_S - \mu)^2}{2\sigma^1} \right\} \text{ for } G_S > 0$$
(2.6)

In this study, solar irradiance G_s is assumed to follow a lognormal PDF, characterized by a mean (μ) and a standard deviation (σ) . The functional form of this probability distribution, which defines the likelihood of a specific irradiance value occurring, is provided in Ref [51]. This formulation is crucial for accurately modeling the power output of solar photovoltaic (PV) systems, especially under uncertainty, and it serves as a foundation for the reserve and penalty cost evaluations discussed in the following sections.

The lognormal fitting and the corresponding frequency distribution of solar irradiance, as shown in Figure 2-7, are derived using a Monte Carlo simulation with a sample size of 8,000. The resulting fit provides a visual and statistical representation of how well the lognormal model aligns with the simulated irradiance data [55].

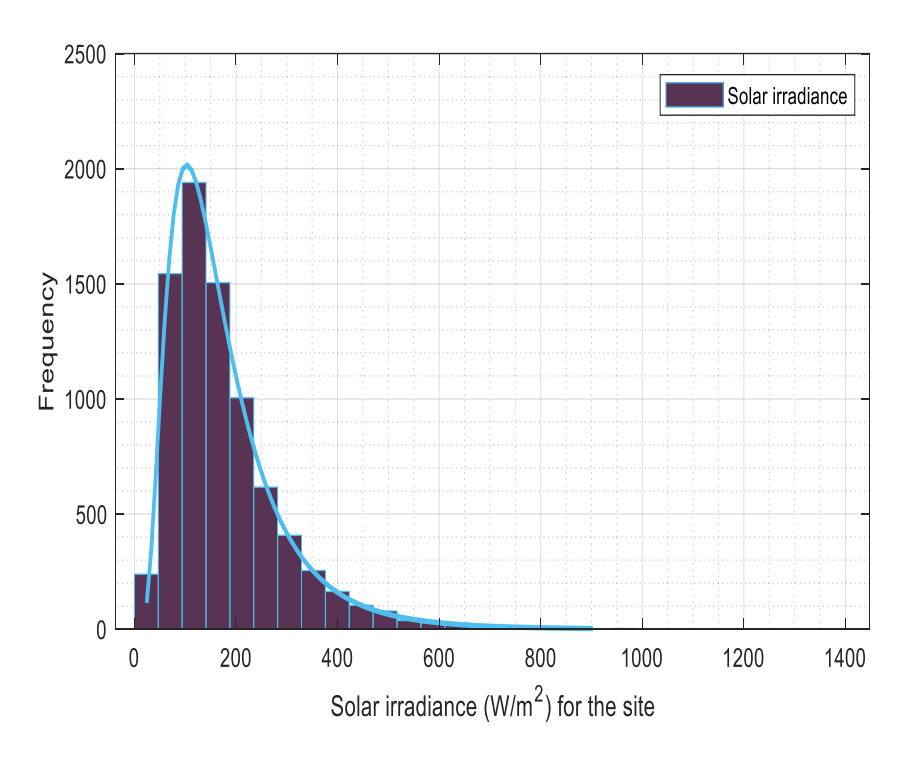


Figure 2-6: Solar Irradiance Frequency For The Site

2.5.2.1 Generated Power Modeling in Solar Power Plant

the process of converting solar irradiance into energy for photovoltaic plants can be expressed as follows [56]:

$$P_{s}(G) = \begin{cases} P_{sr}\left(\frac{G^{2}}{G_{std}R_{c}}\right) & \text{for } 0 \leq G \leq R_{c} \\ P_{sr}\left(\frac{G^{2}}{G_{std}}\right) & \text{for } G \geq R_{c} \end{cases}$$

$$(2.7)$$

Here, G_{std} represents the standard solar irradiance in standard environment, which is typically set at 1000 W/m^2 . The parameter R_c denotes a specific reference irradiance threshold, chosen as 120 W/m^2 in this study. These irradiance values are consistently applied to both solar PV plants connected to the system. Furthermore, P_{sr} refers to the rated output power of a single solar PV unit, corresponding to the maximum power it can produce under standard test conditions. These parameters play a key role in determining the actual power output of the solar units based on the real-time solar irradiance received, as discussed in subsequent modeling and simulation sections [57].

2.5.3 Hydropower Modeling Using Gumbel Probability Density Function

In hydrological studies, it is well established that river flow rates particularly annual maxima are best described by the Gumbel (Type I extreme value) distribution. Under this model, the probability density function (PDF) for a given flow rate Q_w is expressed in terms of a location parameter λ (which shifts the distribution along the flow axis) and a scale parameter γ (which determines its spread) [58], [59].

$$f_{Q}(Q_{w}) = \frac{1}{\gamma} \exp\left(\frac{Q_{w} - \lambda}{\gamma}\right) \exp\left[-\exp\left(\frac{Q_{w} - \lambda}{\gamma}\right)\right]$$
(2.8)

Figure 2-8 presents both the empirical frequency histogram of simulated flow-rate samples and the fitted Gumbel curve. These samples were generated via 8,000 Monte Carlo iterations, using the specific parameter values listed in table 6-2. The close alignment between the histogram and the theoretical PDF confirms that the Gumbel distribution effectively captures the extreme-value characteristics inherent in river flow data.

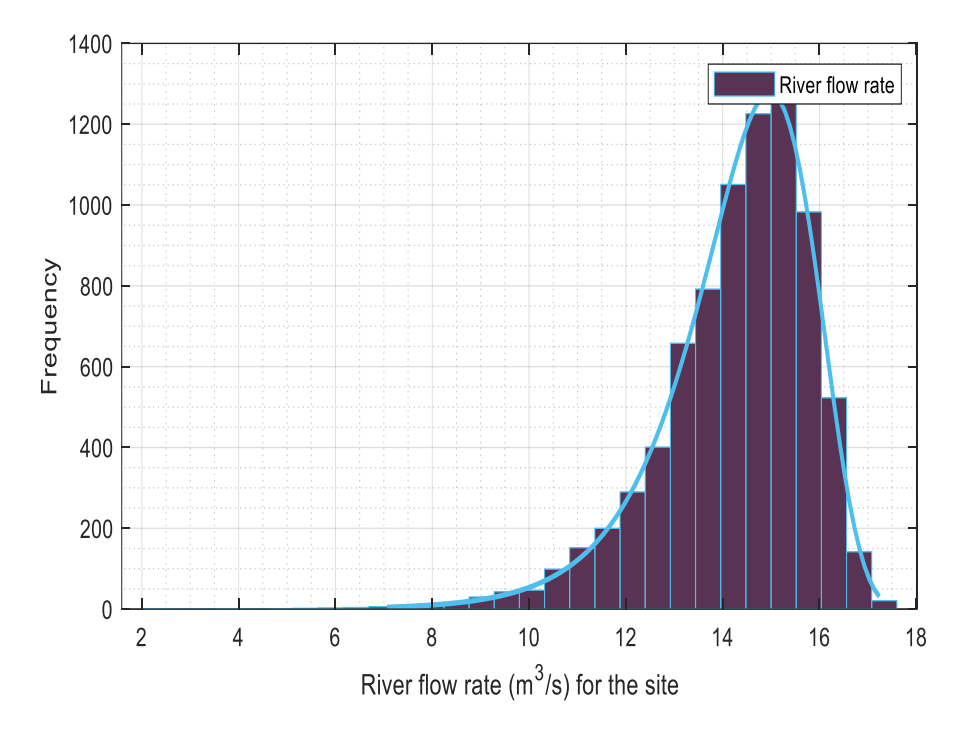


Figure 2-7: River Flow Frequency for the Site

2.5.3.1 Generated Power Modeling in Hydro Power Plant

In a small-hydro installation, the generated power depends on the water flow rate Q_w and the effective pressure head H_w . Mathematically, the output power P_H of the small-hydro unit can be expressed as [57]:

$$P_{H}(Q_{w}) = \eta \cdot \rho \cdot g \cdot Q_{w} \cdot H_{w} \tag{2.9}$$

In this expression, η denotes the efficiency of the turbine generator assembly, ρ is the water density, and g represents the acceleration due to gravity.in this research study based on ref for our calculations, we use the following parameter values:

- $\eta = 0.85$
- $\rho = 1000 \text{ kg/m}^3$
- $g = 9.81 \text{ m/s}^2$
- $H_w = 25 \text{ m}$

2.6 Cost Evaluation Based on Scenarios Outcomes

2.6.1 Cost generation for renewable sources:

One of the main challenges in integrating RES into the power grid is their intermittent and unpredictable nature. Typically, renewable energy installations like wind farms and solar PV farms are owned by private operators who enter into power purchase agreements with the grid or Independent System Operator (ISO) to deliver a specified amount of scheduled power. If these farms fail to generate the agreed-upon power due to the unavailability or insufficiency of renewable

resources, the ISO must compensate for the shortfall by maintaining spinning reserves, which increases overall power generation costs. This situation is referred to as an overestimation of renewable power. Conversely, there are instances when the actual power generated exceeds the scheduled amount an underestimation scenario. In such cases, the surplus power may go unused, and the ISO may incur penalty costs. Therefore, the total cost of renewable energy includes the direct cost of scheduled power, penalty costs for underestimation, and reserve costs for overestimation.

2.6.2 Direct Cost of RES Generators (DCost):

Wind, solar, and small hydropower generators operate without the need for fossil fuels. When these plants are owned by the Independent System Operator (ISO), a conventional cost function may not apply unless the ISO chooses to attribute a payback cost for the initial investment or includes it as part of maintenance and renewal expenses. However, when such plants are owned by private operators, the ISO must pay a price proportional to the scheduled power. The scheduled output, agreed upon by the ISO, is a fixed amount and is jointly delivered by the solar PV and small-hydro units. The output of the hydropower unit depends on the river flow rate, assuming a constant head under a run-of-river configuration. Since the capacity and variability of the small-hydro unit are usually minimal compared to the overall system load, it is typically operated at full capacity. Consequently, the available hydropower determined by river flow combined with the solar PV output forms the scheduled power supply [58].

2.6.2.1 Direct Cost of Wind Power Units

The Direct cost for the wind generator, referred to as $Dcost_{W,j}$, can be represented as follows [52]:

$$Dcost_{W,j}(WP_{Sc,j}) = g_j \times WP_{Sc,j}$$
(2.10)

Where g_j represent the direct cost coefficients associated with j-th wind power plant and WP_{Sc} denote the scheduled power from the corresponding wind power plants

2.6.2.2 Direct Cost of Solar Power Units:

Solar generator, referred to as $Dcost_{S,k}$ [60].

$$Dcost_{S,k}\left(SP_{S,k}\right) = h_k \times SP_{Sc,k} \tag{2.11}$$

 h_k represent the direct cost coefficients associated with associated with k-th solar power plant and SP_{sc} denote the scheduled power from the corresponding solar power plants

2.6.2.3 Direct Cost of Hydro Power Units:

The Direct cost of hydro power units referred to as $Dcost_{h,k}$, can be represented as follows [58]:

$$Dcost_{h,k}(hP_{Sh}) = H_i \times hP_{sc,i}$$
(2.12)

 H_i represent the direct cost coefficients associated with i-th hydro power plant and $P_{sc,i}$ denote the scheduled power from the corresponding hydro power plants

The mathematical expression for the DCost function of the combined solar-hydro generation plants is as follows [61]:

$$Dcost_{Sh,k}(ShP_{Sh}) = C(SP_{sc} + hP_{sc}) = h_k SP_{Sc,k} + H_i hP_{sc,i}$$
 (2.13)

2.6.3 Evaluation of Cost Uncertainties in RES Generators

In uncertain conditions, two scenarios can occur: when the actual power generated from wind or solar sources is less than the estimated amount, known as power overestimation, necessitating the use of spinning reserve resources to ensure an uninterrupted power supply. The expense associated with activating these reserve units to make up for the overestimated power is referred to as the reserve cost. For wind, solar PV, and solar-hydro generators, reserve cost is mathematically expressed as follows [62].

2.6.3.1 Uncertain Wind Power Cost Evaluation

As previously mentioned, due to the uncertain nature of wind energy, a wind farm may generate less power than the scheduled amount. In such cases, the Independent System Operator (ISO) must maintain adequate spinning reserves to meet the resulting demand. The cost associated with committing these reserve generating units to compensate for overestimated wind power is referred to as the reserve cost [63].

The reserve cost for a wind power plant is defined as [63]:

$$RCost_{W,j} \left(WP_{Sc,j} - WP_{Av,j} \right) = RK_{W,j} \left(WP_{Sc,j} - WP_{Av,j} \right)$$

$$= RK_{W,j} \int_{0}^{P_{WG,j}} \left(Wp_{Sc,j} - WP_{,j} \right) f_{W} \left(WP_{,j} \right) dp_{W,j}$$
(2.14)

where $RK_{W,j}$ is the penalty cost coefficient associated with *j*th wind power generator, $WP_{r,j}$ denotes the output power from the corresponding wind units, f_W is the wind power probability density function

In the case of underestimation, the actual output power from the wind farm exceeds the scheduled amount. If this surplus power cannot be utilized such as by reducing the output of conventional generators it is wasted. In such scenarios, the Independent System Operator (ISO) incurs a penalty cost for the unutilized energy.

The penalty cost for a wind power plant is given by [52]:

$$PC_{W,j} \left(WP_{Av,j} - WP_{S,j} \right) = PK_{W,j} \left(WP_{Av,j} - WP_{S,j} \right)$$

$$= PK_{W,j} \int_{WP_{S,j}}^{WP_{r,j}} \left(WP_{,j} - WP_{S,j} \right) f_{W} \left(WP_{,j} \right) dp_{W,j}$$
(2.15)

 $PC_{W,j}$ is the penalty cost coefficient for the wind power plant, WP_r is rated power output from the plant.

2.6.3.2 Uncertain Solar Photovoltaic Power Cost Evaluation

The cost evaluation approach for uncertain and intermittent solar PV power is fundamentally similar to that used for wind power. However, solar radiation is widely recognized to follow a lognormal probability distribution function (PDF). For mathematical convenience, the reserve and penalty cost models are developed based on the methodologies presented in [64].

The reserve cost associated with the overestimation of solar PV power is given by [64]:

$$\begin{split} &RCost_{RS,k}\left(SP_{Sc,k} - SP_{Av,k}\right) = RK_{S,k}\left(SP_{Sc,k} - SP_{Av,k}\right) \\ &= RK_{S,k} \times f_{S}\left(SP_{Av,k} < SP_{Sc,k}\right) \times \left[SP_{Sc,k} - E\left(SP_{Av,k} < SP_{S,k}\right)\right] \end{split} \tag{2.16}$$

 $RK_{S,k}$ is the reserve cost coefficient associated with the solar PV plant and $SP_{Av,k}$ is the actual available power from the plant , $f_S\Big(SP_{Av,k} < SP_{Sc,k}\Big)$ is the probability of occurrence of solar power shortage from the scheduled power $SP_{Sc,k}$, and $E\Big(SP_{Av,k} < SP_{S,k}\Big)$ represents the expectation of solar PV power below $SP_{Sc,k}$.

On contrary to overestimation, penalty cost for underestimation of solar PV power is [64]:

$$PC_{S,k}\left(SP_{A,k} - SP_{Sc,k}\right) = PK_{S,k}\left(SP_{Av,k} - SP_{Sc,k}\right)$$

$$= PK_{S,k} \times f_S\left(SP_{Av,k} > SP_{Sc,k}\right) \times \left[E\left(SP_{Av,k} > SP_{Sc,k}\right) - SP_{Sc,k}\right]$$
(2.17)

 $PK_{S,k}$ is the penalty cost coefficient for the solar PV plant, $f_S\left(SP_{Av,k} > SP_{Sc,k}\right)$ is the probability of solar power being excess of the scheduled power and $E\left(SP_{Av,k} > SP_{Sc,k}\right)$ is the expectation of solar PV power above $SP_{Sc,k}$.

2.6.3.3 Cost Evaluation of Uncertain Combined Solar Photovoltaic and Small-Hydro Power

Large hydropower plants, with their substantial reservoir capacities, are ideal sources for providing spinning reserves. However, in contrast, the capacity of small hydropower units is typically insignificant relative to total system generation and demand. As a result, the ISO may not consider their spinning reserve capacity meaningful. In practice, private operators of small hydropower plants often do not qualify for reserve or penalty payments.

In our case, the third-generation system consists of a combination of a solar PV unit and a small-hydro unit. The output of the small-hydro unit depends on river flow rate, which is commonly modeled using a Gumbel distribution [61].

The solar PV component is eligible for reserve and penalty payments. Since the small-hydro unit contributes only about 10–20% of the total power from the combined system, we treat reserve and penalty payments based on the total power output of the system [61].

The reserve cost for overestimation of the combined generation system power is:

$$RCost_{sh}(ShP_{sc} - ShP_{Av}) = RK_{SH,i}(ShP_{sc} - ShP_{Av})$$

$$= K_{RSH} * f_{SH}(ShP_{Av} < ShP_{sc}) * [P_{SHG} - E(ShP_{Av} < ShP_{sc})]$$
(2.18)

 $RK_{SH,i}$ is the reserve cost coefficient associated with ith combined solar hydro power plant ShP_{Av} represent the actual available power from the plant, $f_{SH}(ShP_{Av} < ShP_{sc})$ is The probability that the combined system delivers less power than the scheduled amount ShP_{sc} and the expectation of delivered power below ShP_{sc} is $E(ShP_{Av} < ShP_{sc})$.

The penalty cost associated with the underestimation of the combined generation system's power occurs when the actual available power is represented as follows:

$$PCost_{sh}(ShP_{Av} - ShP_{sc}) = PK_{SH}(ShP_{Av} - ShP_{sc})$$

= $PK_{SH} \times f_{SH}(ShP_{Av} > ShP_{sc}) \times [E(ShP_{Av} > ShP_{sc}) - ShP_{sc})]$ (2.19)

In this context PK_{SH} represent the penalty cost coefficient related to ith combined solar-hydro power plan. While $f_{SH}(ShP_{Av} > ShP_{sc})$ represents the likelihood of energy exceeding the scheduled power ShP_{sc} , while $E(ShP_{Av} > ShP_{sc})$ denotes the forecast of the combined system power surpassing (ShP_{sc}).

2.7 Conclusion

This chapter presented modeling of uncertainties in wind, solar, and hydro generation by fitting site-specific statistical distributions a Weibull distribution for wind speed variability, a lognormal PDF for solar irradiance fluctuations, and a Gumbel distribution to capture extreme hydro inflow events. We detailed the implementation of Monte Carlo simulation to propagate these uncertainties through system operation scenarios, highlighting sampling strategies and convergence assessment to ensure robust statistical characterization of renewable outputs. Cost evaluation was performed for direct generation costs and imbalance-related costs, including reserve procurement for under generation and penalty fees for over generation, based on scenario outcomes and cost coefficients reflective of different technologies. By linking probabilistic output distributions to economic impacts, this framework enables informed decision-making in renewable energy planning, supporting capacity expansion, scheduling, and risk mitigation; future enhancements could incorporate correlated sampling and variance-reduction techniques to further refine accuracy and computational efficiency.

Chapter 3: POWER SYSTEM AND POWER FLOW MODELING

3.1 Introduction

Reliable and economical operation of modern power systems requires accurate modeling and efficient optimization. As electrical networks become larger, more interconnected, and increasingly integrated with renewable resources, system operators face the challenge of ensuring both security and cost-effectiveness. Fundamental to this task are two key analyses: power flow (or load flow), which determines the steady-state voltages, angles, and line flows for a given operating condition, and (OPF), which extends this analysis by optimizing control variables to minimize costs or improve performance while respecting system limits.

The (OPF) is one of the most studied nonlinear optimization problems. The OPF goal is optimizing the production and transmission of electrical energy in distribution networks while considering system constraints and control limits. There is a wide diversity of OPF formulations and solution methods available. The nature of the OPF continues to change due to the modernization of electricity markets and the addition of renewable resources [65]. This chapter begins by introducing the fundamentals of power-flow analysis defining key state variables (bus voltages and angles) and control variables (generator real/reactive outputs, transformer tap settings). We then derive the AC OPF formulation via the Newton Raphson method, detailing how real and reactive power balance equations form the equality constraints, while generator capability curves, voltage limits, and line thermal ratings impose inequality constraints.

Next, we systematically classify decision variables and constraints into continuous, discrete, linear, and nonlinear categories, and demonstrate construction of typical objective functions:

- Fuel cost curves (quadratic or piecewise-linear)
- Loss minimization
- Emission cost fonctions
- Composite indices for voltage stability or security

We also review popular constraint-handling techniques, penalty functions, Lagrangian relaxation, interior-point methods, and mixed-integer programming for discrete controls. Finally, the chapter concludes with a concise summary of the general OPF formulation, setting the stage for the advanced metaheuristic and multi-objective solution methods developed in the subsequent chapters.

3.2 Power Flow Definition and Objectives

3.2.1 Definition of Power Flow

The power flow problem (load flow) study in an electrical network refers to the analysis and calculation of the variables of an electric network under normal balanced operation in steady state. These variables include node voltages, injected powers at nodes, and power flows in the lines. Losses and currents can be derived from these variables in a given network. So, in simpler language we can say It involves studying and analyzing the flow of electrical power from sources (the generation sources such as power plants) through the transmission and distribution networks to the numerous loads (consumers) linked to the system. The study of power flow involves calculating the voltage values within an electrical network for specified ends and given conditions at bus sets, from these

voltages, the active and reactive power flows in each line and transformer are calculated. The set of equations representing the electrical network is nonlinear in nature [66].

3.2.2 Objective

In practical applications, power flow calculation methods utilize the network configuration and the equipment properties to determine the complex voltage at each node. Additionally, these methods assume perfect symmetry between the three phases of the three-phase system in the electrical network by considering these factors, accurate assessments of voltage conditions within the network can be obtained.

Power flow studies are used for planning the construction and expansion of electrical networks, as well as for their operation and control the result of a power flow problem informs the operator or network planner about how the network lines are loaded, what the voltages are at different bus sets, how much generated power is lost, and where the limits are exceeded.

In power flow calculation, a bus bar is defined by four parameters which are classified are follows

3.2.3 Classification of Bus Bars According to Their Specifications

We can classify bus bars into three categories based on the specifications of the variables used.

For each bus bar, two variables need to be specified beforehand, and the other two variables are to be calculated.

• Reference bus bar (slack bus): It's a generator bus bar that can be classified based on two specified variables: the voltage magnitude (V) and the phase angle (δ). The power values (P and Q) at this bus bar are initially unknown and need to be determined through calculations.

To establish a reference point for voltage angles, the reference bus bar is selected from the generator bus bars with the highest active power. This reference bus bar serves as the benchmark for determining the voltage angles at other bus bars in the system.

- Load bus bar: This bus bar supplies a load characterized by its active power P and reactive power Q. Therefore, (P, Q) are specified, while (V, δ) are to be calculated.
- Generator bus bar: This bus bar is connected to a generator that delivers an active power P under a constant voltage V controlled by an Automatic Voltage Regulator (AVR). Therefore, (P, V) are specified, while (Q, δ) are to be calculated.

Table 3-1: Classification of bus bars according to their specifications

Types of bus bars	Known variables	Unknown variables
Reference bus bar (V δ)	V, δ	P, Q
Generator bus bar (PV)	P, V	Q, δ
Load bus bar (PQ)	P, Q	V,δ

3.2.4 Formulation of Power Flow Equations

The study of power flow involves calculating the voltages of the electrical network for specified endpoints and given conditions at the buses, such as capacitive or inductive loads that need to be supplied, generated powers, and voltage magnitudes at all buses. From these values, the currents in the transmission lines, power flows, and power losses can be obtained. The nodal currant and voltage equations of an electrical network with N buses are written in the following matrix form:

$$\begin{bmatrix} I_1 \\ I_2 \\ \vdots \\ I_N \end{bmatrix} = \begin{bmatrix} Y_{11} & Y_{12} & \cdots & Y_{1N} \\ Y_{21} & Y_{22} & \cdots & Y_{2N} \\ \vdots & \vdots & \ddots & \vdots \\ Y_{N1} & Y_{N1} & \cdots & Y_{NN} \end{bmatrix} * \begin{bmatrix} V_1 \\ V_2 \\ \vdots \\ V_N \end{bmatrix}$$
(3.1)

Where:

$$I_{BUS} = Y_{BUS} * V_{BUS} \tag{3.1}$$

 $I_{BUS} = [I_1, I_2, ... I_N]^T$: The vector of currents injected into each bus bar represents the external source currents. The current flowing from bus bar i to bus bar j is considered positive, while the current flowing in the opposite direction is considered negative.

 $V_{BUS} = [V_1, V_2, ... V_N]^T$: The vector of complex voltages at each bus bar and Y_BUS represents the nodal admittance matrix of the system, which has a size of (N * N), where N is the number of bus bars in the system.

 Y_{ii} : The diagonal element of the admittance matrix represents the sum of all the components connected to that particular bus bar. This can be expressed mathematically by the following equation:

$$Y_{ii} = \sum_{\substack{i=0 \ i \neq k}}^{N} y_{ik} \tag{3.2}$$

 y_{ik} : The off-diagonal element i, k of the admittance matrix represents the negative sum of all the components connected between bus bar i and bus bar j. In other words, it can be expressed as follow:

$$Y_{ik} = -\sum_{k \neq i} y_{ik} \tag{3.3}$$

According to equation (1.1), the net injected current at bus bar i can be expressed as follows:

$$I_1 = \sum_{k=1}^{N} Y_{ik} * V_k \ i = 1, 2 \dots, N$$
 (3.4)

Where:

$$\bar{Y}_{ik} = G_{ik} + j * B_{ik} = Y_{IK}(\cos\delta_{ik} + j\sin\delta_{ik})$$
(3.5)

$$\bar{V}_k = R_{Ek} + j * Im_k = V_K(cos\delta_k + jsin\delta_k)$$
(3.6)

 G_{ik} , B_{ik} are respectively the conductance and susceptance of \bar{Y}_{ik} ; R_{Ek} and Im_k are respectively the real and imaginary parts of \bar{V}_k ; δ_k is the phase of the voltage at the busbar k;

 δ_{ik} : the phase of the element ik;

The expression of the injected apparent power \bar{S}_i at a busbar can be written as follows:

$$S_i^* = P_i - jQ_i = V_i^* * \sum_{k=1}^N \bar{Y}_{ik} * \bar{V}_k$$
 (3.7)

 \bar{P}_i, \bar{Q}_i : where \bar{P}_i and \bar{Q}_i are the active and reactive powers at busbar i. By substituting equations (3.5) and (3.6) into equation (3.7), we obtain:

$$P_{i} = \sum_{k=1}^{N} V_{i} V_{k} Y_{ik} \cos(\delta_{ik} + \delta_{k} - \delta_{i}) \quad i = 1, 2, ..., N$$
(3.8)

$$Q_{i} = \sum_{k=1}^{N} V_{i} V_{k} Y_{ik} \sin(\delta_{ik} + \delta_{k} - \delta_{i}) \quad i = 1, 2, ..., N$$
(3.9)

The equations (1.9) and (1.10) represent the power flow equations as follows:

$$P_i = P_{Gi} - P_{Di} \tag{3.10}$$

$$Q_i = Q_{Gi} - Q_{Di} \tag{3.11}$$

Where P_{Gi} , Q_{Gi} are the active and reactive powers generated, respectively.

 P_{Di} , Q_{Di} are the active and reactive powers demanded at the bus i, respectively.

3.2.5 Power Flow Problem Solution Methods

Generally, the method used to solve this problem is Newton-Raphson due to its fast convergence and reduced number of iterations compared to other methods (such as Gauss-Seidel). The Taylor series expansion is given by:

$$\begin{bmatrix} \Delta P \\ \Delta Q \end{bmatrix} = J * \begin{bmatrix} \Delta \delta \\ \Delta Q \end{bmatrix} \Rightarrow \begin{bmatrix} \Delta P \\ \Delta Q \end{bmatrix} = \begin{bmatrix} J_1 & J_2 \\ J_3 & J_4 \end{bmatrix} * \begin{bmatrix} \Delta \delta \\ \Delta V \end{bmatrix}$$
(3.12)

$$J_1 = \frac{\partial P_i}{\partial \delta_K}, J_2 = \frac{\partial P_i}{\partial V_K}, J_3 = \frac{\partial Q_i}{\partial \delta_K}, J_4 = \frac{\partial V_i}{\partial V_K}$$
(3.13)

Where: ΔP and ΔQ represent the differences between the specified and calculated active powers, and the differences between the specified and calculated reactive powers.

 $\Delta\theta$ and Δv represent the differences between the specified and calculated angles, and the differences between the specified and calculated voltages; J is the Jacobian matrix.

$$\Delta P_i = P_i^{sp\acute{e}} - P_i^{cal} \tag{3.14}$$

$$\Delta Q_i = Q_i^{sp\acute{e}} - Q_i^{cal} \tag{3.15}$$

For a network with N buses, with NG generator buses, there are 2(N - 1) - NG equations to solve. Consequently, there are (N - 1) equations for active power and (N - 1 - NG) equations for reactive power, resulting in a Jacobian matrix of size $(2N - 2 - NG) \times (2N - 2 - NG)$ elements.

The calculation of the Jacobian matrix elements is done as follows:

The diagonal and off-diagonal elements of J1 are:

$$\frac{\partial P_i}{\partial \delta_i} = \sum_{k \neq 1} |V_k| |Y_{ik}| |V_i| \sin(\delta_{ik} + \delta_k - \delta_i)$$
(3.16)

$$\frac{\partial P_i}{\partial \delta_k} = -|V_k||Y_{ik}||V_i|\sin(\delta_{ik} + \delta_k - \delta_i) \quad K \neq i$$
(3.17)

The diagonal and off-diagonal elements of J2 are:

$$\frac{\partial P_i}{\partial V_i} = 2|Y_{ii}||V_i|\cos(\delta_{ii}) + \sum_{k \neq 1}|V_k||Y_{ik}||V_i|\cos(\delta_{ik} + \delta_k - \delta_i)$$
(3.18)

$$\frac{\partial P_i}{\partial V_i} = |V_{ij}| |V_i| \cos(\delta_{ik} + \delta_k - \delta_i) \quad K \neq i$$
(3.19)

The diagonal and off-diagonal elements of J3 are:

$$\frac{\partial Q_i}{\partial \delta_i} = \sum_{k \neq 1} |V_k| |Y_{ik}| |V_i| \cos(\delta_{ik} + \delta_k - \delta_i)$$
(3.20)

$$\frac{\partial Q_i}{\partial V_i} = -2|Y_{ii}||V_i|\sin(\delta_{ii}) + \sum_{k \neq 1}|V_k||Y_{ik}||V_i|\sin(\delta_{ik} + \delta_k - \delta_i)$$
(3.21)

The diagonal and off-diagonal elements of J4 are:

$$\frac{\partial Q_i}{\partial V_i} = -2|Y_{ii}||V_i|\sin(\delta_{ii}) + \sum_{k \neq 1}|V_k||Y_{ik}||V_i|\sin(\delta_{ik} + \delta_k - \delta_i)$$
(3.22)

$$\frac{\partial Q_i}{\partial V_k} = -|V_k||V_i|\sin(\delta_{ik} + \delta_k - \delta_i) \quad K \neq i$$
(3.23)

3.3 Optimal Power Flow

Optimal Power Flow is a mathematical optimization problem in the field of electrical power systems, it is widely regarded as a fundamental tool in this field and has been the subject of wide research since it was introduced by Carpentier in 1962. The objective of the OPF problem is to identify the optimal settings for a given power system network in order to optimize a specific objective function, while satisfying the power flow equations, system security, and operational limits of equipment. This involves manipulating various control variables, including generator real power outputs, voltages, transformer tap settings, phase shifters, switched capacitors, and reactors, to achieve an optimal network configuration based on the defined problem formulation. Moreover, OPF can offer valuable support to operators in addressing various challenges encountered in the planning, operation, and control of power networks [67].

The primary objective of OPF is to minimize a cost function or maximize a performance index while ensuring that the power system operates within specified limits. The performance index can be related to efficiency, voltage stability, system reliability, or any other desired system performance parameter. The most utilized objective function in OPF is the minimization of overall fuel cost. However, other traditional objectives such as minimizing active power loss, bus voltage deviation, emissions from generating units, the number of control actions required, and load shedding. With the deregulation of the electric power industry. One of the major challenges in the OPF problem lies in

the nature of the control variables, as some are continuous (such as real power outputs and voltages), while others are discrete (such as transformer tap settings, phase shifters, and reactive injections) [67].

The application domains of OPF can be classified as follows

- Minimization of fuel cost.
- Minimization of losses.
- Improvement of voltage profile and stability.
- Maximization of power transfer capability

3.3.1 Problem Formulation Optimal Power Flow Model

The main objective in solving OPF problems is to identify the optimal values for control variables, which involves minimizing a specific objective function while adhering to all physical and security constraints. Mathematically, the OPF problem can be expressed as follows:

$$Minimize f(x, u) (3.24)$$

Subject to:

$$G(x, u) = 0 \tag{3.25}$$

$$h(x, u) \le 0 \tag{3.26}$$

Where:

F(x,u) presents the objective function;

x represents the state variables vector of a power system network;

u represents the control variables vector;

g(x,u) represents the equality constraints;

h(x,u) represents inequality constraints, where, h_{max} and h_{min} are the upper and lower boundary limits

3.3.2 Optimal Power Flow Variables Classification

In optimization problems, two main types of variables are considered: independent variables, also known as control or decision variables, and dependent variables, also known as state variables. The optimization process involves first determining the optimal values for the control variables and then calculating the corresponding values for the state variables based on those optimal control values.

In the OPF problem, control variables may include:

• Active power generation of all generator buses except slack bus;

- Voltage of all generator buses;
- Tap setting of all transformers;
- Reactive power injection of shunt capacitor banks;
- Moreover, state variables may also include;
- Active power output of the slack bus;
- Load bus voltages;
- Reactive power generated from generators;
- Transmission line loadings;

It is important to note that the number of control variables determines the dimensionality of the solution space. In other words, a problem with n control variables will result in an n-dimensional solution space [68].

3.3.3 Constraints Formulation

OPF Constraints in the OPF problem are typically classified into two types: equality constraints and inequality constraints. These conditions define the feasible region of the problem, and any solution must fall within this region in order to satisfy all the constraints.

3.3.3.1.1 Equality Constraints

The equality constraints in load flow analysis are derived from the physical laws that govern the behavior of an electrical network. These constraints are expressed as nonlinear equations in the power flow equations, which ensure that the net injection of active and reactive powers at each bus is equal to zero.

$$\begin{cases} P_{Gi} - P_{di} - V_i \sum_{j=1}^{NB} V_j \Big[G_{ij} \cos(\delta_{ij}) + B_{ij} \sin(\delta_{ij}) \Big] = 0 \\ Q_{Gi} - Q_{di} - V_i \sum_{j=1}^{NB} V_j \Big[G_{ij} \sin(\delta_{ij}) - B_{ij} \cos(\delta_{ij}) \Big] = 0 \end{cases}$$
(3.27)

Where:

NB is the total number of busses of the power system;

 P_{Gi} is the active power of generation;

 Q_{Gi} is the reactive power of generation;

 P_{di} is the active power of demand;

 Q_{di} is the reactive power of demand;

 G_{ij} the conductance of the corresponding lines between the (i, j) buses;

 B_{ii} the susceptance of the corresponding lines between the (i, j) buses.

3.3.3.1.2 Inequality Constraints

In the context of the OPF problem, inequality constraints typically impose limitations on various physical components in the electrical system. These components can include generators, tap-changing transformers, and phase-shifting transformers. Additionally, system security requirements and reactive power compensation limits contribute to the set of inequality constraints. Specifically, when considering generators, these constraints are concerned with maintaining active and reactive power levels within acceptable boundaries.

$$P_{Gi}^{min} \le P_{Gi} \le P_{Gi}^{max} \tag{3.28}$$

$$Q_{Gi}^{min} \le Q_{Gi} \le Q_{Gi}^{max} \tag{3.29}$$

The inequality constraints for load tap-changing transformers involve maximum and minimum tap positions, which determine the voltage level relative to the nominal voltage. These constraints are utilized to adjust voltage magnitudes and regulate reactive power flows. On the other hand, phase-shifting transformers have maximum and minimum phase angle shifts to control voltage phases and regulate active power flows. These specific constraints are considered for both types of transformers.

$$T_{ik}^{min} \le T_{ik} \le T_{ik}^{max} \tag{3.30}$$

$$\alpha_{ik}^{min} \le \alpha_{ik} \le \alpha_{ik}^{max} \tag{3.31}$$

Reactive power compensators such as Batteries, reactors, etc. have limits defined by minimum and maximum values, which determine their operating range. These limits ensure that the devices operate within acceptable bounds and can effectively compensate for reactive power in the system.

$$Q_{Ci}^{min} \le Q_{Ci} \le Q_{Ci}^{max} \tag{3.32}$$

Bounds on the apparent power flow in power transformers and transmission lines are set to uphold network security and avoid issues such as instability or thermal losses in conductors. These limits ensure that the power flow in these components remains within safe operating conditions, avoiding excessive heating and potential damage to the system.

$$|S_{ik}|^2 \le |S_{ik}^{max}|^2 \tag{3.33}$$

To preserve the quality of system security and electrical service, it is essential to limit violations on voltage constraints, which must remain within their tolerable limits.

$$V_i^{min} \le V_i \le V_i^{max} \tag{3.34}$$

3.3.4 Constraint Handling (CH) Methods

Constraint handling is a crucial aspect of meta-heuristic optimization algorithms, especially for solving constrained engineering problems such as (OPF) and Optimal Reactive Power Dispatch (ORPD). Numerous techniques have been developed, which can generally be classified into the following six categories

- 1) **Preserving Feasible Solution Method**: The key concept of this approach is to place the solutions into feasible research-space and keeping within by updating process that produces only feasible ones [69].
- 2) Penalty Function Method: In this technique a penalty terms is added to the objective function once any constraint violation happens [70].
- 3) Rejection of Infeasible Solutions: Also called death penalty, in which rejects any infeasible solution as soon as they are generated. In addition, it has an efficient computational, because with any violate solution, it is assigned a fitness of zero [69].
- 4) Superiority of Feasible Solutions Method: This approach is based on the assumption of the superiority of feasible points over infeasible ones [52].
- **5) Stochastic Ranking Method**: first introduced by Runarsson and *Yao* in 2000: In this technique a control factor Pf (0 < P < 1) is predefined by the user to check a balance between objective optimization value (feasibility) and whole of constraint violation (infeasibility points). The process is to determine whether the objective function value or the all constraint violation is used to rank a solution. The ranking process is performed as follow:

If both solutions are feasible or rand < Pf, rank is performed only on the objective value. Otherwise, rank is conducted on the constraint violations only [71].

Since the selecting of the suitable constraint handling method is highly depending on the problem's nature. The problem formulation treating in this dissertation confirm that both of penalty function (PF) method and superiority of feasible solutions (SF) method are more appropriate than other ones. In other words, due to their relative success and the most commonly used ones in the power system optimization. To this context, we give more detail of these methods, and how to handling with different formulation of OPF and ORPD problems in guarantying the feasibility of solutions.

3.3.4.1 Penalty Function Method (PF)

Penalty function method is the simplest and oldest handling technique which transform a constrained problem into an unconstrained one throughout discarding infeasible solutions during the search process even after sufficient number of feasible solutions. Also known as static penalty function method, values of the penalty factors are chosen by trial and error process. Because this method requires proper adjustment of the penalty factors, a small penalty factors over-explores the infeasible region, thus delaying the process of finding feasible solutions, and may prematurely converge to an infeasible solution. On the other hand, large penalty factors may not explore the infeasible region properly, thereby resulting in premature convergence. For this reason, it is preferable to choose the trial to start with the small values of factors until the suitable coefficients will be properly selected that ensure at the same time the convergence rate with feasibility of solution [71].

Among different formulations of the penalty method, the Powell-Skolnik method where incorporates all the constraints with feasibility:

$$\rho(x) = \begin{cases} 1 + \mu \left[\sum_{j=1}^{N} \max\{0, h_i(x)\} + \sum_{i=1}^{M} |g_i(x)| \right] & \text{if not feasible} \\ f(x) & \text{if feasible} \end{cases}$$
(3.35)

Where the constant $\mu > 0$ is fixed, so this approach is a static penalty method.

The penalty-based method transforms the objective function f(x) to a modified objective function F_m in the following from,

$$F_{\rm m}(x) = f(x) [\text{objective}] + P(x) [\text{Penalty}]$$
 (3.36)

Where the penalty term P(x) may take different forms, depending on the actual ways or variants of constraint handling techniques. For instance,

$$P(x) = \sum_{i=1}^{M} \mu_{i} g_{i}^{2}(x) + \sum_{i=1}^{N} k_{j} \max\{0, h_{i}(x)\}^{2}$$
(3.37)

Where $\mu_i > 0$ and $k_i > 0$ are penalty factors. In order to avoid too many penalty factors, a single penalty constant $\lambda > 0$ can be used as follows:

$$P(x) = \lambda \left[\sum_{i=1}^{M} g_i^2(x) + \sum_{j=1}^{N} \max\{0, h_i(x)\}^2 \right]$$
 (3.38)

Where λ is fixed factor, independent of iteration t, this basic form of penalty is the well-known static penalty method. Some studies show that it may be beneficial to vary λ over the course of iterations,

$$\lambda = (\alpha t)^{\beta} \tag{3.39}$$

Where $\alpha = 0.5$ and $\beta = 1.2$

In short, there are other forms of penalty approaches such as adaptive penalty and death penalty.

3.4 Objective Function

In OPF, the objective function signifies the objective or target to be reached when optimizing the operation of a power system. The objective function is usually defined mathematically and measures the system's performance or cost.

Typically, the most commonly utilized objective in the OPF problem formulation is the minimization of the overall cost associated with the active power generation from real energy production units. The cost of each production unit is assumed to be solely dependent on the active power generated and is represented by quadratic curves. Consequently, the total objective function of the electrical system can be expressed as the sum of the quadratic cost models for all generators involved. By minimizing this objective function, the OPF algorithm aims to optimize the operation of the system by determining the optimal values for the control variables that minimize the total generation cost.

Minimise

$$F = \sum_{i=1}^{NG} f_i = \sum_{i=1}^{NG} a_i P^2 + b_i P_i + c_i \quad (\$/h)$$
(3.46)

Or

$$P_{Gi\,min} \le P_{Gi} \le P_{Gi\,max} \tag{3.46}$$

$$P_{Gi} = P_{Di} + P_{Li} (3.47)$$

Where ai, bi, ci signify the cost coefficients of the i-th generation unit, and PDi, PLi are the demanded power and the active transport losses, respectively.

3.4.1 Classical Methods Applied to The Optimal Power Flow Problem

There are several classical optimization techniques that have been applied to solve (OPF) problems. Here are six categories of these techniques, along with a brief description of each and their application statistics:

- **Newton's Method**: in general, these are nonlinear equations that need to be solved using iterative methods. The Newton method is particularly preferred because of its quadratic convergence properties [73].
- **Linear Programming**; Linear programming is a mathematical optimization technique used to solve problems that involve linear constraints and an objective function. In this method, both the objective function and constraints are represented as linear equations or inequalities, and the variables are required to be non-negative [74].
- Quadratic Programming; Quadratic programming is a specific type of nonlinear programming where the objective function is quadratic, and the constraints are either linear or linearized [74].
- Nonlinear Programming: Nonlinear programming (NLP) is a branch of optimization that focuses on solving problems with nonlinear objective functions and constraints. In NLP, the constraints can be either from equalities or inequalities or both. The inequality constraints can be bounded, meaning they have specified upper and lower limits. This allows for more flexibility in defining the feasible region and finding optimal solutions [75].
- Interior Point Method: The interior point method, which has recently been rediscovered, offers a faster and potentially superior alternative to the conventional simplex algorithm for solving linear programming problems. Furthermore, this method has been extended to tackle nonlinear programming (NLP) and quadratic programming (QP) problems, showing remarkable qualities and yielding promising results. By introducing nonnegative slack variables, the interior point methods transform inequality constraints into equalities. A logarithmic barrier function, incorporating the slack variables, is subsequently added to the objective function, multiplied by the barrier parameter. Throughout the solution process, this parameter is gradually reduced to zero, ensuring convergence within the feasible region [75].

Limitations of Classical Methods

Addressing optimization problems using classical or traditional techniques can be challenging due to various factors depending on the nature of the problem. Difficulties arise when dealing with problems that have multiple local optima, involve discontinuities, exhibit changes in optimal

solutions over time, or have constraints within the search space. Additionally, classical search techniques often struggle with problems that have large and complex exploration or search spaces, limiting their ability to thoroughly explore all potential solutions. Large-scale problems may be computationally expensive to solve using classical methods.

Overall, these limitations highlight the need for alternative approaches, such as metaheuristic optimization methods, in complex optimization scenarios. These methods will be discussed in the second chapter of this thesis.

3.5 Conclusion

This chapter has developed a comprehensive framework for modeling power systems and solving the Optimal Power Flow (OPF) problem using classical methods. We began by formulating the nonlinear power flow equations that govern real and reactive power balances across buses, emphasizing their role as equality constraints in OPF formulations. Classical solution techniques were then reviewed, ranging from early gradient and Newton–Raphson approaches to modern interior-point algorithms. Key OPF objectives including generation cost minimization, loss reduction, and voltage profile improvement were shown to influence the choice of optimization algorithms and impact practical dispatch decisions. The chapter also detailed the structure of equality constraints (power balance and network equations) and inequality constraints (generator output limits, bus voltage bounds, and line flow ratings), and surveyed traditional constraint-handling methods that enforce feasibility while ensuring efficient convergence. However, due to the inherent limitations of these classical methods, more advanced optimization techniques are needed to address increasing system complexity and uncertainty topics that will be explored in the next chapter.

Chapter 4: METAHEURISTIC OPTIMIZATION TECHNIQUES

4.1 Introduction

Metaheuristic optimization algorithms are high level strategies designed to find near optimal solutions for hard (often NP-hard) problems where classic methods fail, by balancing global exploration and local exploitation across a search space. These methods draw inspiration from diverse sources biological evolution, collective animal behavior, physical laws, and human social processes and can be grouped accordingly into four main classes: evolutionary, swarm-intelligence, physics-based, and human-related techniques. Each class differs in its metaphor (what real-world process it mimics), its algorithmic operators (e.g. genetic crossover vs. velocity update), and its typical balance of exploration vs. exploitation [76]. Metaheuristic algorithms are general-purpose, problem-independent strategies for finding high-quality solutions to complex optimization problems, especially those with nonlinear, multimodal, or combinatorial search spaces that defeat exact methods. They operate as "black-box" optimizers: they do not require gradient information or problem convexity, and can handle discrete, continuous, noisy, or dynamic objective functions. Two central principles guide their design [77].

Exploration: Exploration refers to the capability of a metaheuristic algorithm to investigate broadly across diverse and unvisited regions of the solution space, thereby reducing the chance of becoming trapped in local optima and increasing the likelihood of finding the global optimum. By generating varied candidate solutions and sampling uncharted areas, exploration mechanisms maintain population diversity and ensure the algorithm does not prematurely converge on suboptimal regions. Techniques such as random perturbations, large neighborhood jumps, and high-temperature acceptance in Simulated Annealing enable metaheuristics to escape local traps and discover promising basins in multimodal landscapes. In population-based methods like Genetic Algorithms, exploration is further enhanced through elevated mutation rates and diverse crossover operations, which introduce new genetic material and facilitate sampling of previously unexplored search-space regions. Effective exploration strategies are particularly critical in high-dimensional or noisy problem domains, where the search landscape contains numerous peaks and valleys, as they significantly improve the algorithm's ability to locate the true global optimum [76].

Exploitation: Exploitation emphasizes the intensification of the search around high-quality solutions to refine and improve them through local search operations, thereby accelerating convergence toward optima. This process focuses computational effort on the neighborhoods of promising solutions by performing small, directed moves such as greedy improvement steps or tabu-guided exchanges to fine-tune solution quality. In Particle Swarm Optimization, for example, exploitation is realized by biasing particle velocities toward their personal-best and the global-best positions, causing the swarm to sample more intensively in regions that have already demonstrated superior performance. Trajectory-based metaheuristics like Iterated Local Search and Tabu Search explicitly exploit local neighborhoods via systematic descent heuristics or memory-based forbidding of recent moves to climb toward local optima. However, excessive exploitation characterized by overly small perturbations can limit exploration and increase the risk of premature convergence to suboptimal basins if diversity mechanisms are not maintained [76].

4.2 Classification of Metaheuristic Algorithms

A common taxonomy divides metaheuristics into four main families based on their source of inspiration and operational paradigm:

Evolutionary Techniques: draw on biological evolution, typically population-based with operators like crossover and mutation.

Swarm Intelligence Techniques: model collective behaviors of decentralized agents (e.g., ant colonies, bird flocks).

Physics-based Techniques: mimic natural physical processes (e.g., annealing, gravity, electromagnetism).

Human-related Techniques: simulate social, cognitive, or organizational behaviors (e.g., teaching, brainstorming).

4.2.1 Evolutionary Techniques:

Evolutionary algorithms (EAs) simulate the principles of biological evolution notably selection, crossover (recombination), mutation, and survival of the fittest to iteratively improve a population of candidate solutions toward better fitness levels. These methods are inherently population-based and derivative-free, making no assumptions about continuity or differentiability in the underlying objective function. Their generality and applicability make them robust across diverse optimization challenges, ranging from engineering design to scheduling and power system optimization. One comprehensive review covering these characteristics including algorithm classes, operators, exploration–exploitation balance, and problem applicability is provided by Eiben & Smith in their foundational text on evolutionary computing [78].

Mechanisms:

Evolutionary techniques follow a generational cycle comprising six main steps:

- 1. **Initialization:** A population of candidate solutions is randomly generated to uniformly sample the search space's diverse regions.
- 2. **Evaluation:** Each individual's fitness is computed by assessing the objective function, providing a scalar measure of solution quality.
- 3. **Selection:** Candidates are probabilistically chosen as parents based on fitness higher-fitness individuals have a greater chance to reproduce thereby enforcing survival of the fittest.
- 4. **Crossover (Recombination):** Pairs of parents exchange segments of their encoding to create offspring, combining successful traits from both and pro moting exploration of new regions.
- 5. **Mutation:** Random perturbations are applied to offspring to introduce novel genetic material and maintain population diversity, guarding against stagnation.
- 6. **Replacement:** A new generation is formed by selecting among parents and offspring often retaining elite individuals to balance retention of good solutions with introduction of new ones.

Genetic Algorithms (GAs):

Genetic Algorithms (GAs) encode candidate solutions as fixed-length strings typically binary vectors or real-valued arrays and iteratively evolve them using biologically inspired operators. In each generation, a population's fitness is evaluated, parents are probabilistically selected based on fitness, and offspring are generated through crossover (one-point, two-point, uniform) and mutation (bit-flipping or real-value perturbations). Elitism preserves the best individuals directly into the next generation, ensuring no loss of high-quality solutions. GAs are derivative-free, require no continuity or differentiability assumptions, and can seamlessly handle discrete, continuous, and mixed-integer problems. A comprehensive review detailing genetic operators, population dynamics, exploration-exploitation balance, and inheritance mechanisms is available in ref [79].

4.2.2 Swarm-intelligence (SI):

Swarm-intelligence algorithms are population-based metaheuristics inspired by the collective behavior of social organisms ants, bees, birds that self-organize through local interactions to perform tasks beyond the capability of any individual agent. They rely on simple behavioral rules at the agent level such as movement, sensing, and updating internal states and on indirect or direct communication stigmergy or information sharing to produce coherent, intelligent global search patterns without any central coordinator. Core emergent properties include robustness (tolerance to agent failures), adaptability (response to dynamic landscapes), and scalability (performance with increasing agent numbers), which together enable SI methods to maintain diversity and avoid premature convergence in complex, multimodal search spaces [80].

Mechanisms

Three fundamental mechanisms drive SI search dynamics:

- 1. **Decentralized control**: each agent follows local rules without a global leader, enabling parallel exploration and fault tolerance.
- 2. **Indirect communication:** agents modify shared environmental markers (e.g., pheromone trails) that influence subsequent agent behaviors, creating positive and negative feedback loops to balance intensification and diversification.
- 3. **Iterative adjustment:** agents iteratively update their positions or solution components based on personal experience (memory of past successes) and communal information (global or neighborhood best), which dynamically steers the swarm toward high-fitness regions while still exploring new areas.

Particle Swarm Optimization (PSO)

Particle Swarm Optimization (PSO) represents candidate solutions as particles moving through the search space. Each particle's velocity is adjusted based on its personal best position (pbest) and the global best position (gbest) discovered by the swarm. This mechanism effectively blends individual learning with social influence, enabling PSO to converge toward optimal regions without relying on gradient information or continuity assumptions [81].

4.2.3 Physics-Based Techniques

Physics-based metaheuristics translate optimization variables into physical quantities and leverage well-understood natural laws such as thermodynamics, gravity, and electromagnetism to drive search dynamics toward minima or equilibria. By modeling solution candidates as particles, masses, or charges, these algorithms exploit analogues of energy minimization or force interactions to balance global exploration and local exploitation. Some operate on a single trajectory (e.g., Simulated Annealing), while others maintain a population of interacting agents (e.g., Gravitational Search), but all share the principle of mapping problem structure onto physical processes to guide search adaptively [82].

Core Principles

- 1. **Physical Mapping:** Each solution is encoded as a physical entity (e.g., a particle with mass or charge), and its "fitness" determines a corresponding physical property (mass magnitude, energy level, temperature).
- 2. **Interaction Laws:** Agents interact according to laws such as Newton's law of gravitation or Coulomb's law of electrostatics, inducing movements that bias the search toward high-fitness regions while still permitting exploration via weaker forces or thermal fluctuations.
- 3. **Control Schedules:** Parameters analogous to temperature schedules or force attenuation functions govern the transition from exploration (high energy/weak forces) to exploitation (low energy/strong forces), ensuring convergence properties can be tuned or guaranteed under certain conditions.

Gravitational Search Algorithm (GSA)

In GSA, each agent is assigned a "mass" proportional to its fitness; masses attract one another via a gravitational constant, so that heavier (better) masses exert stronger pull, guiding lighter agents toward promising regions. Over time, the gravitational constant is decreased to shift focus from exploration to exploitation [83].

4.2.4 Human-related Techniques

Human-related metaheuristics emulate social interactions, cognitive behaviors, and organizational processes to generate and refine solutions. They may be population-based (teams, crowds) or hybrid, integrating human-inspired operators with classical heuristics [84].

Mechanisms:

Idea exchange: Pooling and recombining individual insights (e.g., brainstorming, teaching).

Role-based interaction: Teachers and students (TLBO), leaders and followers (MLO).

Game-theoretic dynamics: Competition (War Strategy Optimization) or cooperation (Teamwork Optimization).

Learning and adaptation: Individuals improve via practice (Skill Optimization Algorithm) or advice (Mother Optimization Algorithm).

Teaching-Learning-Based Optimization (TLBO)

Teaching-Learning-Based Optimization frames the search process as a classroom where the "teacher" (the current best solution) guides the entire population of "learners" toward improved performance by shifting the mean solution vector, while subsequent peer-to-peer interactions among learners foster further refinement and diversity in the search space. This dual-phase mechanism teacher phase for global intensification and learner phase for local exploration eliminates algorithm-specific parameters and leverages simple yet effective knowledge transfer to achieve rapid convergence without extensive tuning [85].

4.2.5 Differences Between Classes:

Source of Inspiration: biological evolution vs. social swarms vs. physical laws vs. human behaviors.

Population Structure: evolutionary and swarm algorithms are strictly population-based; physics-based may be single-solution (SA) or multi-agent (GSA); human-related can blend both paradigms.

Operators: evolutionary methods use genetic operators; swarm intelligence uses movement and pheromone rules; physics-based use energy/force dynamics; human-related use interaction and learning metaphors.

Exploration vs. Exploitation: physics-based often rely on temperature or force schedules, evolutionary on diversity maintenance, swarm on social learning, and human-related on role transitions and knowledge sharing.

Table 4-1: Metaheuristic Algorithms Classification

Aspect	Evolutionary	Swarm Intelligence	Physics-Based	Human-Related
Inspiration	Natural selection, genetics	Collective animal/insect behavior	Physical laws/phenomena	Human teaching, learning, social processes
Population vs. trajectory	Population of solutions	Population with local interactions	Either population (GSA) or single- solution trajectory (SA)	Population with social/knowledge exchanges
Key operators	crossover, mutation	Velocity/position updates, pheromone laying, attraction	Temperature schedule, force calculations	Teacher–learner updates, knowledge sharing
Exploration mechanism		Randomness in movement, pheromone evaporation	High "temperature," low attraction	Random peer interactions, brainstorming
Exploitation mechanism	Selection pressure, elitism	Attraction to best peers or global best	Cooling schedule, increasing force focus	Teacher guidance, knowledge aggregation

Aspect	Evolutionary	Swarm Intelligence	Physics-Based	Human-Related
Memory usage	_	best, pheromone map	temperature), agent	Shared knowledge pool, teacher's record

4.3 Kepler Optimization Algorithm (KOA):

4.3.1 Inspiration

In ancient times, it was widely believed that the Earth was the center of the universe, with the Sun, planets, stars, and moons revolving around it. This geocentric view persisted until 1543, when the Polish astronomer Nicolaus Copernicus challenged it by proposing the heliocentric theory that the Earth and other planets orbit the Sun. Although Copernicus lacked the means to prove his theory, it laid the foundation for future discoveries. In 1609, German astronomer Johannes Kepler confirmed the heliocentric model through extensive calculations. He formulated three fundamental laws that describe the motion of planets around the Sun. These laws, known as Kepler's laws of planetary motion, are outlined below [86], [87]:

Kepler's First Law:

All planets travel in elliptical orbits with the Sun located at one of the two foci. This law defines the shape of planetary orbits as ellipses rather than perfect circles, as illustrated in Figure 4-1. An ellipse resembles an oval and has two focal points; the Sun occupies one of these. The eccentricity of an ellipse, represented by e, quantifies how elongated the shape is. It is calculated by dividing the distance from the center of the ellipse to a focus by the length of the semi-major axis. When e = 0, the orbit is a perfect circle; when e = 1, it becomes a straight line. Figure 4-2 shows examples of various elliptical shapes.

Kepler's Second Law:

A line segment connecting a planet to the Sun sweeps out equal areas during equal intervals of time. This law explains the changing speed of a planet in its orbit. A planet travels more quickly when it is closer to the Sun and more slowly when it is farther away. Despite these changes in speed, the imaginary line from the planet to the Sun covers equal areas over equal time periods, maintaining a consistent areal velocity. The velocity of a planet around the Sun can be calculated as follows [88]:

$$V = \left[\mu(M_S + m)(\frac{2}{R} - \frac{1}{a}) \right]^2 \tag{4.1}$$

 M_S and m denote the mass of the Sun and a planet, respectively, R is the Euclidean distance between the Sun and a planet at this time, μ is the gravitational constant and α is the semi major axis of the orbit.

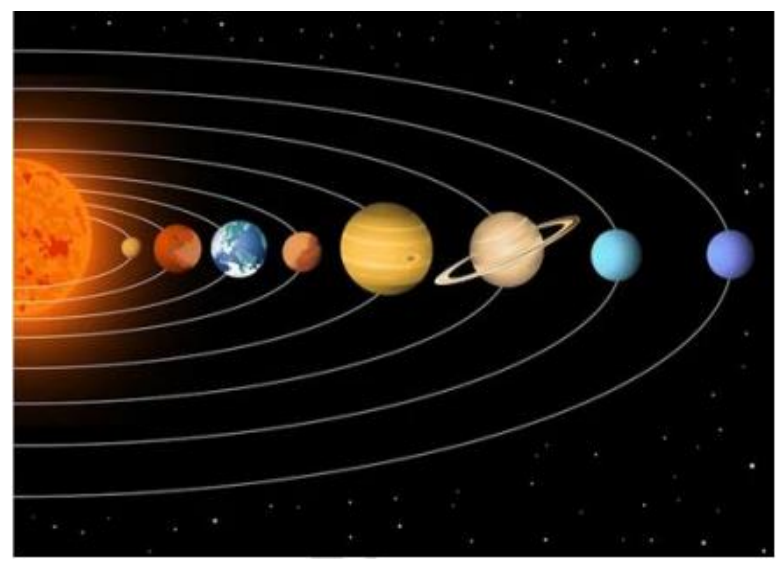


Figure 4-1: The trajectory of planets motion [86]

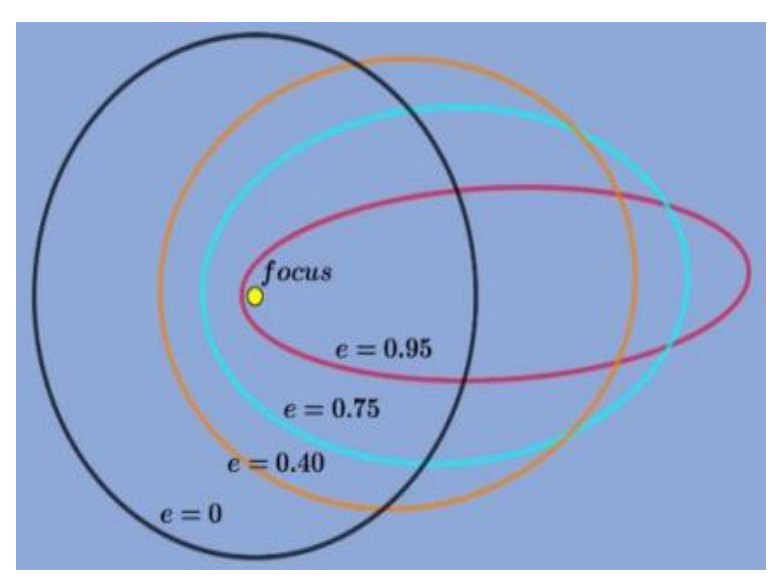


Figure 4-2: Different Ellipse Shapes [86]

Kepler's Third Law:

For any planet, the square of its orbital period is proportional to the cube of the semi-major axis of its orbit. In simpler terms, planets that are farther from the Sun take longer to complete one orbit, and this relationship follows a precise mathematical pattern. This law can be expressed as:

$$T^2 = \left[\frac{4\pi^2}{\mu(M_S + m)} \right] a^3 \tag{4.2}$$

Here, T is the orbital period, a the semi-major axis, μ the gravitational constant, M_S the Sun's mass, and m the planet's mass. Most solar system bodies rotate counterclockwise, but exceptions like Venus rotate clockwise likely due to early collisions. Four key factors influence a planet's orbit: position, mass, gravitational force, and orbital velocity. These form the foundation of the mathematical model behind the proposed algorithm. Kepler's laws enable predicting a planet's position and velocity at any moment directly inspiring KOA.

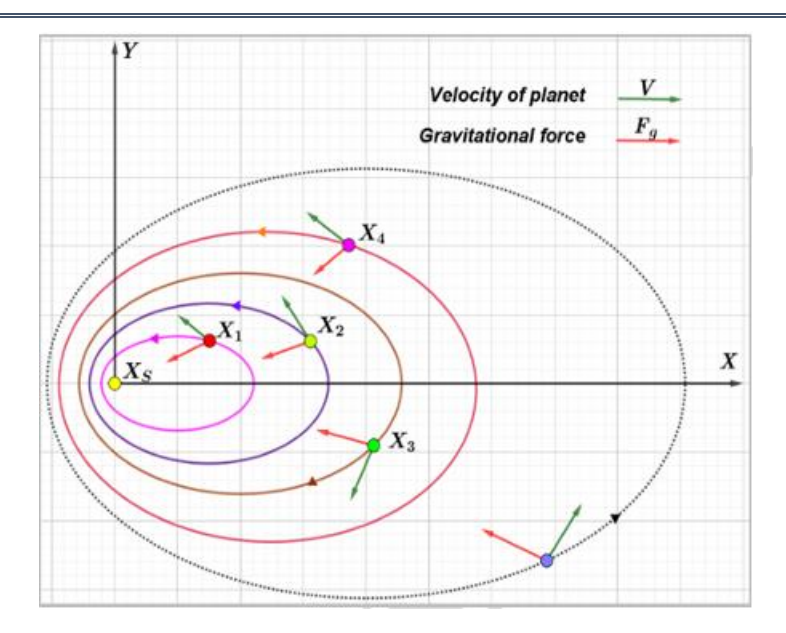


Figure 4-3:2D Dimension Of Planets Motion[86]

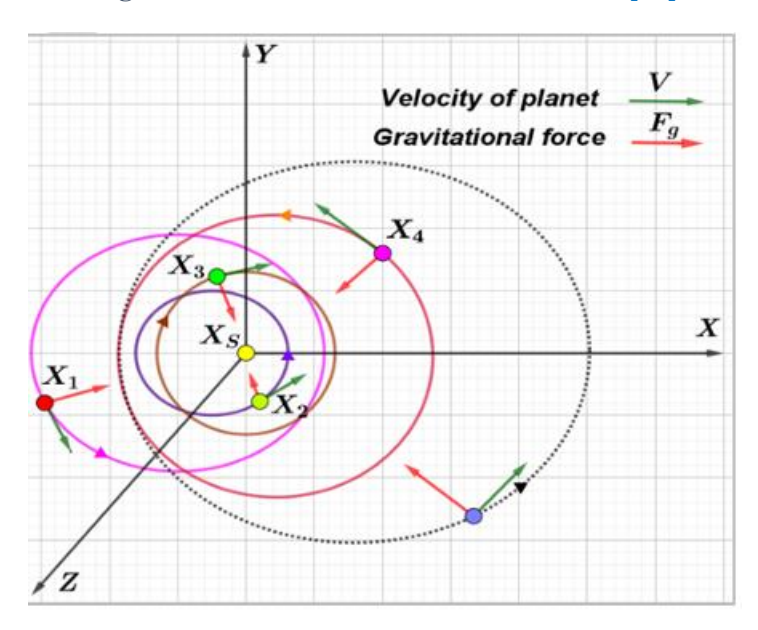


Figure 4-4:3D Dimension Of Planets Motion[86].

4.3.2 Mathematical model of Kepler optimization algorithm (KOA):

This section presents a new optimization algorithm inspired by Kepler's laws of planetary motion [88]. In our proposed algorithm, Kepler's first law is simulated as follows. The Sun and the planets (or objects) revolving around it in (imaginary) elliptical orbits can be used to represent the search space, as shown in Fig 4-3. In KOA, the planets (candidate solutions) are under different situations from the Sun (the best solution) at various times, and thus, the search space is explored and exploited more efficiently. Fig 4-4 illustrates how the position of an object, its mass, the force of attraction between the object and the Sun, and the velocity with which it orbits the Sun change its position around the best solution, i.e., the Sun. The figure also depicts the rotation of most objects in a clockwise direction.

Fig. 4-4 can also be used to explain how the searcher's position changes in 3D space. Similar to other metaheuristic population-based algorithms, KOA starts the search process with an initial set

of objects (candidate solutions) with stochastic orbitals. Each object is initialized with its random position in orbit during this stage. After evaluating the fitness of the initial set, KOA runs in iterations until the termination condition is met. In the current study, we use the term "time" instead of "iteration" because it is a common term in solar system theory and cosmology. During optimization, the following rules are applied to KOA.

- The orbital period of a planet (the candidate solution) is chosen randomly in accordance with the normal distribution.
- The eccentricity of a planet's orbit is selected at random from a range of 0 to 1.
- The fitness of a solution is calculated on the basis of the objective function.
- The best solution, in iteration, is the central star (the Sun).
- The distance between the Sun and the planet is changed in accordance with the current time.

The rest of this section presents the mathematical model of KOA. In brief, the pseudocode and flowchart of KOA are presented in Fig 4-6, respectively. The time complexity of the steps listed in this algorithm is of O(NTmax), where N represents the population size, and Tmax is the termination criteria of the proposed KOA based on the maximum number of function evaluation. Theoretically, KOA can be considered a global optimization algorithm because it includes exploration and exploitation phases. Mathematically, the processes of the proposed KOA are described in detail as follows.

Phase 1: Initialization process

In this process, a number of planets equal to N, referred to as the population size, will be randomly distributed in d-dimensions, representing the decision variables of an optimization problem, in accordance with the following formula:

$$X_{i}^{j} = X_{i,low}^{j} + rand_{[0,1]} \times (X_{i,up}^{j} - X_{low}^{j}), \begin{cases} i=1,2,\dots,N. \\ j=1,2,\dots,d. \end{cases}$$
(4.3)

where X_i indicates the *i*th planet (candidate solution) in the search space; N represents the number of solution candidates in search space; d represents the dimension of the problem to be optimized; $X_{i,up}^j$ and X_{low}^j represent the upper and lower bounds, respectively, of the *j*-th decision variable; and rand[0,1] is a number generated randomly between 0 and 1.

The orbital eccentricity (e) for each ith object is initialized using equation eq.(4):

$$(e) = rand_{[0,1]}, i = 1, \dots, N$$
 (4.4)

Where $rand_{[0,1]}$ is a random value generated within interval [0,1]. finally, the orbital period (T) for each i-th object is initialized using Eq. (5):

$$T_i = |r|, i = 1, \dots, N$$
 (4.5)

where r is the number generated randomly on the basis of the normal distribution.

Step 2: Defining the gravitational force (F)

The Sun is the main element of the solar system; it represents the largest object in the solar system and controls the movement of the group through its gravity [89]. The primary reason why planets orbit the Sun is because the Sun's gravity keeps them in their orbit. If the Sun does not exist, then planets will move in a straight line toward infinity, however, the Sun's gravity constantly changes direction to enable planets to move around it in an elliptical shape. Gravity is known as the fundamental force that controls the orbits of planets around the Sun. Each planet has its own gravity that is proportional to its size. Notably, the velocity of a planet depends on the gravity of the Sun. The closer a planet is to the Sun, the greater its orbital velocity, and vice versa. The attraction force of the Sun Xs and any planet Xi is given by the universal law of gravitation, which is defined as

$$Fg_{i}(t) = e_{i} \times \mu(t) \times \frac{\overline{Ms} \times \overline{m}_{i}}{\overline{R}_{i}^{2} + \varepsilon} + r_{1}$$

$$(4.6)$$

where \overline{Ms} and $\overline{m_i}$ denote the normalized values of Ms and mi, which represent the mass of Xs and Xi, respectively, and given by Eqs. (4.8) and (4.9); ε is a small value; μ is the universal gravitational constant; e_i is the eccentricity of a planet's orbit, which is a value between 0 and 1 that was proposed to endow a stochastic characteristic to KOA; r_1 is a value that is generated randomly between 0 and 1 to give more variation to the gravitation values within the optimization process; and $\overline{R}i$ is the normalized value of Ri that represents the Euclidian distance between Xs and Xi, and is defined as

$$R_{i}(t) = \|Xs(t) - X_{i}(t)\|_{2} = \sqrt{\sum_{i=1}^{N} (Xs(t) - X_{i}(t))^{2}}$$
(4.7)

 $||Xs(t) - X_i(t)||_2$ represents the Euclidean distance between the dimensions of Xs and these of Xi. The mass of the Sun and object i at time t is simply calculated using the fitness evaluation as follows (considering a minimization problem):

$$M_{s} = \frac{fit_{s}(t) - worst(t)}{\sum_{K+1}^{N} (fit_{s}(t) - worst(t))}$$

$$(4.8)$$

$$m_i = r_2 \frac{fit_s(t) - worst(t)}{\sum_{K=1}^{N} (fit_s(t) - worst(t))}$$
(4.9)

$$fit_s(t) = best(t) = k \in {\text{min } 1, 2, ..., N} fit_k(t)$$
 (4.10)

$$worst(t) = k \in {^{\max}_{1}, 2, ..., N} fit_k(t)$$
 (4.11)

where r_2 is a number generated randomly between 0 and 1 to diverge the mass values for various planets. $\mu(t)$ is a function that exponentially decreases with time (t) to control search accuracy and is defined as follows:

$$worst(t) = k \in {\text{max } 1, 2, ..., N} fit_k(t)$$
 (4.12)

where γ is a constant; μ_0 is an initial value; and t and t and t are the current iteration number and maximum number of iterations, respectively.

Phase 3: Calculating an object' velocity

The velocity of an object depends on its position relative to the Sun. That is, a planet's velocity increases if it is close to the Sun and decreases if it is far from it. If an object is close to the Sun, then the Sun's gravity is considerably strong, and the planet attempts to increase its speed to avoid being pulled toward the Sun. However, if an object is far from the Sun, then its velocity will slow down because the Sun's gravity is weak. Mathematically, this behavior is formulated in Eq. (4.13) to compute the velocity of an object around the Sun according to the vis-viva equation. This equation is twofold. The first fold determines the velocities of planets close to the Sun by multiplying the distance between the current solution and a randomly selected solution, or the distance between two solutions that are randomly selected from the current population. This helps KOA diversify its search strategies. However, the diversity of the population's solutions during the optimization process may be minimized, and thus, velocity may be minimized in cases wherein a planet is close to the Sun. Accordingly, another step size based on the distance between the lower and upper bounds of the optimization problem is integrated into the first fold to assist in preserving the velocity of planets throughout the optimization process and avoiding being stuck in local minima. Second, on the basis of the proposition that planets are far from the Sun, the equation computes the velocity of the planet in accordance

with the distance between a randomly selected solution and the current solution to reduce the velocity of planets compared with the first fold. The major shortcoming in the second fold is the lack of diversity between solutions, which may minimize the opportunity for KOA to escape local optima because changes in the current solution are too small. To address this flaw, a second step size based on the distance between the lower and upper bounds of the optimization issue is incorporated into the second fold

$$v_{i}(t) = \ell \times (2r_{4}\overrightarrow{X}_{i} - \overrightarrow{X}_{b}) + \rho(\overrightarrow{X}_{a} - \overrightarrow{X}_{b}) + (1 - R_{i-norm}(t)) \times F \times \overrightarrow{U} \times (\overrightarrow{X}_{i,up} - \overrightarrow{X}_{i,low})$$
(4.13)

if
$$R_{i-norm}(t) \leq 0.5$$

else

$$r_4 \times L \times (\overrightarrow{X}_a - \overrightarrow{X}_i) + (1 - R_{i-norm}(t)) \times F \times \overrightarrow{U}_1 \times (r_3 \overrightarrow{X}_{i,un} - \overrightarrow{X}_{i,low})$$
 (4.14)

$$\ell = \overrightarrow{U} \times M \times L, \tag{4.15}$$

$$L = \left[\mu(t) \times (M_S + m_i) \left(\frac{2}{R_i(t) + \varepsilon} - \frac{1}{a_i(t) + \varepsilon}\right)\right]^{\frac{1}{2}}$$
(4.16)

$$M = (r_3 \times (1 - r_4) + r_4) \tag{4.17}$$

$$\vec{U} = \begin{cases} 0 & \vec{r_5} \le \vec{r_6} \\ 1 & else \end{cases} \tag{4.18}$$

$$F = \begin{cases} 1 & \text{if } r_4 \le 0.5 \\ -1 & \text{else} \end{cases}$$
 (4.19)

$$\rho = (1 - \overrightarrow{U}) \times \overrightarrow{M} \times L \tag{4.20}$$

$$\vec{M} = (r_3 \times (1 - \vec{r_5}) + \vec{r_5}) \tag{4.21}$$

$$\overrightarrow{U}_1 = \begin{cases} 0 & r_5 \le r_4 \\ 1 & else \end{cases} \tag{4.22}$$

$$\overrightarrow{U_2} = \begin{cases} 0 & r_3 \le r_4 \\ 1 & else \end{cases} \tag{4.23}$$

where $\overrightarrow{v_i}(t)$ represents the velocity of object i at time t $\overrightarrow{X_i}$ represent object i, r_3 and r_4 are randomly generated numerical values at interval [0, 1], and $\overrightarrow{r_5}$ and $\overrightarrow{r_6}$ are two vectors that include random values between 0 and 1. $\overrightarrow{X_a}$ and $\overrightarrow{X_b}$ represent solutions that are selected at random from the population; M_s and m_i represent the mass of X_s and X_i , respectively; $\mu(t)$ represents the universal gravitational constant; ε is a small value for preventing a divide-by-zero error; Ri(t) represents the distance between the best solution X_s and the object X_i at time t; and ai represents the semimajor axis of the elliptical orbit of object i at time t, and it is defined by Kepler's third

law mentioned in eq 4.24 as follows:

$$a_i(t) = r_3 \times \left[T_i^2 \times \frac{\mu(t) \times (M_S + m_i)}{4\pi^2} \right]^{\frac{1}{3}}$$
(4.24)

where T_i represents the orbital period of object i and is determined by Eq. (4.25). In our proposed algorithm, the semimajor axis of the elliptical orbit of object i is assumed to decrease gradually with generations wherein the solutions move toward the promising region in which the global best solution is likely to be found. $R_{i-norm}(t)$ represents normalizing the Euclidian distance between X_s and X_i , and it is defined as follows:

$$R_{i-norm}(t) = \frac{R_i - R_{i-norm}(t)}{\max(R(t)) - \min(R(t))}$$
(4.25)

The purpose of Eq. (4.16) is to calculate the percentage of steps that each object will change. If $R_{i-norm}(t) \le 0.5$, then the object is close to the Sun and will increase its speed to prevent drifting toward the Sun because of the latter's tremendous gravitational force. Otherwise, the object will slow down

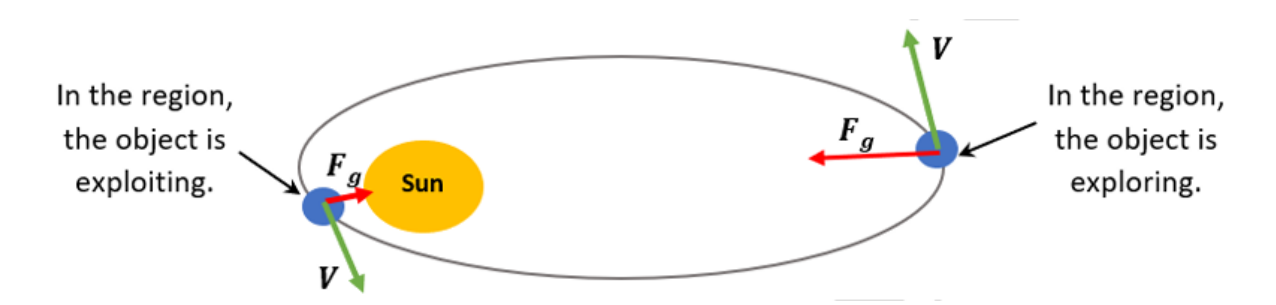


Figure 4-5: Exploration And Exploitation Regions In The Search Space[86]

Step 4: Escaping from the local optimum

In the solar system, most objects revolve counterclockwise around the Sun, and they all rotate on their owns axes, however, some objects revolve around the Sun in a clockwise direction. The proposed algorithm uses this behavior to escape from local optimum regions. The proposed KOA simulates this behavior by using a flag \mathcal{F} that changes the search direction such that agents have a good chance of scanning the search space accurately.

Step 5: Updating objects' positions

As mentioned earlier, objects revolve around the Sun in their own elliptical orbits. During rotation, objects move closer to the Sun for a certain time and then move away from it. The proposed algorithm simulates this behavior through two major phases: the exploration and exploitation phases. KOA explores objects far from the Sun to find new solutions, while using solutions close to the Sun more accurately as it searches for new places near the best solutions. Fig 4-5 shows the regions of exploration and exploitation around the Sun. The exploration and exploitation phases are subsequently described in detail. In the exploration phase, the objects are far from the Sun, indicating that the proposed algorithm explores the entire search area more efficiently. In accordance with the previous steps, a new position of each object far from the Sun is updated using Eq. (4.26):

$$\vec{X}_i(t+1) = \vec{X}_i(t) + \vec{F} \times \vec{v}_i \times (Fg_i(t) + |r|) \times \vec{U} \times (\vec{X}_s(t) - \vec{X}_i(t))$$
(4.26)

where $\vec{X}_i(t+1)$ is the new position of object i at time t+1, $\vec{v}_i(t)$ is the velocity of object i required to reach the new position, $X_s(t)$ is the best position of the Sun found thus far, and \mathscr{F} is used as a flag to change search direction. Eq. (4.26) simulates the gravitational force of the Sun to the planets, where this equation employs

another step size on the basis of calculating the distance between the Sun and the current planet multiplied by the gravitational force of the Sun to help KOA explore the regions around the best-so-far solution and find better outcomes in less number of function evaluations. In general, the velocity of planets will represent the exploration operator of KOA when a planet is far from the Sun. However, this velocity is affected by the gravitational force of the Sun, which helps the current planet slightly exploit regions near the optimal solution. Meanwhile, when a planet approaches the Sun, its velocity increases dramatically, allowing it to escape the Sun's gravitational pull. In such case, velocity represents local optimum avoidance if the best-so-far solution, referred to as the sun, is local minima, and the Sun's gravitational pull represents the exploitation operator to assist KOA in attacking the best-so-far solution to find better solutions

Step 6: Updating distance with the Sun

To further improve the exploration and exploitation operators of planets, we attempt to mimic the typical behavior of the distance between the Sun and planets, which naturally varies over time. When planets are close to the Sun, KOA will focus on optimizing the exploitation operator; when the Sun is far, KOA will optimize the exploration operator. These rules depend on the value of the regulating parameter h. When this value is large, the exploration operator is employed to expand planetary orbital separation from the Sun; conversely, when this value is small, the exploitation operator is used to exploit the regions around the best-so-far solution if the distance between the Sun

and planets is small. This principle is randomly exchanged with Eq. (4.26) to improve the exploration and exploitation operators of KOA further, as listed in Algorithm 1. The mathematical model of this principle is described as follows:

$$\overrightarrow{X}_{i}(t+1) = \overrightarrow{X}_{i}(t) \times \overrightarrow{U}_{1} + (1 - \overrightarrow{U}_{1}) \times \left(\frac{\overrightarrow{X}_{i}(t) + X_{s} + \overrightarrow{X}_{a}}{3.0} + h \times \left(\frac{\overrightarrow{X}_{i}(t) + X_{s} + \overrightarrow{X}_{a}}{3.0} - \overrightarrow{X}_{b}(t)\right)\right)$$
(4.27)

where h is an adaptive factor for controlling the distance between the Sun and the current planet at time t, as defined below:

$$h = \frac{1}{a^{rr}} \tag{4.28}$$

where r is a number that is generated randomly on the basis of the normal distribution, while η is a linearly decreasing factor from 1 to -2, as defined below:

$$\eta = (a_2 - 1) \times r_4 + 1 \tag{4.29}$$

where a_2 is a cyclic controlling parameter that is decreasing gradually from -1 to -2 for \overline{T} cycles within the whole optimization process as defined below:

$$a_2 = -1 - 1 \times \left(\frac{t \times \frac{T_{\text{max}}}{T}}{\frac{T_{\text{max}}}{T}} \right) \mu \tag{4.30}$$

Step 7: Elitism

This step implements an elitist strategy to ensure the best positions for planets and the Sun. This procedure is summarized using Eq. (4.31):

$$\overrightarrow{X}_{i,new}(t+1) = \begin{cases} \overrightarrow{X}_i(t+1), & \text{if } f(\overrightarrow{X}_i(t+1) \leq \overrightarrow{X}_i(t)) \\ \overrightarrow{X}_i(t), & \text{else} \end{cases}$$
 (4.31)

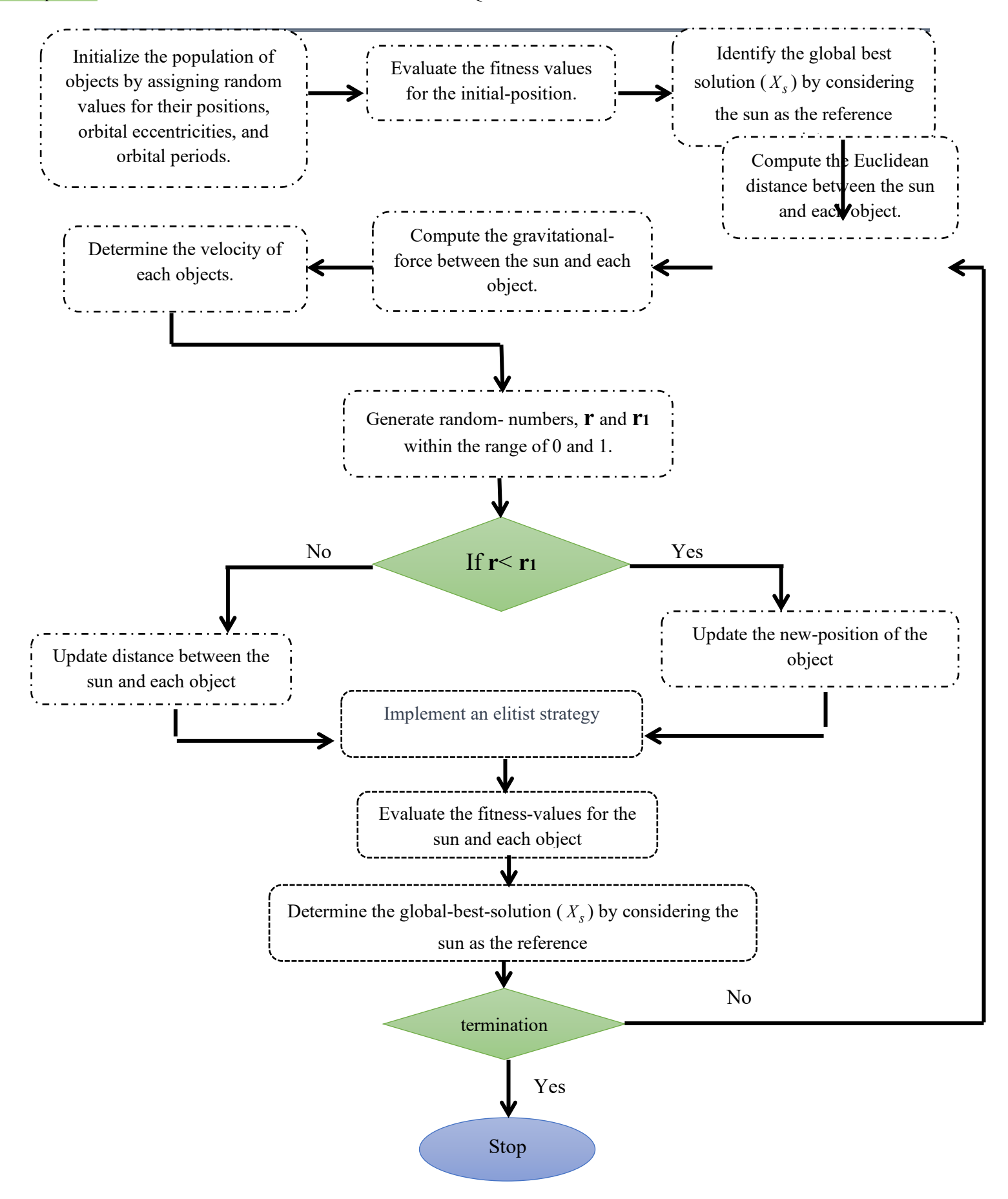


Figure 4-6: Flowchart of (KOA)

4.4 Enhanced Kepler Optimization Algorithm

It is recognized that the performance of meta-heuristic technique can be ameliorated by fulfilling the suitable equilibrium between the two opposing phases. The initial phase, focused on local search, referred to as exploitation, while the subsequent phase, which aims to search globally, is known as exploration. The global minima can be guaranteed, and reducing the search space through these phases helps prevent the technique from becoming trapped in local minima. A slight modification to this technique is introduced to generate a substantial exploration through a deeper search for new neighbor solutions in the search space. Hence, an operator phi is suggested to strike a better balance between the exploration and exploitation stages. More precisely, this operator also acts significantly on the acceleration of algorithm convergence rate. This operator decreases linearly during iterations from 1 to 0.5 using the subsequent equation [62]:

$$\psi = 0.75 + 0.25 \times \cos\left(\pi \frac{t}{\text{Tmax}}\right) \tag{4.32}$$

Where Tmax is the basic stopping criterions and t is the Instant iteration. The operator ψ is combined with the equation 4.27.

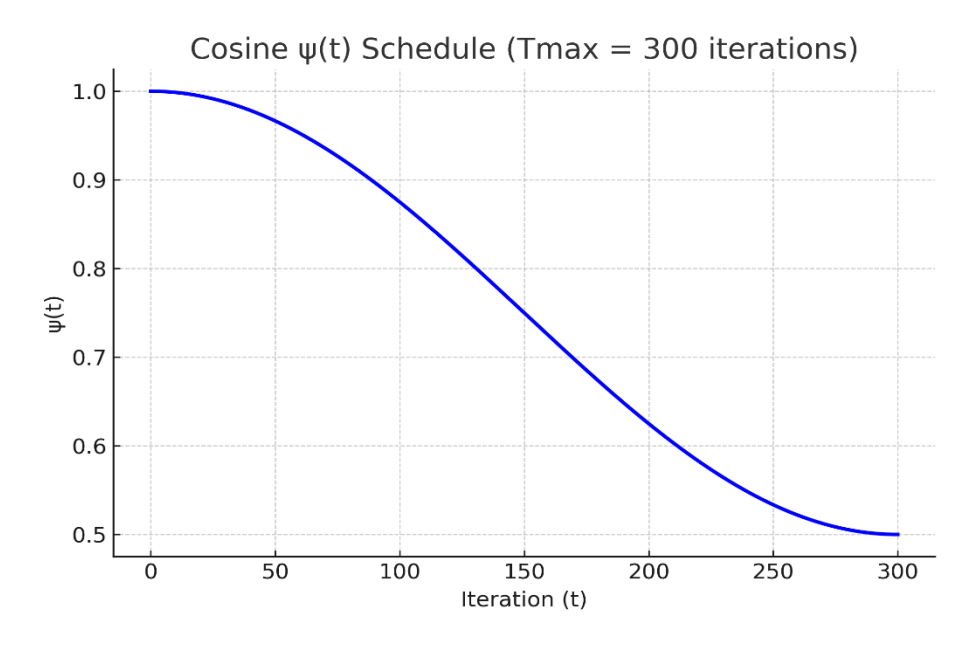


Figure 4-7: ψ variation with iteration

- 1. Early iterations ($\mathbf{t} \approx \mathbf{0} \to \mathbf{\psi} \approx \mathbf{1.0}$): $\mathbf{h} \cdot \mathbf{\psi} \approx \mathbf{h}$, $\mathbf{\psi}(\mathbf{t}) = 1$. Planets make big jumps \to they spread widely across This phase = Exploration.
- **2. Middle iterations** ($\rightarrow \psi \approx 0.75$): $\psi(t)$ has decreased smoothly to about 0.75. Exploration is moderated: jumps are smaller, but still large enough to search new regions. Balance between exploration and exploitation: algorithm explores, but also starts to refine.
- 3. Late iterations ($\rightarrow \psi \approx 0.5$): $h \cdot \psi < h$, $\psi(t)$ reaches its minimum value 0.5. Exploration is reduced by half compared to the start. Planets make small jumps around the best-known regions. Focus shifts to exploitation: fine-tuning around optimal solutions, ensuring convergence

4.5 Non-Dominated Sorting Kepler Optimization Algorithm (NSKOA)

In the original version of the Kepler optimization algorithm (KOA), the algorithm was designed to solve mono-objective optimization problems, where a single global best solution was determined as the "Sun" (XS) based on fitness values. The algorithm updated the positions and velocities of the objects (planets) accordingly, aiming to improve their fitness relative to this singular objective.

To extend KOA into a multi-objective framework, the key modification was the integration of the non-dominated sorting procedure, allowing the algorithm to handle multiple conflicting objectives simultaneously [90]. The key changes are as follows:

4.5.1 Non-Dominated Sorting Principle

This mechanism is essential for navigating trade-offs in multi-objective problems by ranking solutions based on Pareto dominance. In the modified version, after initializing the population and calculating the objective functions, non-dominated sorting is performed to assign ranks to solutions. Non-dominated solutions, which are not outperformed in all objectives, receive a rank of 1, while subsequent ranks are assigned iteratively to solutions that are dominated by others. This ranking system helps preserve a diverse set of optimal solutions, ensuring that different trade-offs between objectives are explored [91].

4.5.2 Concept of Dominance

In the Pareto sense,

$$U_1$$
 domine U_2 if
 $\forall i \in [1,2]$, $F_i(U_1) \leq F_i(U_2)$
and $\exists i \in [1,2], F_i(U_1) < F_i(U_2)$

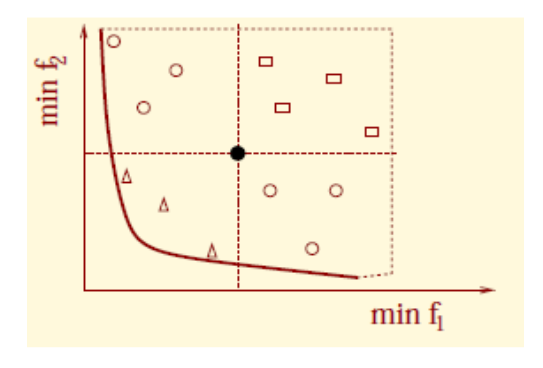


Figure 4-8: Concept Of Dominance [91]

Example: The point odominates squares, is dominated by triangles, and is not comparable with circles.

4.5.3 classification of the population

We classify the population using non-domination. This returns two columns for each object. These are the rank and the crowding distance corresponding to their position in the front.

3.7.1 Rank:

- Undominated → rank 1
- Dominated except by rank $1 \rightarrow \text{rank } 2$

•

4.5.4 Crowding Distance (CD)

An important aspect of this approach is the calculation of crowding distance, which measures the proximity of solutions to their neighbors in the objective space. A higher crowding distance indicates a less crowded region, helping to maintain diversity among solutions and favoring those that are well-distributed along the Pareto front.

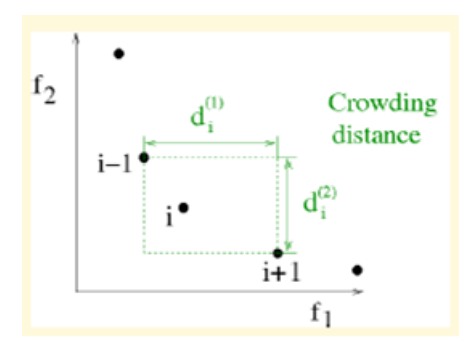


Figure 4-9: Crowding Distance[91].

By evaluating solutions based on both rank and crowding distance, the algorithm ensures a balance between convergence toward the Pareto front and the preservation of solution diversity across the front. This process ensures that, instead of converging to a single global best solution, a set of non-dominated solutions is maintained, offering multiple viable options that address different trade-offs between the conflicting objectives.

4.5.5 Elitism and Population Combination

In this Algorithm, the current population (Pt) of size N and a new population (Qt) of size N are assembled to form a population (Rt = Pt \cup Qt), as shown in Figure 4-9. This assembly ensures elitism. The population of size (2N) is then sorted according to the non-dominance criterion to identify the different fronts F1, F2, etc. The best individuals will end up in the first front(s). A new parent population (Pt + 1) is formed by adding the fronts in full (first front F1, second front F2, etc.) as long as they do not exceed N. If the number of individuals present in (Pt + 1) is less than N, a crowding procedure is applied on the first edge following Fi not included in (Pt + 1).

The goal of this operator is to insert the $N - |P_{t+1}|$ best individuals that are missing in the population (Pt + 1). The individuals in this front are used to calculate the crowding distance between two neighboring solutions.

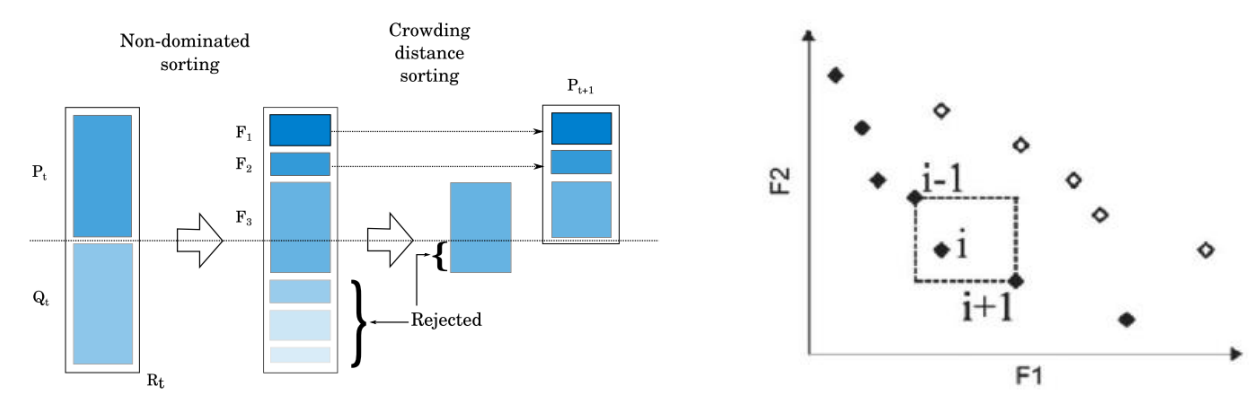


Figure 4-10:Non-Dominated Selection [91]

Figure 4-11: Crowding Distance [91]

4.5.6 Best Compromise Solution (BCS)

Fuzzy set theory is frequently employed to effectively select a candidate Pareto-optimal solution from numerous options along the Pareto front. Given the inherent irrationality of decision-makers, the i-th objective function of a solution within the Pareto-optimal set, denoted as f_i , is expressed through a membership function μ_i [92], defined as:

$$\mu_{i} = \begin{cases} 1 & f_{i} \leq f_{i}^{\min} \\ \frac{f_{i}^{\max} - f_{i}}{f_{i}^{\max} - f_{i}^{\min}} & f_{i}^{\min} \leq f_{i} \leq f_{i}^{\max} \\ 0 & f_{i} \geq f_{i}^{\max} \end{cases}$$
(4.33)

where f_i^{max} and f_i^{min} represent the maximum and minimum values of the i-th objective function, respectively.

The normalized membership function μ^k is calculated for each non-dominated solution k as follows:

$$\mu^{k} = \frac{\sum_{i=1}^{Nof} \mu_{i}^{k}}{\sum_{i=1}^{M} \sum_{i=1}^{Nof} \mu_{i}^{j}}$$
(4.34)

Where the number of non-dominated solutions is denoted as M. The best compromise solution is determined as the one with the highest value of μ^k . By organizing all solutions in descending order based on their membership function, a priority list of non-dominated solutions is generated. This prioritized list serves as guidance for the decision-maker, aiding in navigating through the current operational circumstances.

4.6 Conclusion:

This chapter delved into the foundational principles of metaheuristic algorithms, emphasizing the critical balance between exploration and exploitation that underpins their efficacy in solving complex optimization problems. A systematic classification of metaheuristic frameworks was presented, highlighting the core mechanisms of distinct algorithmic classes (e.g., swarm intelligence, evolutionary algorithms). We then introduced the Kepler Optimization Algorithm (KOA) whose astrophysics-inspired dynamics were analyzed in depth, particularly its ability to model celestial mechanics for navigating search spaces. To address limitations in KOA's exploratory capabilities, a novel equation was introduced, enhancing its diversity-seeking behavior during the initial search phases. This modification ensures a more rigorous exploration of the solution space, reducing premature convergence risks while maintaining computational efficiency.

Building on this enhanced KOA, the chapter further proposed a multi-objective adaptation of the algorithm through the integration of non-dominated sorting. By hierarchically ranking solutions based on Pareto dominance and employing crowding distance metrics, the revised framework (MO-KOA) efficiently balances competing objectives. The inclusion of a best compromise solution mechanism leveraging decision-maker preferences or objective weighting provides a practical pathway to select optimal trade-offs in multi-objective landscapes. In the next chapter, the enhanced KOA (EKOA) will be applied to solve the (SOPF) problem in the presence of (RES) and its performance will be compared with the original KOA to evaluate the proposed improvements.

Chapter 5: POWER FLOW ANALYSES IN PRESENCE OF RENEWABLE ENERGY SOURCES

5.1 Introduction:

Modern electrical networks are undergoing profound transformations to meet rising demand for fossil-fuel-based energy, contain escalating production costs, and mitigate the environmental impact of pollutant emissions from thermal power plants. These pressures have driven a shift toward cleaner, more sustainable energy sources and more sophisticated grid-management strategies pivotal among them is the (OPF) problem, first formulated over half a century ago, remains a central, large-scale, nonlinear optimization task in power-system research. Its objective is to minimize total generation cost by selecting optimal settings for control variables real-power outputs, generator bus voltages, transformer tap positions, and so on while enforcing power-balance equations and respecting equipment limits (generator capabilities, line thermal ratings, voltage bounds). Traditionally focused on dispatching controllable thermal units, OPF must now accommodate intermittent (RES) such as wind and solar, whose variable outputs introduce stochasticity into generation scheduling. Early OPF solutions relied on classical techniques Newton Raphson programming, quadratic and nonlinear programming, interior-point methods, and linear programming. While effective for small, wellbehaved problems, these approaches often stall at local optima, struggle with high nonlinearity, and incur heavy computational burdens as system size and complexity grow. Their sensitivity to initial conditions further complicates convergence to a global solution. To overcome these limitations, metaheuristic and hybrid algorithms have gained traction. By enhancing population diversity and combining complementary search strategies, these methods reduce the risk of stagnation and improve exploration-exploitation balance. In particular, recent studies have explored hybridizations and modifications of evolutionary, swarm-intelligence, and physics-inspired techniques to better handle the stochastic OPF (SOPF) challenge presented by high RES penetration [93].

This chapter introduces power flow analyses in the presence of (RES) and examines their impact on power production and pollutant gas emissions. It also presents a novel Enhanced Kepler Optimization Algorithm (EKOA) specifically designed for Stochastic Optimal Power Flow (SOPF). By embedding advanced exploration—exploitation operators, EKOA effectively navigates complex search spaces, avoids local optima, and balances competing objectives such as economic cost, system losses, voltage stability, and environmental impact. The uncertainty of RES is modeled using Weibull distributions for wind and lognormal distributions for solar irradiance. Extensive simulations on large-scale test systems demonstrate both the impact of RES integration and EKOA's superior convergence, solution quality, and computational efficiency compared to existing methods.

- · A detailed formulation of SOPF with RES uncertainty and classical OPF constraints
- Critique of traditional optimization approaches and their limitations in stochastic, large-scale settings
- Development of the Enhanced Kepler Optimization Algorithm (EKOA) with augmented exploration—exploitation mechanisms
- Application of appropriate probability models (Weibull, lognormal, Gumbel) for RES output
- Statistical validation of EKOA's performance against benchmark algorithms

By combining rigorous uncertainty quantification, tailored metaheuristics, and robust constraint handling, this work lays a scalable foundation for integrating renewable energies into future resilient and low-carbon power grids.

5.2 Optimal Power Flow Problem Formulation:

The optimization problem in this paper aims to solve the (OPF) for a power system that includes thermal and stochastic wind and solar PV power generations. The primary goal is to optimize power system variables and determine the optimal settings for control in power system components. This is achieved by minimizing selected objective functions while ensuring that all the equality and inequality constraints are satisfied, formulated Mathematically as-follows [94]:

Minimize
$$OF(d,c)$$
 (5.1)

Subject to
$$g(d,c)$$
 $\begin{cases} g(d,c) = 0 \\ h(d,c) \le 0 \end{cases}$ (5.2)

Where $_{OF(d,c)}$ denotes the objective function, g(d,c) the equality constraints, h(d,c) define inequality constraints, d and c are the dependent variables vector and the control variables vector respectively. Maintaining system security and achieving optimal solutions in an electric power system necessitates the adherence to limits on dependent variables. These limits are vital for preserving feasibility, ensuring system stability, and striking a balance between optimization and operational constraints.

Where:

- $_{OF(d,c)}$ denotes the objective function that needs to be minimized. The specific form of this objective function would depend on the objectives identified in the paper.
- g(d,c) represents the collection of equality constraints that must be fulfilled. These constraints ensure that the power flow equations and other system requirements are met.
- c represents the vector of decision variables, which includes the control settings for power system components, and d represent the vector of state variables which represent states of the power system, these variables describe the system's dynamic behavior

5.2.1 Optimization Problems:

5.2.1.1 Cost of Generation for Thermal Units:

The fuel cost function for multiple thermal generator units can be modeled as a convex and differentiable quadratic function. It can be represented by the equation (5.3):

$$C_{TH}(P_{TG}) = \sum_{i=1}^{N_{TG}} a_i + b_i P_{TGi} + c_i P_{TGi}^2$$
(5.3)

However, the mentioned above model ignores the valve point loading, which introduces oscillations or fluctuations to the actual input-output curve, can be addressed by modifying the equation (5.3). This modification involves the addition of an extra sin term to capture the valve point effects [95].

$$TC_{TH}(P_{TG}) = \sum_{i=1}^{N_{TG}} a_i + b_i P_{TGi} + c_i P_{TGi}^2 + \left| d_i \times \sin\left(e_i \left(P_{TG}^{\min} - P_{TG}\right)\right) \right|$$
 (5.4)

 a_i, b_i, c_i, d_i , and e_i coefficients represent the cost coefficients for the i-th thermal generator, indicating the relationship between power output and fuel cost. The system consists of N_{ThG} thermal generators, and P_{ThG}^{min} is the minimum rated power of the conventional thermal generator.

5.2.1.2 Emission and Carbon Tax:

The adverse environmental impact of conventional energy sources is well acknowledged, particularly in terms of emitting harmful gases. The release of sulfur oxide (SOx) and nitrogen oxide (NOx) tends to escalate with the rise in power generation from thermal power generators, as illustrated by the correlation outlined in Equation (5.5). The emission level, quantified in tons per hour (t/h), can be computed using the following equation [96]:

$$E = \sum_{i=1}^{N_{TG}} \left[\left(\alpha_i + \beta_i P_{TGi} + \gamma_i P_{TGi}^2 \right) \times 0.01 + \omega_i \exp\left(\mu_i P_{TGi} \right) \right]$$
 (5.5)

Where ω_i , μ_i α_i , β_i , γ_i signifies emission-coefficients related to the i^{-th} generator. These coefficients represent the emissions intensity or emission rate of specific gases, such as SOx or NOx, per unit of power generated by that particular generator.

In recent years, to tackle the global warming, numerous countries have been exerting significant pressure on the entire energy industry to minimize carbon emissions. a carbon tax C_{tax} is imposed on emitted greenhouse gases. The emission cost is calculated by multiplying the carbon tax rate C_{tax} by the emissions (E) in \$/h. This encourages investment in cleaner power sources like wind and solar and addresses the environmental impact of emissions. The cost of emission in (\$/h) is represented as [51]:

Emission cost:
$$Em = C_{tax} \times E$$
 (5.6)

5.2.1.3 Real Power Losses:

In the (OPF) problem, additional system parameters such as the power loss in the network transmission. These parameters are crucial indicators of system efficiency and stability. Power loss in the transmission system is an inherent outcome, primarily stemming from the resistance within the transmission lines. The commonly employed equation for calculating network loss is as follows [97]:

$$pl = \sum_{q=1}^{nl} G_{q(ij)} \left[V_i^2 + V_j^2 - 2V_i V_j \cos(\delta_i - \delta_j) \right]$$
 (5.7)

Where nl is the total number of transmission lines, $G_{q(ij)}$ is the conductance of the branch i-j, V_i and V_j are the voltages at bus i and j respectively, $\delta_{ij} = \delta_i - \delta_j$, is the difference in voltage angles between them.

5.2.1.4 Voltage Deviation:

Voltage deviation is a parameter used to evaluate the quality of voltage in a network. It represents the cumulative difference between the voltages of all load buses (PQ buses) and the nominal value of 1 per unit (p.u.). Mathematically, it is calculated as the sum of the deviations of each load bus voltage from the nominal value. The voltage deviation is expressed by the following equations [98]:

$$VD = \left(\sum_{p=1}^{NL} \left| VL_p - 1 \right| \right) \tag{5.8}$$

5.2.2 Objective Functions

5.2.2.1 Minimization of Total Generation Cost

The first objective function formulates the cost of energy production taking into account presence of (RES), whereby all the cost-functions above-mentioned are involved. This objective aims to minimize the total generation cost of all types of generators in the system, including thermal, wind, and solar sources. It can be mathematically expressed as:

$$OF^{1} = TC_{Th}(P_{TG}) + \sum_{j=1}^{N_{WG}} \left[C_{W,j}(WP_{Sc,j}) + RC_{W,j}(WP_{G,j} - WP_{Av,j}) + PC_{W,j}(WP_{Av,j} - WP_{Sc,j}) \right] + \sum_{k=1}^{N_{SG}} \left[C_{S,k}(SP_{Sc,k}) + RC_{S,k}(SP_{Sc,k} - SP_{Av,k}) + PC_{S,k}(SP_{Av,k} - SP_{Sc,k}) \right]$$

$$(5.9)$$

Where N_{SG} and N_{WG} represent the number of PV solar and wind generators in the grid.

5.2.2.2 Minimization of Emission Gases with Carbon Tax

In this case, the carbon tax C_{tax} was considered as penalty implemented through minimizing the emission and power generation costs, which can be expressed mathematically as follows:

$$OF^2 = OF^1 + C_{tax} \times Em (5.10)$$

the carbon tax C_{tox} is equal to 20 (\$/h).

5.2.2.3 Minimization of The Real Power Losses

The equation (17) used for minimizing the overall real power losses of the network is as follows:

$$OF^{3} = ploss = \sum_{q=1}^{nl} G_{q(ij)} \left[V_{i}^{2} + V_{j}^{2} - 2V_{i}V_{j}\cos(\delta_{i} - \delta_{j}) \right]$$
 (5.11)

5.2.2.4 Minimization of The Voltage Deviation

The equation (14) used for minimizing the voltage deviation on all buses of the network as follows:

$$OF^{4} = VD = \left(\sum_{p=1}^{NL} |VL_{p} - 1|\right)$$
 (5.12)

5.2.3 **System Constrains**

5.2.3.1 Equality-Constraints

The equality constraints in power systems consist of the power balance equations, which require that the total active power and reactive power generated within the power system is equal to the total demand and losses in the network.

$$P_{TGi}^{\min} \le P_{TGi} \le P_{TGi}^{\max}, \qquad i = 1, 2, ..., N_{TG}$$
 (5.13)

$$P_{Wsj}^{\min} \le P_{Wsj} \le P_{Wsj}^{\max}, \qquad j = 1, 2, \dots, N_{WG}$$
 (5.14)

$$P_{SG,k}^{\min} \le P_{SG,k} \le P_{SG,k}^{\max}$$
 $k = 1, 2 \dots N_{SG}$ (5.15)

$$Q_{TGi}^{\min} \le Q_{TGi} \le Q_{TGi}^{\max}, \tag{5.16}$$

$$Q_{Wsj}^{\min} \le Q_{Wsj} \le Q_{Wsj}^{\max}, \qquad i = 1, 2, ..., N$$
 (5.17)

$$Q_{SG,k}^{\min} \le Q_{SG,k} \le Q_{SG,k}^{\max} \qquad k \in N_{SG}$$
 (5.18)

$$Q_{C_i}^{\min} \le Q_{C_i} \le Q_{C_i}^{\max} \qquad i \in N_C \tag{5.19}$$

$$V_{Gi}^{\min} \le V_{Gi} \le V_{Gi}^{\max}, \tag{5.20}$$

$$V_{Li}^{\min} \le V_{Li} \le V_{Li}^{\max} \qquad i \in NLB$$
 (5.21)

5.2.3.2 Security Constraints

$$T_k^{\min} \le T_k \le T_k^{\max} \qquad k \in NT \tag{5.22}$$

$$T_k^{\min} \le T_k \le T_k^{\max}$$
 $k \in NT$ (5.22)
 $S_i \le S_i^{\max}$ $i \in LN$ (5.23)

Equations (5.13) - (5.15) establish the active power constraints for thermal power plants, wind power generators, and solar PV power generators respectively. Equations (5.16) - (5.19) represent the reactive power capabilities of thermal power plants, wind and solar PV generators, and shunt reactive power sources. Equation (5.20) outlines the generator voltage, while Equation (5.21) define the voltage limits for load buses, where NLB represents the number of load buses. Security constraints related to tap changing transformers and line capacities are expressed in Equations (5.22) and (5.23) respectively, with LN denoting the number of lines in the electric grid.

When dealing with constraints, the static-penalty function method has been widely used, typically involving a trial-and-error process. However, selecting inappropriate penalty coefficients can lead to constraint violations. To address this issue, a technique of constraint handling known as the Superiority of Feasible Solutions is employed to ensure the feasibility of solutions. more details are given in [52].

Table 5-1: EKOA Process Dealing With OPF

Step 1	Read KOA input and data of the test system
	Read input data: Line-data, Bus-data, transformers-data and generation-data.
	• Dimension (dim =12 for 30-bus, 60 for 114-bus)
	• Population size: $N \ (N = 30 \text{ for and } N = 60 \text{ for } 30 \text{ bus and } 114\text{-bus respectively })$
	• Stopping criteria (TMAX) the iterations maximum number
	Min and Max control variables values
Step 2	• Specify objective functions ($OF^1, OF^2,$)
Step 3	• Calculate the anticipated -output power of WG and SPV generators.
Step 4	• create the initial population of N individuals in the range [LB , UB]
Step 5	• Execute power-flow (runpf) for every updated individual within the population, assess the fitness of all individuals, and subsequently evaluate constraint the functions along with constraint violations.
Step 6	Apply the KOA update equations to generate a new population.
Step 7	 During the selection phase, individuals are substituted in the next population if they demonstrate improved values in the objective function, following every update, any new individual will be considered better if they yield negligible or zero constraint violations compared to the corresponding individual in the old population. Otherwise, the previous individuals are maintained.
Step 8	• Repeat the steps 5 and 7 until (TMAX) the iterations maximum number is reached.
Step 9	• Present the optimal results corresponding to the best pathfinder, along with its fitness value

5.3 Simulation Results

for the purpose of proving the effectiveness and practicality of the EKOA for addressing stochastic OPF problems that incorporate solar pv and wind power generators, we conducted an analysis on the modified IEEE 30 bus network and the Algerian electricity network DZA 114bus. Table 5-1 represent the process of EKOA dealing with the optimization data. Various objective functions were considered during the examination. The implementation of the proposed algorithm was carried out using the MATLAB software, and the simulations were performed on a personal computer equipped with an Intel CoreTM i7-8300H 2.22 GHz processor and 8.00 GB RAM. In order to determine an appropriate population size for the Kepler Optimization (KOA) algorithm, empirical tests were conducted by executing the algorithm with varied population sizes, such as 20, 40, 60, and 80. The specific results of these tests are not provided in this document; however, we only mention the population sizes that yielded the best outcomes. Consequently, for all simulation cases, a population size of 30 individuals was selected for the IEEE 30-bus network, while 60 individuals

were chosen for the DZA 114-bus system. Furthermore, the iterations maximum number was set to 300 for the IEEE 30-bus network 400 and for the practical 114-bus power system. To ensure an equitable comparison, the control variables of the two test systems were treated as continuous variables.

5.3.1 Test System 1: Modified IEEE 30 Bus Power System

With the aim of demonstrating the effectiveness of the Enhanced Kepler optimization algorithm, a series of case studies were conducted on the IEEE-30 bus system, which was modified by incorporating two wind generators at buses 5 and 11, as well as a solar PV generator at bus 13. The configuration of the system represented in Figure 5-1. Detailed data can be found in reference [64]. The deterministic (OPF) scenarios for the modified system configuration were analyzed, specifically excluding the wind turbine generators (WT) and photovoltaic (PV) units. Four different cases were examined, each with their respective objective functions as outlined in the previous section. The findings of the case studies utilizing the Kepler algorithm are presented in a tabulated format, along with corresponding explanations provided in this section.

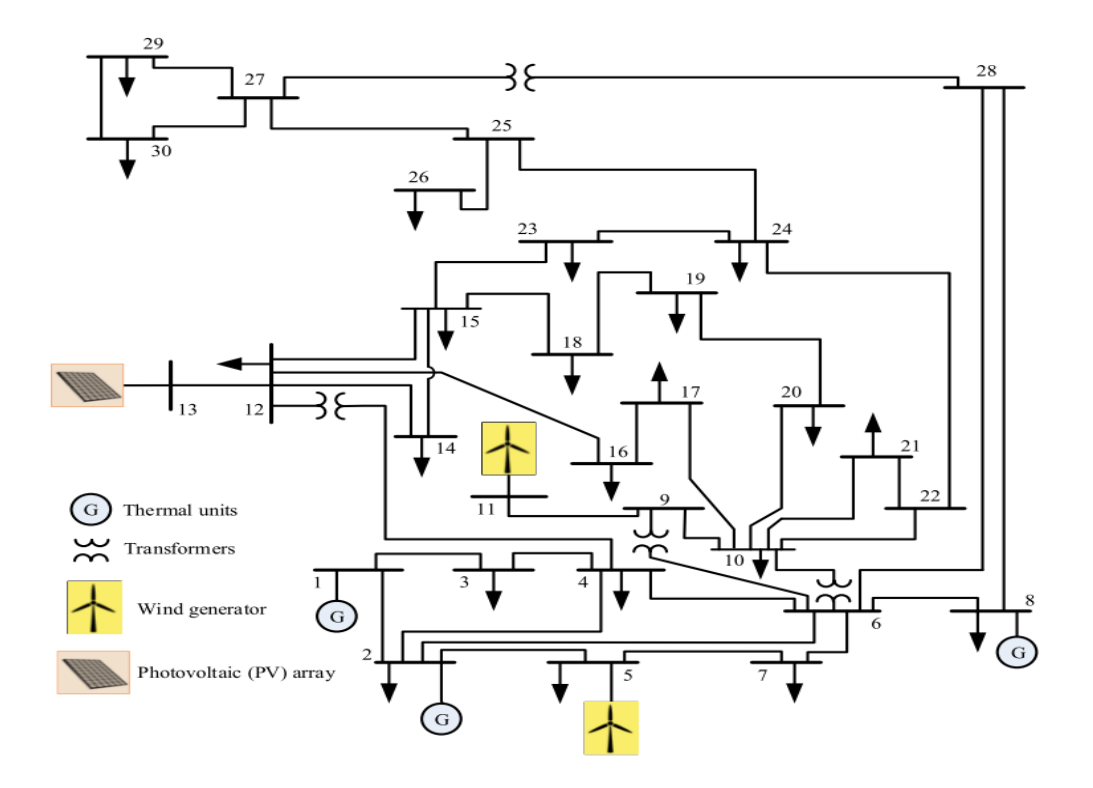


Figure 5-1: Modified IEEE 30 Bus System Configuration [51]

Table 5-2: Emission And Cost Coefficients Of Thermal Generators Of IEEE 30 Bus Network [62]

Generator	Bus	a	b	c	d	e	α	β	γ	ω	μ
ThG1	1	0	2	0.0038	18	0.037	0.04091	-0.05554	0.06490	0.0002	6.667
ThG2	2	0	1.75	0.0175	16	0.038	0.02543	-0.06047	0.05638	0.0005	3.333
ThG3	8	0	3.25	0.0083	12	0.045	0.05326	-0.03550	0.03380	0.0020	2.000

 Table 5-3:PDF Parameter Of Wind And Solar Pv Units[51]

		Wind-pow	er generating farm	
Position of	No of	Rated power, P _{wr}	Weibull PDF	Weibull mean, M _{wbl}
Windfarm	turbines	(MW)	parameters	
Bus # 5	25	75	c = 9 k = 2	v = 7.976 m/s
Bus #11	11 20 60		c = 10 k = 2	v = 8.862 m/s
		Photovo	ltaic power plant	
Position of Solar	Rated p	ower, P_{rv} (MW)	Lognormal PDF	Lognormal mean
system	system		parameters	
Bus #13	Bus #13 50		μ = 6, r = 0.6	$G = 483 \text{ W/m}^2$

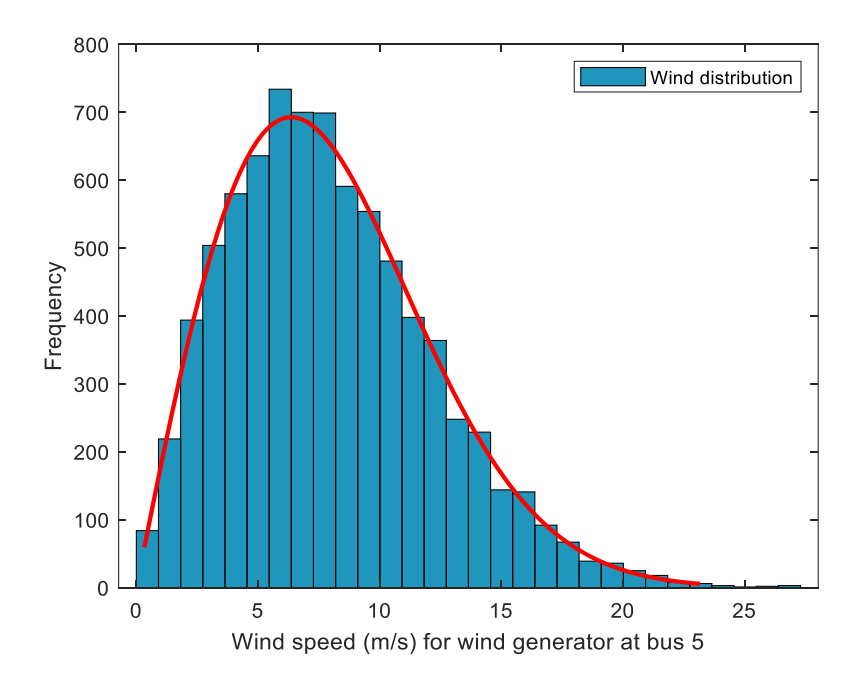


Figure 5-2: Speed Of Wind Frequency For Wind Generator At Bus 5

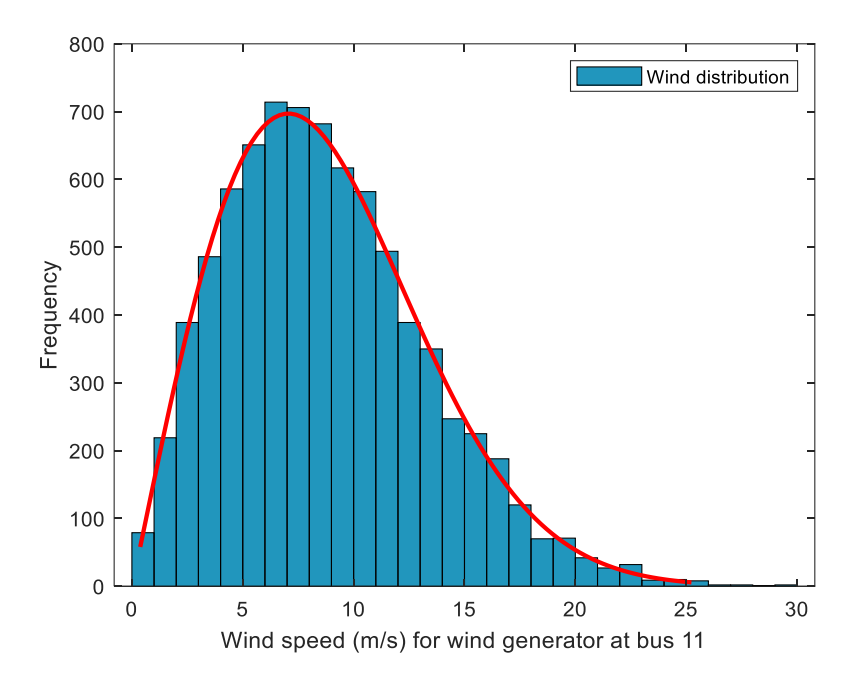


Figure 5-3: Wind Speed Frequency For Wind Plant At Bus 11

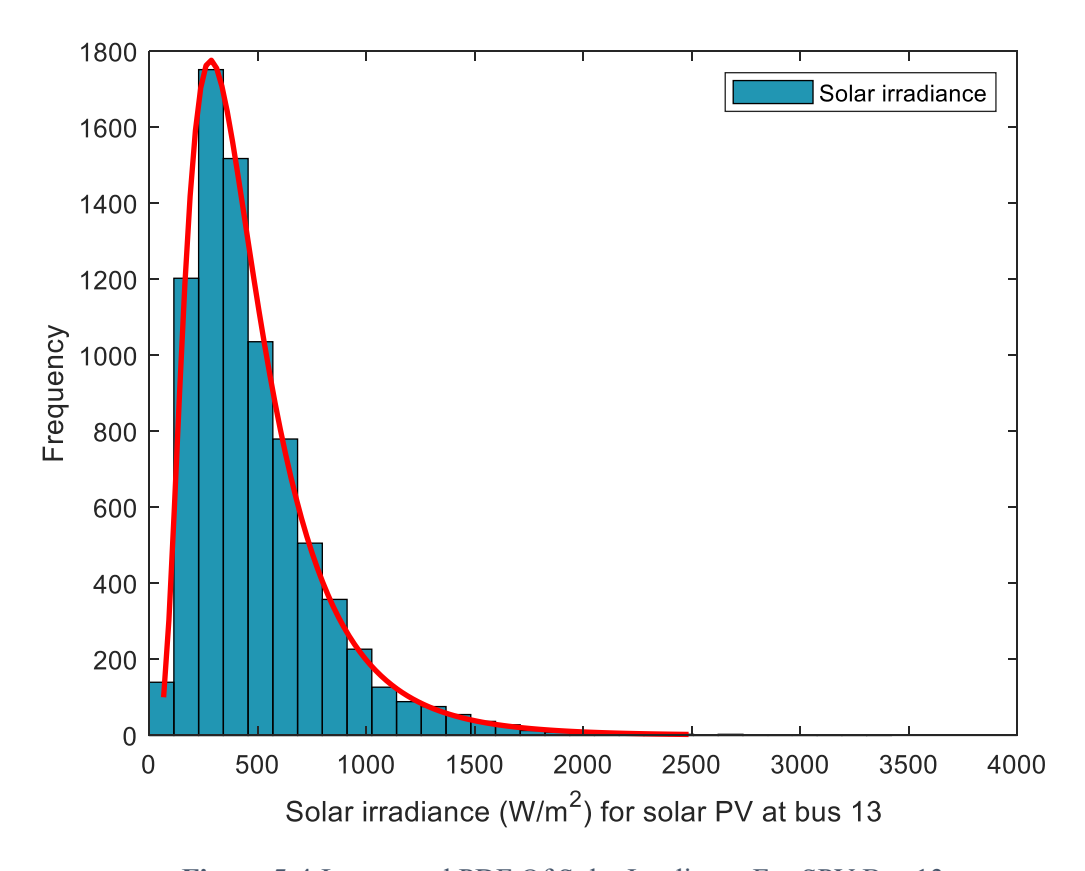


Figure 5-4:Lognormal PDF Of Solar Irradiance For SPV Bus 13

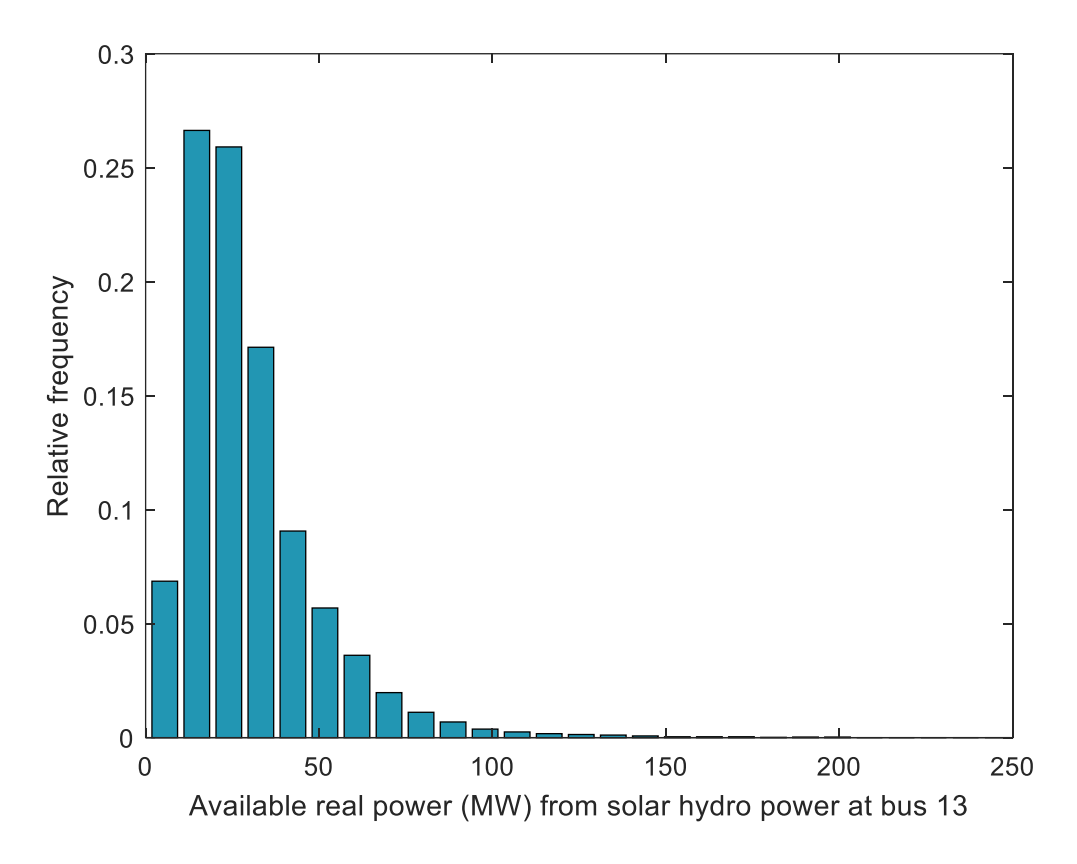


Figure 5-5: Aviable Real Power From Solar PV Unit

5.3.1.1 Case 1: Total Generation Cost Minimization

In the first case, the main objective is to minimize the total generation cost, taking into account the contributions from wind, solar. Where these last two both have the direct, penalty and reserve costs, the results obtained are based on the parameters of Weibull, lognormal probability density functions (PDFs). The specific PDF parameters for the RES can be found in Table 5-2, which is referenced in [51]. The fitting of the Weibull distribution and the frequency distribution of wind speeds are depicted in Figure 5-2, generated via the simulation of 8000 Monte-Carlo scenarios. Additionally, Figure 5-4 displays the fitting of the lognormal distribution and the frequency distribution of solar irradiance, obtained from the simulation of a sample size of 8000 Monte Carlo scenarios. The selection of optimal sites for wind farms and PV power generation is influenced by various factors, including wind speed and solar radiation [29].

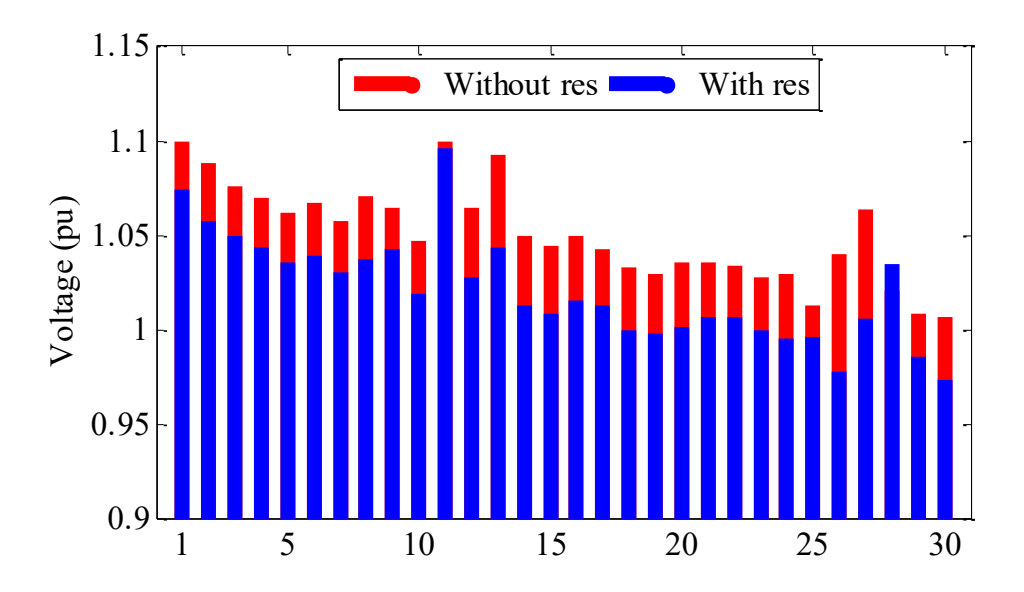


Figure 5-6: Voltage Profile Of 30 BUSS With And Without RES

The results indicate that among the compared optimizers, EKOA consistently achieves the lowest generation cost. as demonstrated in Table 5-3. The optimal generation cost attained by EKOA is **780.939** and 781.18 MW by the KOA, while other optimization techniques, such as PSO (Particle Swarm Optimization), yield 784.3400 \$/h, TLBO (Teaching-Learning-Based Optimization) results in 782.676 (\$/h), SHADE-SF (Shade-based Success-History Feedback) generates 782.50 \$/h, jellyfish optimization produces 781.638 (\$/h),the artificial ecosystem optimizer achieves 781.521(\$/h), the hunger games search obtains 781.86 (\$/h),, orca predation algorithm generates 782.076 (\$/h),and the gorilla troops optimizer (GTO) obtains 781.26 (\$/h),,(GBLCSBO) 781.80 (\$/h), and slim mould algorithm (SMA) 781.07(\$/h).

Based on the literatures and the simulation results presented in Table 5-3, It can be inferred that the integration of (RES) leads to a decrease in the total power production cost. The initial reference cost of thermal power production is about 800.00 \$\frac{1}{2}\$/h reduced to 780.939\$/h, resulting in a cost reduction of approximately 19.06 \$\frac{1}{2}\$/h. To put it more precisely, if this cost-saving rate of 19.06 \$\frac{1}{2}\$ per hour is maintained throughout the operating time of 7500 hours per year, the proposed optimizer EKOA can save a total of 142950 \$\frac{1}{2}\$ annually. This clearly indicates that the incorporation of solar PV power plants and wind generators substantially contributes to decreasing the total generation cost when compared to the initial system configuration without renewable energy sources. For further comparison and statistical analysis for the case 1 of the EKOA algorithm with other algorithms, please refer to Table 5-4.

Table 5-4:Optimal results for variables and objective function in Case 1

Variables	Min	Max	SHADE -SF[51]	PSO [64]	JS [99]	GTO [60]	TLBO [52]	SMA [52]	GBLCSB O[100]	KOA	EKOA
P _{TG1}	50	140	134.908	134.90	134. 905	134.907	134.843	134.91	134.9079	134.909	134.91
P _{TG2}	20	80	28.564	28.037	29.0226	28.1779	29.0639	29.4961	28.955	28.8857	27.47
Pwg1	0	75	43.774	43.744	43.9696	43.2909	44.045	42.2527	43.9896	43.7583	43.36
P _{TG3}	10	35	10	10.000	10.0006	10.0000	10.0606	10.0034	10	10.0004	10.00
PwG2	0	60	36.949	37.193	37.0193	36.5917	36.6258	37.1432	37.1254	37.1741	36.32
P _{SG1}	0	50	34.976	35.303	34.2532	36.1438	34.5823	35.3402	34.1873	34.3757	37.0.5
V_1	0.95	1.1	1.072	1.0815	1.07725	1.0725	1.0756	1.07226	1.0724	1.0743	1.073
V ₂	0.95	1.1	1.057	0.9500	1.05698	1.0578	1.0587	1.0590	1.0575	1.0584	1.057
V ₅	0.95	1.1	1.035	1.1000	1.03507	1.0374	1.0411	1.0349	1.0354	1.0365	1.035
V ₈	0.95	1.1	1.04	1.1000	1.03705	1.0395	1.0353	1.0396	1.0398	1.0383	1.040
V ₁₁	0.95	1.1	1.1	1.1	1.0983	1.1000	1.0874	1.100	1.0988	1. 0959	1.100
V_{13}	0.95	1.1	1.055	1.0626	1.04571	1.0548	1.0359	1.0511	1.0543	1.0439	1.056
Q _{TG1}	-20	150	-1.903	15.679	-0.6835	-2.6423	4.51	-4.5670	-1.8791	1.08	-1.0644
QTG2	-20	60	13.261	- 20	11.0011	12.5121	12.0447	17.6960	13.2879	13.15	11.5386
QwG4	-30	35	23.181	35.00	22.6673	4.65643	29.9474	1.9840	23.1688	3.89	2.8333
Q _{TG3}	-15	40	35.101	40.00	40.0	32.0473 0	30.7341	32.6825	35.1479	32.30	32.7563
QwG5	-25	30	30	27.85	30	29.7031	27.9642	29.9006	30	29.15	29.6765
QsG6	-20	25	17.346	17.73	14.0246	16.0907	11.8604	14.7003	17.2537	12.61	16.3878
Tc	ost (\$/h)		782.503	781.90	781.638	781.262	782.676	781.078	781.80	781.189	780.939
V	D(pu)		/	/	0.4421	0.4838	/	0.4701	0.4627	0.45932	0.4852
PLos	ss (MW)	/	/	5.7738	5.7117	/	5.7117	5.7653	5.6977	5.7019

Algorithm	Minimum (\$/h)	Maximum (\$/h)	Mean (\$/h)	Std
PSO [64]	781.9047	794.4220	784.904776	2.52e + 00
GOA [64]	785.7109	823.4731	804.016837	9.52e + 00
ALO [64]	781.6562	791.9234	784.325274	2.49e + 00
GWO [64]	781.6645	783.3359	783.041218	2.75e - 01
GSA [64]	782.2237	794.8995	785.860254	2.43e + 00
BMO [64]	781.6519	783.5283	781.81867	3.44e - 01
MFO [64]	781.6928	783.9304	782.49197	4.77e - 01
SMA [52]	781.07	782.990	781.9726	4.53e - 01
HGS [52]	781.86	782.9445	782.4106	3.649e - 01
AEO [52]	781.3979	782.8744	781.8199	3.095e - 01
GTO [60]	781.2626	782.7022	782.082	3.77e - 01
CSBO [100]	782.2169	783.2244	782.8519	9.1e-01
TLBO [100]	782.3418	783.6428	782.6428	1.48e+00
SOA [100]	785.6410	782.5584	783.8291	3.37e+00
MVO [100]	782.6425	786.1347	783.9558	4.15e+00
GBL	781.8010	782.0075	781.9034	8.00e-2
CSBO [100]	/81.8010			0.00C-2
KOA	781.1895	783.0159	782.1351	4.44e - 01
EKOA	780.9396	782.3084	781.7237	4.13e-01

Table 5-5: Statistical Analysis For Case 1 Of EKOA With Other Algorithms

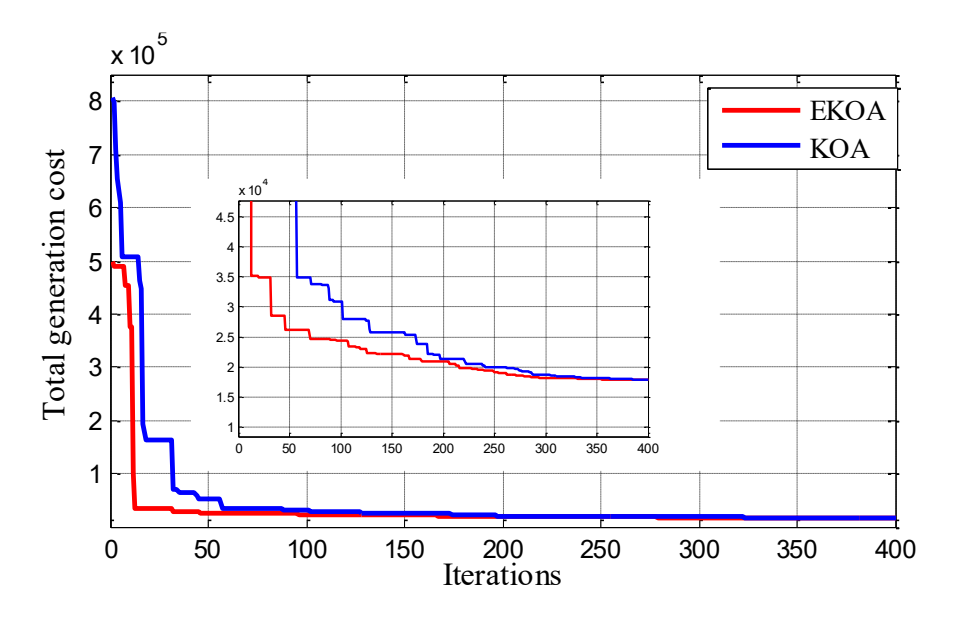


Figure 5-7: Convergence Curve For Case 1 30-Bus System

5.3.1.2 Case 2 Minimizing the Total Cost with Emission-Carbon Tax

In the second case, the minimization of the quadratic emission and total power production cost functions was conducted, taking into account the carbon tax referred to as (Ct) applied to thermal power generators. The specified carbon tax value is set at 20 \$/ton. The introduction of the carbon tax notably increases the level of (RES) penetration, as evident in the simulation

results listed in Table 5-6. The penetration ratio of RES in the optimal generation schedule is determined by the emission rate, influenced by carbon tax value. The primary objective is scheduling more power from the (RES) to keep the emission volume at minimum level.

Table 5-6: Optimal Results For Variables And Objective Function In Case 2

Variables	SHADE-SF	MFO [64]	BMO [64]	JS [99]	SMA[52]	GTO[60]	GBLCSB O[100]	KOA	EKOA
P _{TG1}	123.020 33.047	123.637 33.2996	123.127 31.947	123.572 33.1626	123.6670 33.5199	123.3721 32.7853	123.1690 33.1017	123.37 32.5293	123.28 32.5222
PwG1	46.021	46.1099	45.402	46.0806	46.2945	45.8351	45.5216	45.7033	45.7553
P _{TG3}	10.00	10.0000	10.000	10.00	10.000	10.00	10	10.00	10.00
PwG2	38.748	38.8443	38.270	38.8011	39.2413	38.5999	38.3516	38.5416	38.5304
P _{SG1}	37.336	36.7199	39.865	37.0628	35.9774	38.0833	39.5323	38.4039	38.4683
\mathbf{V}_1	1.071	1.0782	1.0777	1.07066	1.0731	1.0702	1.0703	1.0765	1.0703
V_2	1.057	1.0645	1.0640	1.05715	1.0589	1.0569	1.0568	1.0626	1.0567
V ₅	1.036	1.0432	1.0426	1.03604	1.0378	1.0357	1.0357	1.0410	1.0354
V_8	1.04	1.0473	1.0471	1.04038	1.0414	1.0403	1.0403	1.0451	1.0396
V ₁₁	1.099	1.1000	1.1000	1.0983	1.0980	1.0985	1.0999	1.100	1.1000
V ₁₃	1.056	1.0591	1.0602	1.05575	1.0581	1.0580	1.0566	1.0588	1.0552
QTG1	-2.678	- 1.738	- 1.8489	-2.6666	2.4424	-3.24025	-2.7561	-1.4312	-2.6159
QTG2	12.319	12.565	12.4064	12.3540	17.9378	12.55509	12.2171	11.6961	11.8523
QwG4	35.27	22.889	22.9177	35.2538	25.9879	22.83972	23.0089	2.1329	2.4963
Q _{TG3}	22.964	35.847	35.6862	22.9990	39.5619	34.9987	35.1591	33.3865	32.8828
QwG5	30	28.500	28.5058	30.00	29.8480	30.00	30.00	28.1412	29.9101
QsG6	17.779	16.659	17.0942	17.7114	18.5039	18.50504	18.0477	15.	16.3490
T _{Cost} (\$/h)	810.346	811.422	810.7982	810.120	810.3875	810.4412	810.5507	810.1167	809.89
Emission (t/h)	0.891	/	0.88338	0.8937	0.8986	0.8836	0.87348	0.8836	0.8812

5.3.1.3 Case 3: Optimized Cost Vs the Reserve Cost

In this case, all parameters remain unchanged from case 1, except for the reserve-cost coefficients. Specifically, the coefficients of solar PV and wind units were incrementally adjusted in discrete steps of 1, commencing from 4 and reaching 6. Specifically, we considered three cases: (RK)=4 (case3-1), RK= 5 (case3-2), and up to RK= 6 (case3-3). However, the coefficients of penalty-cost for all (RES) remain unchanged from case 1. The optimal power schedules of the generators are depicted with a bar graph in Figure 5-8, allowing for a comparison with the schedules obtained in the base case (case 1).

When examining this case study, it was Noticed that as the reserve cost coefficient increased, the participation of the wind and solar PV generators gradually decreased as shown in figure (5-8,5-9), leading to a shortfall in the scheduled power. Consequently, an immediate provision of spinning reserve became necessary to address this deficit. The compensatory measure involved thermal generators, which consequently raised the thermal power generation cost due to the amplified output power, in contrast the cost of solar PV wind units decreases as depicted in Figure 5-10.

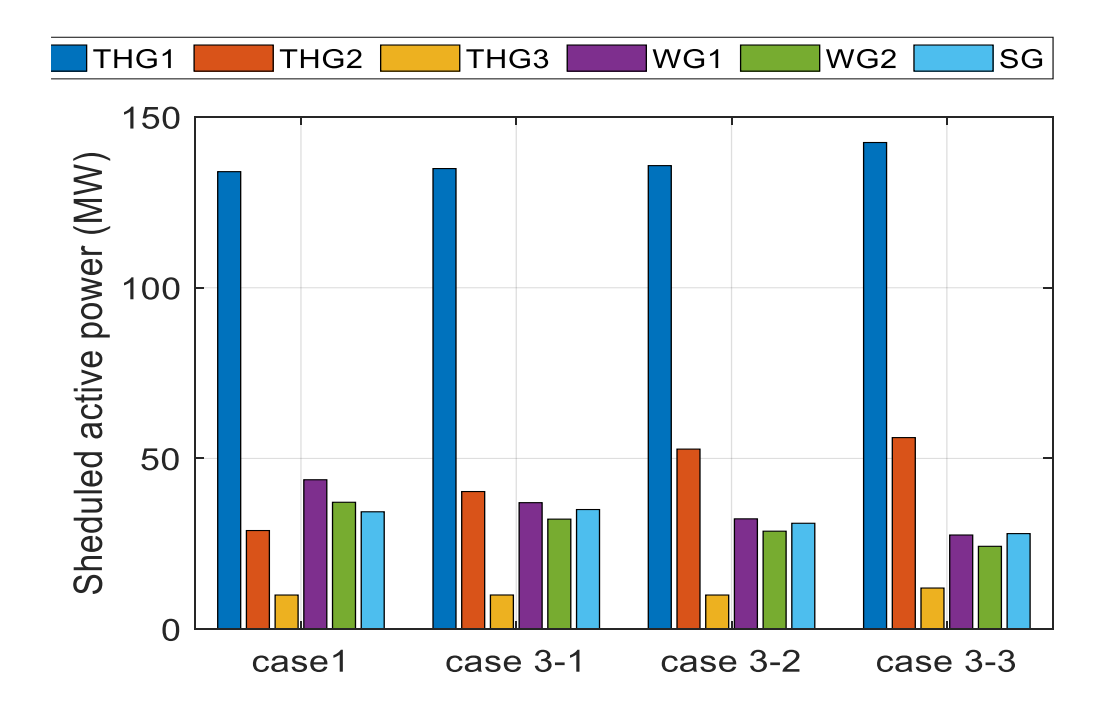


Figure 5-8: Variation Of The Scheduled Active Power Vs The Reserve Cost

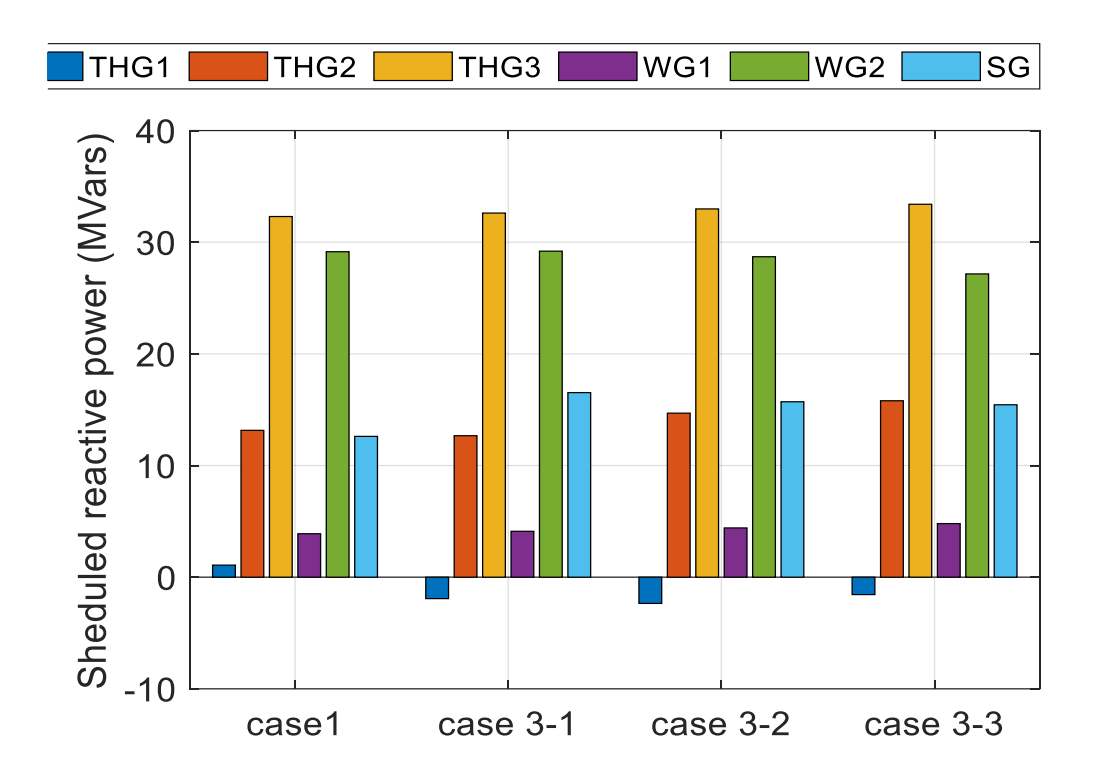


Figure 5-9: Variation Of The Scheduled Reactive Power Vs The Reserve Cost Coefficients

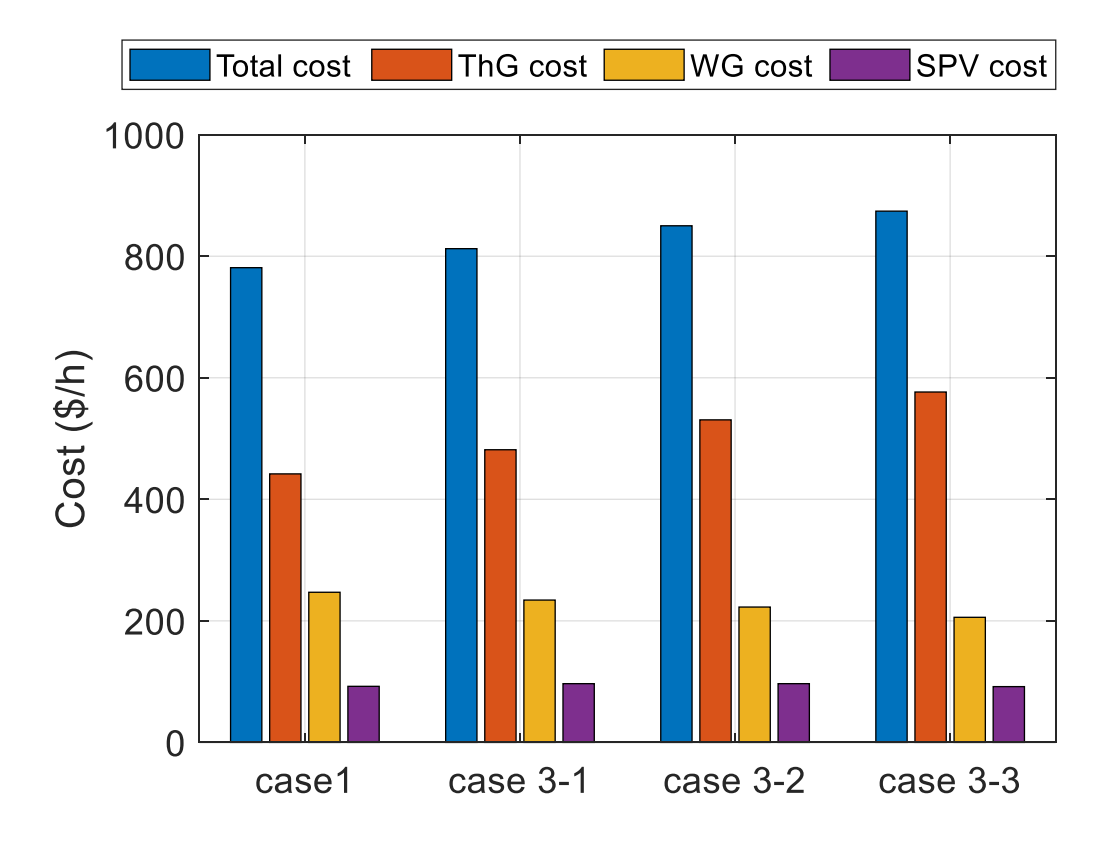


Figure 5-10: Variation Of Production Cost Against Reserve Cost Coefficients

5.3.1.4 Case 4: Optimized Cost vs the Penalty Cost

In the fourth case, the reserve cost parameters remain unchanged from case 1, with the exception of the penalty cost coefficients. Specifically, the penalty-cost coefficients for all wind generators and the photovoltaic power plant are elevated from 4 to 6 in a sequential order: PK = 4 (case 4-1), PK = 5 (case 4-2), and PK = 6 (case 4-3). Figure 5-11 and 5-12 presents a bar graph showing the optimal active and reactive power schedules respectively for the six generators in comparison to those obtained in case 1, also shown in the same figure. When figure 5-13 shows the different production costs variations with the variation of penalty cost.

In the fourth scenario, the reserve cost parameters remain consistent with those of case 1, with the exception of the penalty cost coefficients. Specifically, the penalty-cost coefficients for all wind generators and the photovoltaic power plant are elevated from 4 to 6 in a sequential order.

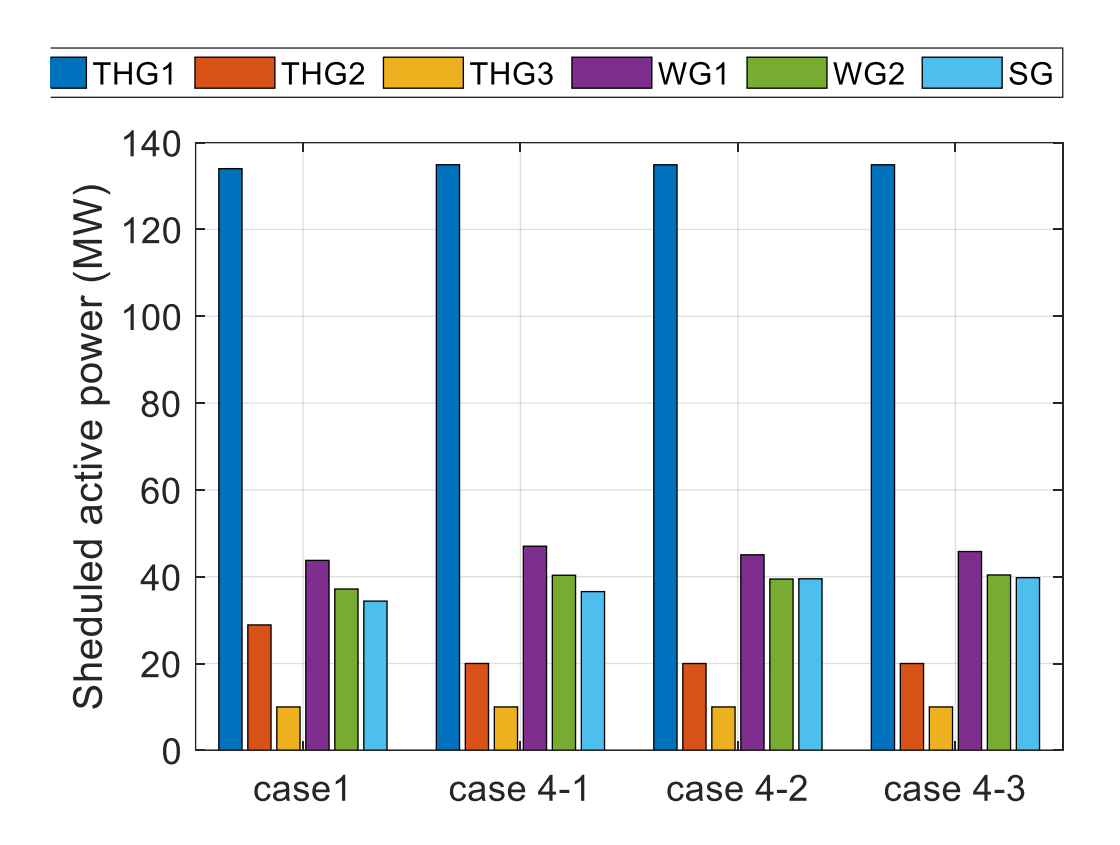


Figure 5-11: Variation Of The Scheduled Active Power Vs The Penalty Cost Coefficients

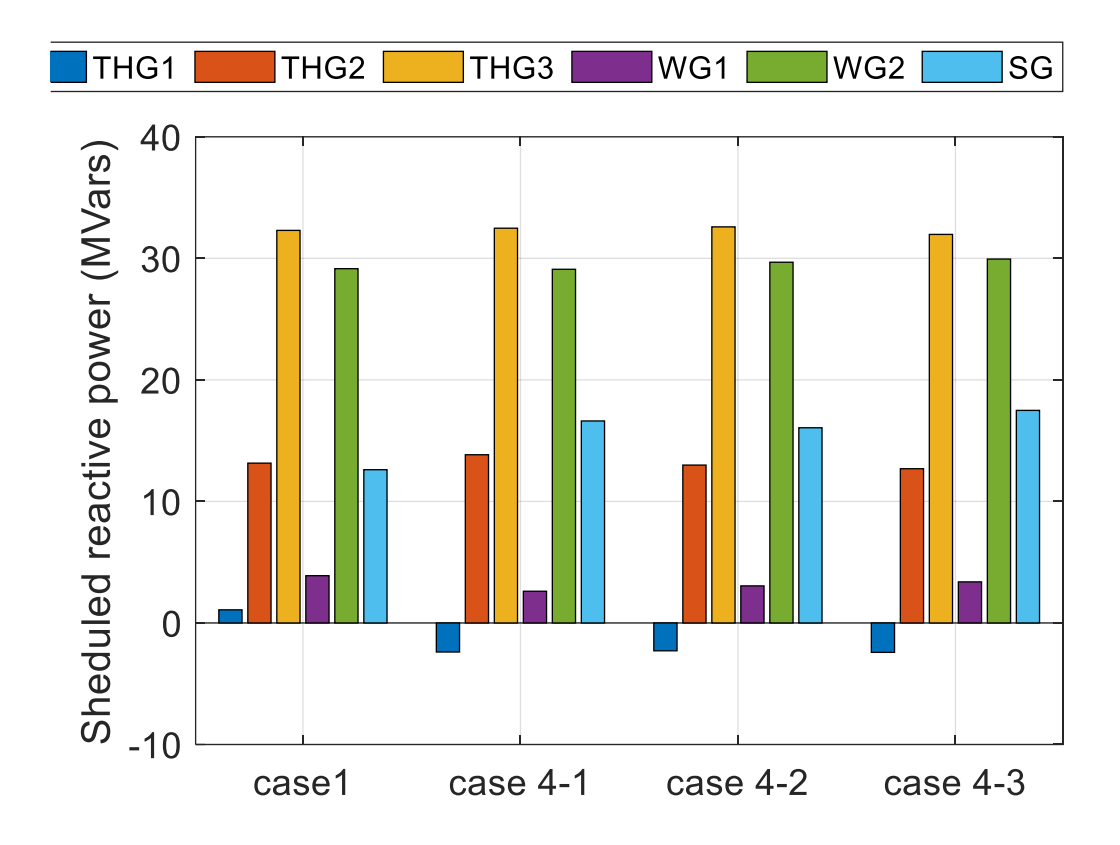


Figure 5-12: Variation Of The Scheduled Reactive Power Vs The Penalty Cost Coefficients

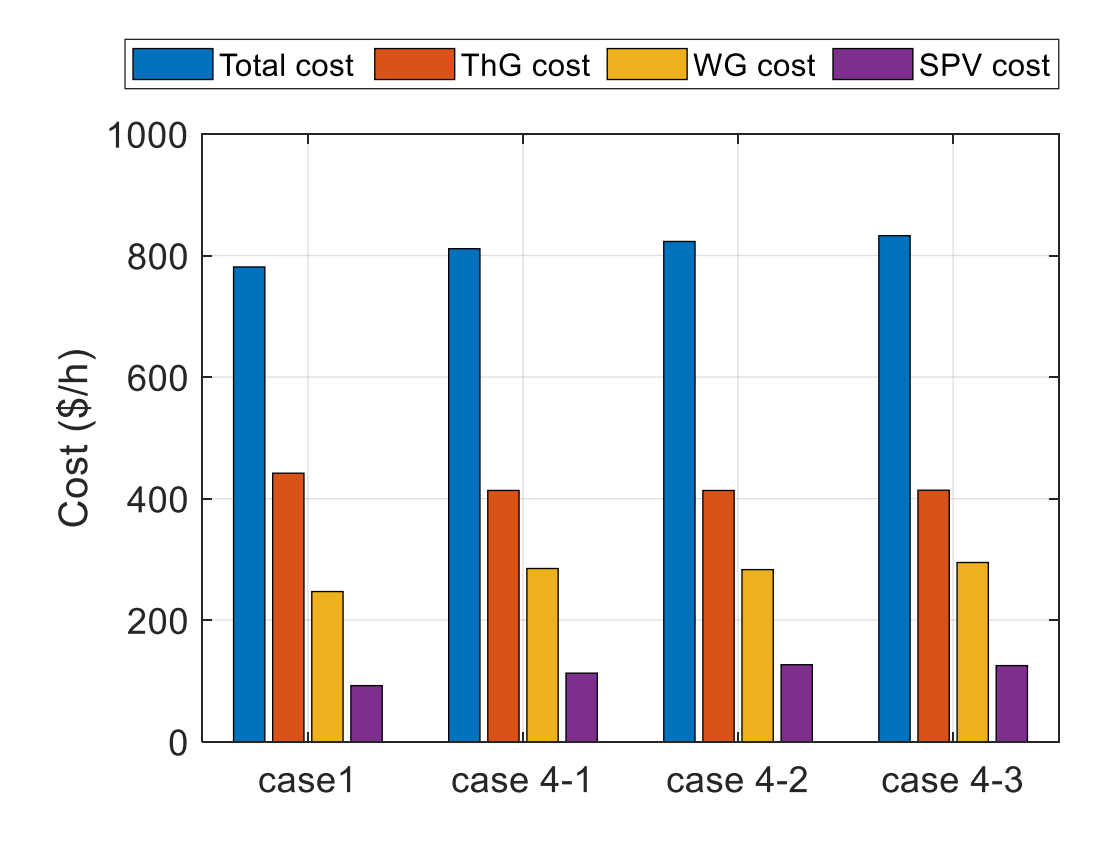


Figure 5-13: Variation Of Production Cost Against Penalty Cost Coefficients

As the penalty cost coefficient increases, the participation of solar PV and wind and generators has gradually increased, leading to an increase in the power scheduled from (RES) generators. As a result, there is a non-uniform decrease in the output of thermal generating units, as shown in Figure 5-13. The economic dispatch analysis among 3 thermal generators indicates that a significant portion of the power is dispatched to the lowest production cost generator. Conversely, the scheduled output of all (RES) also exhibits non-uniform patterns. This variation can be attributed to the inherently nonlinear relationship between the probability density function (PDF) and the reserve and penalty cost associated with solar PV and wind generators. It is worth noting that the cost of thermal generators, decreases while an overall steady increase in the total generation cost is observed.

5.3.1.5 Case 5: Minimization of the Real Power Losses

Case 5 pertains to minimizing the real power losses in transmission lines. MATPOWER is employed to calculate the overall power loss following the execution of the power flow program. Table 5-7 presents a comprehensive overview of the statistical indicators for various algorithms. Notably, the proposed EKOA stands out for its effectiveness and superiority in comparison to KOA and other methods, particularly in terms of power loss results. Table 5-7 reveals that the EKOA consistently produces the lowest values for power losses, underscoring its efficiency in minimizing transmission-related power losses.

Table 5-7: Optimal Results For Variables And Objective Function In Case 5

Variables	Min	Max	TLBO [100]	MVO [100]	SOA [100]	GWO [100]	CSBO [100]	GBLCSB O[100]	КОА	ЕКОА
P _{TG1}	50	140	50.0016	51.3281	50.0004	50.2938	50.0216	50	50.02	50.01
P _{TG2}	20	80	30.178	22.6655	32.5101	35.0292	23.4727	25.089	27.0293	24.86
Pwg1	0	75	74.9997	74.9287	74.999	72.7486	74.959	75	74.993	74.99
P _{TG3}	10	35	34.9989	34.8759	34.998	32.1645	34.882	35	34.923	35
P _{WG2}	0	60	59.9987	59.1338	59.998	58.6623	59.9708	60	59.985	60
P _{SG1}	0	50	40.5396	44.3954	40.5396	36.7714	42.172	40.3852	38.453	40.54
V_1	0.95	1.1	0.9779	1.0072	0.6909	1.052	1.0574	1.0581	1.0580	1.058
V_2	0.95	1.1	1.0546	1.0463	1.0546	1.0505	1.0517	1.0527	1.0522	1.052
V ₅	0.95	1.1	1.0455	1.0195	1.0456	1.036	1.0427	1.0435	1.0431	1.044
V_8	0.95	1.1	1.0784	1.062	1.0836	1.0333	1.0509	1.0995	1.0481	1.049
V ₁₁	0.95	1.1	1.0999	1.0984	1.0991	1.0989	1.0982	1.0968	1.0991	1.099
V ₁₃	0.95	1.1	1.0629	1.0888	1.0628	1.0756	1.0622	1.0567	1.0659	1.060
Q _{TG1}	-20	150	-20	-20	-20	-11.159	-5.3287	-5.2711	-4.613	-4.93
QTG2	-20	60	19.058	317607	18.9776	22.9157	5.1685	6.4460	5.1021	5.93
QwG4	-30	35	20.7905	4.2009	20.9343	20.5827	20.2985	20.4997	0.2937	0.48
Q _{TG3}	-15	40	40	40	40	22.8676	39.6359	40	33.423	30.74
QwG5	-25	30	30	30	30	30	30	30	29.8864	30
QsG6	-20	25	19.4794	25	19.4167	25	19.6931	17.6558	19.9608	17.93
To	T _{Cost} (\$/h)		898.692	887.071	905.958	875.682	880.749	880.638	879.792	880.733
emss	sion(t/h))	0.09766	0.10032	0.09718	0.09703	0.09943	0.09894	0.09842	0.09900
PL	oss (MW)		2.1038	2.2604	2.1038	2.2699	2.0780	2.0741	2.0005	1.9962
V	D(pu)		0.5458	0.4502	0.5452	0.4496	0.52872	0.50841	0.5776	0.55507

5.3.1.6 Case 6: Minimization of Voltage Deviation

Taking into account the importance of voltage in power system analyses, Case 6 is dedicated to minimizing of the voltage deviation of the power system buses. The outcomes of simulations are detailed in Table 5-8, the results underscore the superiority of the EKOA method compared to the KOA and other counterparts, particularly in achieving the minimum voltage deviation. This affirms the efficacy of the EKOA approach.

 Table 5-8: Optimal Results For Variables And Objective Function In Case 6

Variables	Min	Max	TLBO [100]	MVO [100]	SOA [100]	GWO [100]	CSBO [100]	GBLCSB O[100]	KOA	EKOA
P _{TG1}	50	140	74.984	91.002	72.940	82.944	75.208	76.143	84.41	94.60
P _{TG2}	20	80	79.998	79.173	79.421	76.164	79.999	80.00	79.9903	80.00
Pwg1	0	75	74.998	66.035	74.978	72.397	74.999	75.00	68.244	59.5025
P _{TG3}	10	35	34.998	33.602	34.871	32.946	34.999	35.0	34.6914	34.9047
P _{WG2}	0	60	22.812	21.708	27.498	24.093	22.588	22.0151	20.6375	19.5340
P _{SG1}	0	50	0.0004	1.5117	0.2815	0.6766	0.0002	0	0.0676	0.0315
V_1	0.95	1.1	1.0347	1.0119	1.002	0.9996	1.0375	1.0609	1.0462	1.0486
V_2	0.95	1.1	1.0956	1.0687	1.0901	1.0729	1.0937	1.0999	1.0458	1.0484
V_5	0.95	1.1	0.996	0.994	0.9938	0.9951	0.9961	0.9502	0.9932	0.9924
V_8	0.95	1.1	1.098	1.0942	1.0729	1.0451	1.0955	1.0999	1.0247	1.0264
V ₁₁	0.95	1.1	1.0931	1.0992	1.0993	1.0949	1.0965	1.0962	1.0885	1.0905
V ₁₃	0.95	1.1	1.0626	1.098	1.0892	1.0763	1.0598	1.0997	1.0556	1.0573
Q _{TG1}	-20	150	-20	-20	-20	-20	-20	-85837	-16.935	-19.910
Q _{TG2}	-20	60	60	60	60	60	60	60	45.921	50.4937
QwG4	-30	35	-19.66	-17.97	-19.76	-18.95	-19.63	-30	-29.873	-29.871
Q _{TG3}	-15	40	40	40	40	40	40	40	39.9057	39.9916
QwG5	-25	30	30	30	30	30	30	30	29.877	29.9977
QsG6	-20	25	25	25	25	25	25	25	240999	24.9541
To	ost (\$/h)		960.86	956.34	963.97	951.40	960.61	963.205	952.616	942.601
Ems	ssion(t/h)		0.1347	0.1993	0.1298	0.1574	0.1352	0.1376	0.1652	0.2254
	Loss(MW)		4.4405	4.9777	4.3441	4.6582	4.4496	4.7582	4.6413	5.1692
V	D(pu)		0.375	0.3779	0.3766	0.3772	0.3757	0.3752	0.3396	0.3382

5.3.2 Test-system 2: The Modified Algerian DZA 114-BUS Power System

To showcase the efficacy of the suggested EKOA in a real-world practical, large-scale network, the Algerian DZA 114-bus electricity power system has been chosen as the test system the testing ground with some changes in the original configuration. This system encompasses 175 transmission lines with 15 generators, including 16 branches equipped with transformers tap changers. The aggregate power demand stands at (3727 + j 2070) per unit (p.u) with a 100 MVA base.

The 4th bus serves as the slack-bus in the power system. As part of the modification, 2 wind generators have been added to buses 52 and 83, and a solar PV generator has been installed at bus 109. All the necessary data for the test system, in "MATPOWER format," is freely available only to referees. This optimization problem involves a total of 46 variables, which include the active power of 15 generators, also the voltage magnitudes of 15 generators, and adjustments for 16 tap-changers. Additionally, the power system experiences voltage drops at certain buses, posing challenges in ensuring the feasibility of solutions, particularly with regard to reactive power generators. The maximum and the minimum operating limits of the control variables can be found in the table 8.

In this case, only three objective functions were considered, which are the total power production cost minimization and the minimization of the real power losses, and the base case that denotes the total cost generation for the conventional DZA 114 bus system without considering renewable energy sources. These are important cases taken into consideration in both applied aspects and techno-economic studies.

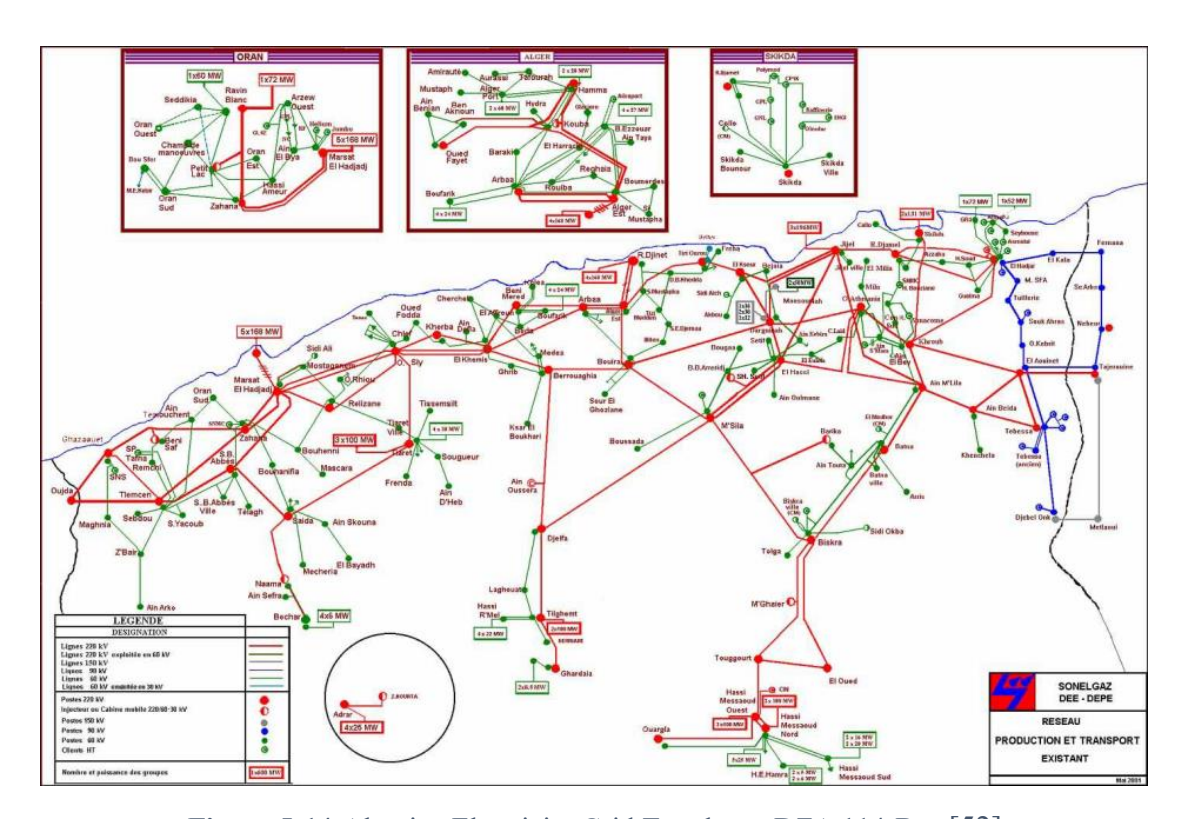


Figure 5-14: Algerian Electricity Grid Topology- DZA 114-Bus [52]

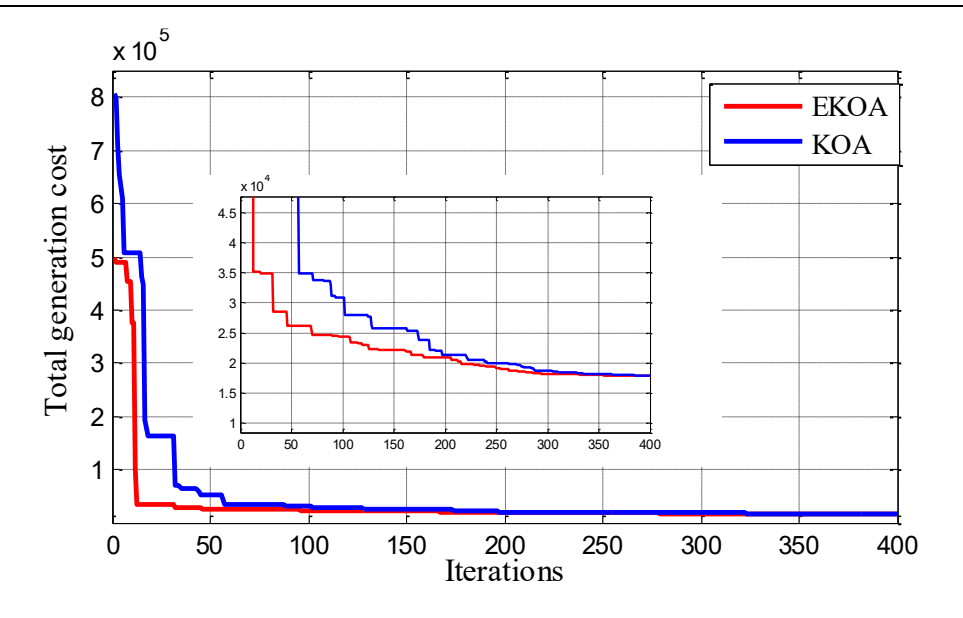


Figure 5-15: Convergence Curve For Case 1 DZA 114-Bus System

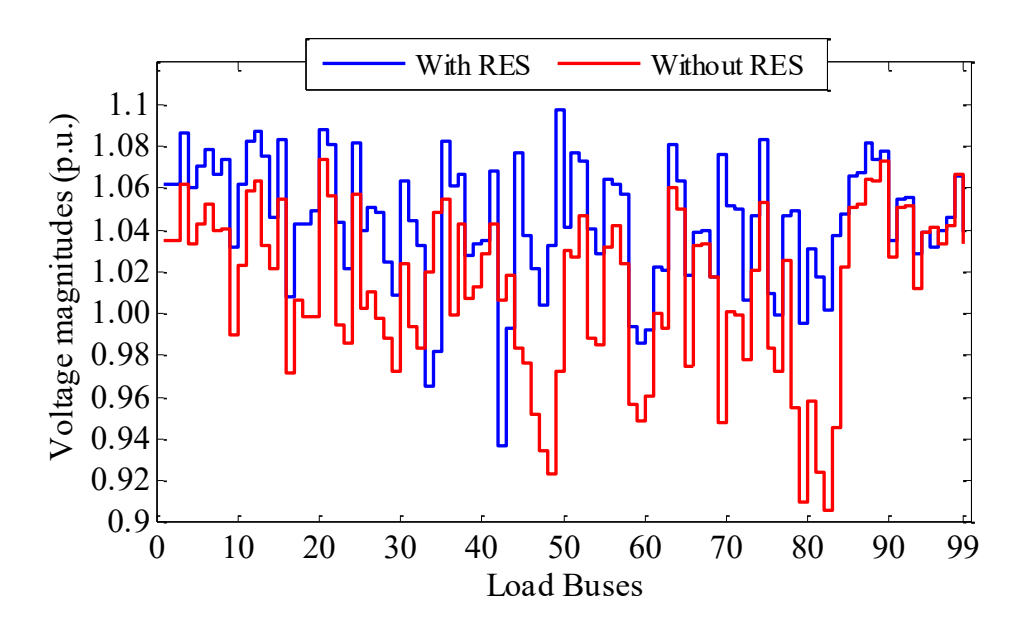


Figure 5-16: Voltage Profile Of DZA 114- Load Buses For Case 1

Table 5-9 presents the maximum and minimum operating limits of control variables, along with the outcomes of various objective functions explored in this case. Notably, the proposed (EKOA) stands out for its remarkable effectiveness and superiority compared to the (KOA).

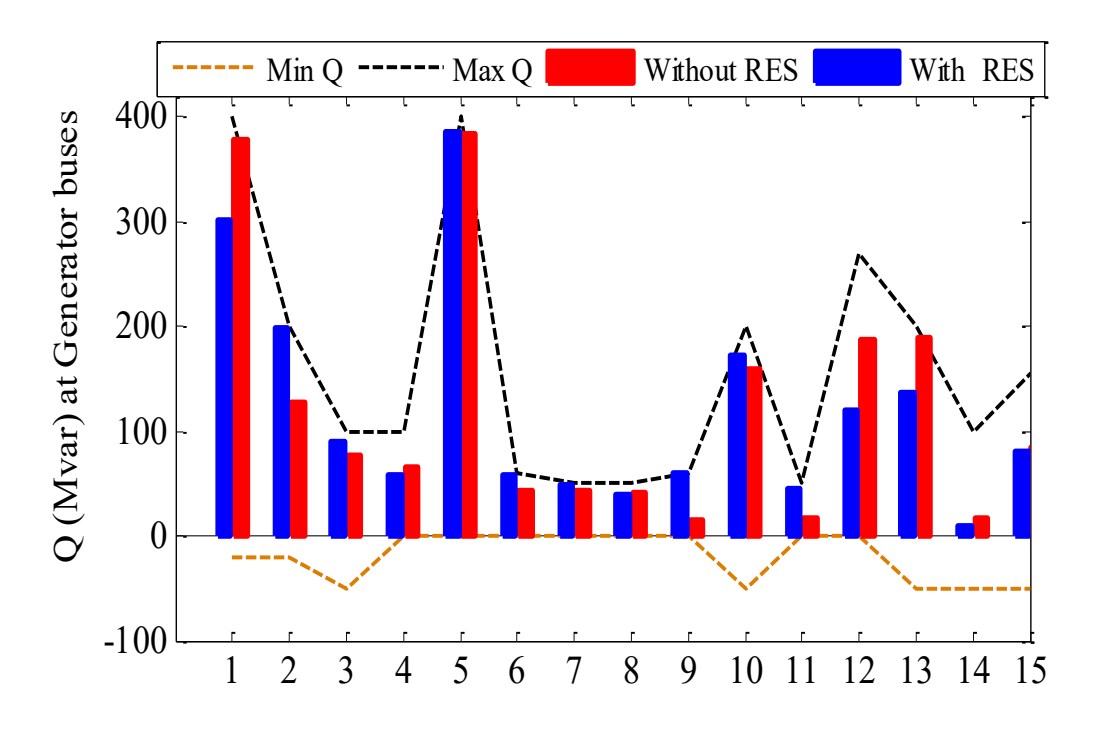


Figure 5-17: Generators Reactive Power For Case 1

In practical system studies, it becomes crucial to demonstrate the advantages resulting from the integration of the (RES), particularly in techno-economic analyses. In the case of the conventional DZA 114-bus system, there is a substantial contrast in the cost of energy production 19,080.9613 (\$/h) before RES integration and \$16,701.773 (\$/h) after integration, reflecting a difference of \$2,379.18 (\$/h), Which makes the profit significant in the long term. This underscores the substantial economic benefits of incorporating wind generators and solar power plants, leading to a notable reduction in the total generation cost compared to the original configuration of system without renewable energy sources. For the technical standpoint, figure 16 and figure 17 show the effect of integrating the RES on the voltage profile load buses and generators reactive power respectively in the both configurations.

Examining the convergence curves in Figure 5-15 which reveals that EKOA converges more rapidly in the initial iterations, reaching a superior solution compared to KOA. The results from the studies conducted on the two test systems affirm the efficacy of the EKOA approach in effectively addressing numerous large scale optimization problems within the realm of power system studies.

Table 5-9: Objective Functions of Test System 2

Control variable	Lin	nits	BASE CASE	CAS	SE 1	CAS	SE 5
s	MIN	MAX	EKOA	KOA	EKOA	KOA	EKOA
P _{TG4}	135	1350	423.4175	402.69	410.25	543.641	554.57
P_{TG5}	135	1350	436.2501	425.2704	419.39 38	426.712	454.6359
P_{TG11}	10	100	93.1889	99.9266	99.9996	95.767	99.2740
P _{TG15}	30	300	197.0996	169.6806	174.657	180.792	143.6250
P _{TG17}	135	1350	440.6231	391.676	395.7364	488.1685	604.6042
P _{TG19}	34.5	345	187.2718	161.7523	166.8785	194.637	179.8764
P _{TG22}	34.5	345	196.5769	159.1196	168.2786	217.616	117.7340
PwG52	0	345	228.2173	345.00	345.0000	146.717	130.7846
P _{TG80}	34.5	345	215.1279	180.1062	157.9774	230.024	254.7381
P _{WG83}	0	300	203.825	299.7106	299.9999	151.303	209.0530
P _{TG98}	30	300	179.4664	165.1998	158.2814	231.569	251.0583
P _{TG100}	60	600	600.00	599.1959	600.0000	500.029	390.2614
P _{TG101}	20	200	200.000	199.826	199.999	190.967	199.0806
P _{TG109}	0	100	93.7766	99.8056	99.992	92.582	99.1006
P _{TG111}	10	100	99.1202	99.9419	99.9990	98.411	99.6812
V_{G4}	0.9	1.1	1.0746	1.0980	1.0975	1.0864	1.0443
V_{G5}	0.9	1.1	1.0618	1.0855	1.0907	1.0764	1.0340
V_{G11}	0.9	1.1	1.0640	1.0918	1.0998	1.0755	1.0344
V_{G15}	0.9	1.1	1.0784	1.0940	1.0998	1.0795	1.0426
V_{G17}	0.9	1.1	1.0786	1.0984	1.0995	1.0783	1.0533
$ m V_{G19}$	0.9	1.1	1.0014	1.0123	1.0521	0.993	0.9753
$ m V_{G22}$	0.9	1.1	1.0240	1.0182	1.061	0.991	0.9774
V_{G52}	0.9	1.1	1.0344	1.0484	1.086	1.0029	0.9804
V_{G80}	0.9	1.1	1.0190	1.0939	1.0560	1.0397	1.0421
V_{G83}	0.9	1.1	1.0659	1.1000	1.0994	1.0752	1.0789
V_{G98}	0.9	1.1	1.0718	1.0938	1.0898	1.0854	1.0672
V_{G100}	0.9	1.1	1.0871	1.1000	1.0999	1.0963	1.0895
V_{G101}	0.9	1.1	1.0925	1.1000	1.0910	1.0972	1.0585
V_{G109}	0.9	1.1	1.0497	1.0621	1.0408	1.0959	1.0785
V _{G111}	0.9	1.1	1.0761	1.1000	1.0750	1.0593	1.0181
Т	Cost (\$/h)		19080.9613	16730.907	16701.773	18992.604	19524.435
,	<i>VD</i> (p.u)		3.4224	4.40771	4.6987	4.454	3.22006
Pl	oss (MW))	66.9613	72.0597	69.4451	61.943	61.0737

5.4 Conclusion

This research presents the development and application of two novel metaheuristic algorithms—the Kepler Optimization Algorithm (KOA) and its enhanced version (EKOA) for solving the (OPF) problem under uncertainty introduced by (RES). The proposed EKOA incorporates an additional operator and cosine-based function to strengthen the exploration process and prevent premature convergence. Both algorithms were implemented on the IEEE 30-bus and the practical DZA 114-bus power systems to evaluate performance across diverse operating conditions for various objective functions. Results demonstrate that EKOA consistently outperforms the original KOA and other optimization methods from the literature, achieving faster convergence, higher solution accuracy, and reduced computational effort. Furthermore, the integration of RES within the OPF framework leads to significant economic and environmental benefits, including reductions in generation cost and pollutant emissions. To further enhance system performance, voltage stability, and operational reliability under high renewable penetration, the next stage of this work introduces Flexible AC Transmission System (FACTS) devices as an integral component of the optimization framework.

Chapter 6: VOLTAGE STABILITY IMPROVEMENT IN PRESENCE OF RENEWABLE ENERGY SOURCES AND FACTS DEVICES

6.1 Introduction:

The Flexible AC Transmission Systems (FACTS) devices are crucial for enhancing system performance because of their capability to manipulate system parameters such as transmission-line impedance, voltage magnitudes, and phases, as well as power flow through the lines. Several works have explored the use of FACTS devices in power flow optimization, demonstrating their potential in enhancing system performance. For instance, the SVC provides reactive power compensation, which helps regulate voltage levels on the transmission line. The TCSC can adjust the effective reactance of the transmission line, allowing for better control of power flow. These can help to reduce the power losses, increase the transmission capacity of the line, and mitigate voltage instability. They can improve voltage stability and reduce voltage fluctuations. Several works have explored the use of FACTS devices in power flow optimization, demonstrating their potential in enhancing system performance [101].

This study aims to investigate the importance of integrating RESs and FACTS devices within contemporary power systems. The focal point of this investigation involves determining the optimal location and size of the TCSC and SVC installations. This optimization aims to minimize overall system costs while concurrently reducing real power losses (RPL) and total voltage deviation (TVD), and improving the voltage stability index (VSI). Despite potential additional costs associated with FACTS technology implementation, integrating RES offers a promising solution. By decreasing the base cost of energy production and mitigating toxic gas emissions, this integrated approach aligns with environmental and economic sustainability objectives, showcasing a comprehensive strategy to tackle the challenges and seize the opportunities within modern power systems.

- This chapter introduces a novel non-dominating sorting KOA referred to as NSKOA, to tackle SOPF problems.
- It addresses the OPF problem by incorporating RESs, namely solar PV, wind, and hydro power systems and FACTs devices such as the SVC and TCSC.
- It optimizes the size and location to maximize the benefits of FACTS devices for the power system.
- Using lognormal, Weibull, and Gumbel Probability Density Functions (PDFs) to effectively model and characterize the RES uncertainties within the system.
- A statistical analysis is performed to confirm the effectiveness of the proposed NSKOA and to highlight the advantages gained from integrating RES and FACTS devices.

6.2 Problem Formulation

The problem presented in this paper aims to solve the SOPF for a power system that incorporates thermal generation as well as stochastic wind and solar PV power generations. The main objective is to determine the optimal settings for control variables in various power system components, while maintaining adherence to all equality and inequality constraints. The mathematical formulation of this problem is as follows:

Minimize

$$OF(d,c) = \{OF_1(d,c), OF_2(d,c), OF_3(d,c), \dots, OF_{Nobj}(d,c)\}$$
(6.1)

Subject to

$$g(d,c) \begin{cases} g(d,c) = 0 \\ h(d,c) \le 0 \end{cases}$$

$$(6.2)$$

Ensuring both system security and optimal outcomes within an electrical network requires strict adherence to constraints placed on control variables. These limits serve as fundamental safeguards, essential for upholding feasibility, guaranteeing system stability.

- OF(d,c) denotes the objective function that needs to be minimized.
- g(d,c) represents the collection of equality constraints that must be fulfilled.
- c represents the vector of decision variables, and d represent the vector of state variables.

6.2.1 Optimization Problem

6.2.1.1 Cost of Generation for Thermal Units

The fuel cost associated with thermal generator units can be represented as a smooth and convex quadratic function. This mathematical representation is denoted by Equation (3):

$$C_{TH}(P_{TG}) = \sum_{i=1}^{N_{TG}} a_i + b_i P_{TGi} + c_i P_{TGi}^2$$
(6.3)

The model described above ignores valve point loading; however, when valve point effects are considered, an additional sinusoidal term is incorporated into the equation to capture the oscillations or fluctuations introduced by the valve points. This modification accounts for the non-linearity in the input—output curve of thermal generators and provides a more accurate representation of the fuel cost function in power system optimization. The valve point-effect can be modeled mathematically using Equation (4) [15]:

$$TC_{TH}(P_{TG}) = \sum_{i=1}^{N_{TG}} a_i + b_i P_{TGi} + c_i P_{TGi}^2 + \left| d_i \times \sin\left(e_i \left(P_{TG}^{\min} - P_{TG}\right)\right) \right|$$
 (6.4)

 a_i, b_i, c_i, d_i , and e_i are the cost coefficients for the i^{th} thermal generator. The system comprises N_{ThG} conventional generators, and P_{ThG}^{in} represents the minimum rated power of these generators.

6.2.1.2 The Investment Cost of FACTS Modeling

6.2.1.2.1 SVC Modeling

The static var compensator (SVC) can exhibit two distinct characteristics: inductive or capacitive. In the former, it absorbs reactive power, while in the latter, it injects reactive power. The SVC is composed of a series capacitor bank that is shunted by a thyristor-controlled reactor, as illustrated in Figure 6-1. According to, the investment cost of static var compensators (SVCs) varies linearly depending on the reactive power of the SVC to be installed. Therefore, the cost at node I is expressed as follows [93]:

$$C_{SVC_i} = 0.0003 \times Q_{SVC_i}^2 - 0.3051 \times Q_{SVC_i} + 127.38$$
(6.5)

The total investment cost is given as follows:

$$C_{SVC} = \sum_{i=1}^{N_{SVC}} (0.0003 \times Q_{SVC_i}^2 - 0.3051 \times Q_{SVC_i} + 127.38)$$
 (6.6)

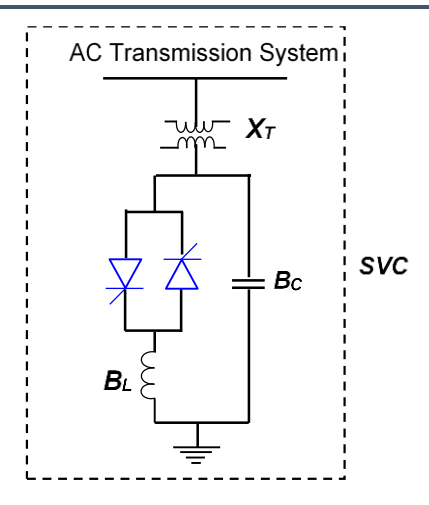
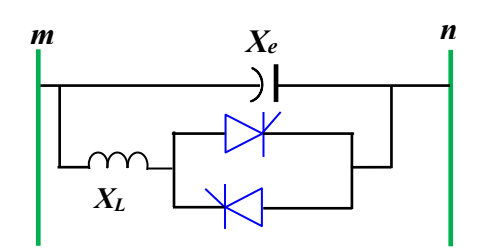


Figure 6-1:SVC Model and Configuration.

where Q_{SVC_i} represent the reactive power generated by *i*-th SVC while C_{SVC_i} represents its associated cost. The total investment cost for all SVC devices is referred to as C_{SVC} , and N_{SVC} is the total number of SVC devices.

6.2.1.2.2 TCSC Modeling

The thyristor-controlled series compensator (TCSC) is a series compensation device comprising a series capacitor bank shunted by a thyristor-controlled reactor. The primary concept behind power flow control using the TCSC is to adjust the overall effective series transmission impedance of the lines, either decreasing or increasing it by introducing capacitive or inductive reactive components, respectively. The TCSC is represented as a variable impedance, as illustrated in Figure 6-2.



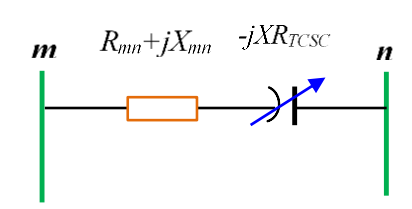


Figure 6-2:TCSC Configuration

Figure 6-3: Schematic Diagram Of TCSC

The total investment cost of TCSCs is a quadratic function of the reactive power to be installed, expressed as follows [93]:

$$C_{TCSC} = \sum_{i=1}^{N_{TCSC}} ((0.0015 \times Q^{2}_{TCSC_{i}} - 0.7130 \times |Q_{TCSC_{i}}| + 153.75) \times 1000 \times Q_{TCSC_{i}})$$
(6.7)

where Q_{TCSC_i} represents the reactive power generated by the *i*-th TCSC. The total investment cost for the all TCSC devices is referred to as C_{TCSC} , and N_{TCSC} is the total number of TCSC devices.

6.2.2 Objective Functions

6.2.2.1 Minimization of Power Production Cost

The first objective function represents the total cost of energy production, incorporating the presence of RESs and all their relevant cost functions. Mathematically, it can be expressed as follows:

$$TGcost = TC_{Th} (P_{TG}) + \sum_{j=1}^{N_{HG}} \left[C_{W,j} (WP_{Sc,j}) + RC_{W,j} (WP_{G,j} - WP_{Av,j}) + PC_{W,j} (WP_{Av,j} - WP_{Sc,j}) \right]$$

$$+ \sum_{k=1}^{N_{SG}} \left[C_{S,k} (SP_{Sc,k}) + RC_{S,k} (SP_{Sc,k} - SP_{Av,k}) + PC_{S,k} (SP_{Av,k} - SP_{Sc,k}) \right]$$

$$+ \sum_{j=1}^{N_{SGG}} \left[C_{Sh,i} (ShP_{sc}) + RC_{SH} (ShP_{sc} - ShP_{Av}) + PC_{Sh,i} (ShP_{Av} - ShP_{sc}) \right]$$

$$(6.8)$$

where N_{WG} , N_{SG} , and N_{ShG} represent the number of wind, solar PV, and solar-hydro power generators, respectively, in the grid.

6.2.2.2 Real Power Losses (RPLs)

In the context of the OPF problem, it is important to consider additional network parameters, including the power loss incurred during system transmission. These parameters play a critical role in assessing the efficiency and stability of the system. The calculation of the (TPL) is expressed through the following equation:

$$RPL = \sum_{q=1}^{nl} G_{q(ij)} \left[V_i^2 + V_j^2 - 2V_i V_j \cos(\delta_i - \delta_j) \right]$$
 (6.9)

where $G_{q(ij)}$ is the conductance of the branch, nl is the number of transmission lines, V_i and V_j are the voltages at bus i and j, respectively, and $\delta_{ij} = \delta_i - \delta_j$ is the difference in voltage angles between them.

6.2.2.3 Total Voltage Deviation (TVD)

Voltage deviation is an indicator used to assess the quality of voltage within a power network. It quantifies the total variation between the voltages at all load buses (PQ buses) and the standard nominal value of one per unit (p.u.). This parameter is determined by summing the absolute differences between the voltage at each load bus and the nominal value. The mathematical expression for calculating voltage deviation is as follows:

$$VD = \left(\sum_{p=1}^{NL} \left| VL_p - 1 \right| \right) \tag{6.10}$$

6.2.2.4 Voltage Stability Index (VSI)

The importance of monitoring and controlling power networks has grown significantly within the operation of contemporary electrical power systems, particularly with regards to enhancing voltage stability amid the increasing integration of renewable energies. To better understand voltage drops, the operational range of index L has been defined as (0, 1) Consequently, the third objective function, aimed at minimizing the voltage stability index within the transmission branches, can be modeled as follows:

$$Min(VSI) = min(max(L_i))$$

where (L_i) of the j-th bus is calculated using the following equation:

$$L_{j} = \left| 1 - \sum_{i=1}^{Ngb} F_{ij} \times \frac{V_{i}}{V_{i}} \angle \left\{ \theta_{ij} + (\delta_{i} - \delta_{j}) \right\} \right| j = 1, 2, ..., N_{lb}$$
(6.11)

$$F_{ij} = |\theta_{ij}, \quad V_i = |V_i| |\underline{\theta_i}, \quad V_j = |V_j| |\theta_j$$

$$(6.12)$$

$$F_{ij} = -[Y_1]^{-1} \times [Y_2] \tag{6.12}$$

 V_i and V_j represent the voltage magnitudes at bus i and j. θ_{ij} signifies the voltage angle difference between bus i and j. Ngb and N_{lb} stand for the number of generator and load buses, respectively. Y_1 , Y_2 , Y_3 , and Y_4 represent the sub-matrices of the system Ybus, obtained through the rearrangement of the generator and load bus parameters as shown in Equation (6.12).

$$\begin{bmatrix} I_{gb} \\ I_{lb} \end{bmatrix} = \begin{bmatrix} Y_1 & Y_2 \\ Y_3 & Y_4 \end{bmatrix} \times \begin{bmatrix} V_{gb} \\ V_{lb} \end{bmatrix}$$

$$(6.12)$$

6.2.3 Constraints

6.2.3.1 Equality Constraints

In this study, the specific equality constraints represent the fundamental power balance in the system, ensuring that the total power generation equals the total demand plus transmission losses. This is critical for maintaining a stable and balanced power system. Mathematically, this is expressed as the sum of power generated at all buses being equal to the load demand plus losses. These constraints ensure the continuous supply of power and the reliable operation of the network, which is essential in both traditional and RES-integrated systems.

$$P_{TGi}^{\min} \le P_{TGi} \le P_{TGi}^{\max}, \qquad i = 1, 2, ..., N_{TG}$$
 (6.14)

$$P_{wsj}^{\min} \le P_{wsj} \le P_{wsj}^{\max}, \qquad j = 1, 2, ..., N_{WG}$$
 (6.15)

$$P_{SS,k}^{\min} \le P_{SS,k} \le P_{SS,k}^{\max}, \qquad k = 1, 2, ..., N_{SG}$$
 (6.16)

$$Q_{TGi}^{\min} \le Q_{TGi} \le Q_{TGi}^{\max}, \tag{6.17}$$

$$Q_{wsj}^{\min} \le Q_{wsj} \le Q_{wsj}^{\max}, \qquad i = 1, 2, ..., N$$
 (6.18)

$$Q_{ss,k}^{\min} \le Q_{ss,k} \le Q_{ss,k}^{\max} \qquad k \in N_{SG}$$

$$(6.19)$$

$$Q_{Ci}^{\min} \le Q_{Ci} \le Q_{Ci}^{\max} \qquad i \in N_C$$
 (6.20)

$$V_{Gi}^{\min} \le V_{Gi} \le V_{Gi}^{\max},\tag{6.21}$$

$$V_{Li}^{\min} \le V_{Li} \le V_{Li}^{\max} \qquad i \in NL$$
 (6.22)

$$b_{SVC}^{\min} \le b_{SVC} \le b_{SVC}^{\max}, \qquad u \in N_{SVC}$$

$$(6.23)$$

$$X_{TCSC}^{\min} \le X_{TCSC} \le X_{TCSC}^{\max}, \quad W \in N_{TCSC}$$
 (6.24)

6.2.3.2 Security Constraints

The inequality constraints, on the other hand, include operational limits such as generator output limits, voltage limits at buses, and thermal limits of transmission lines. These constraints ensure that the system operates within safe and efficient boundaries.

$$T_k^{\min} \le T_k \le T_k^{\max} \qquad k \in NT \tag{6.25}$$

$$S_i^{\min} \le S_i \le S_i^{\max} \qquad i \in NL \tag{1.26}$$

In this context, max and min are the upper and lower boundaries, N_{TG} , N_{WG} , N_{SG} , and N_{ShG} refer to the number of thermal, wind, solar PV, and solar-hydro generators, and NL is the number of load buses the superiority of feasible solutions technique used in this study to ensure solution feasibility.

Algorithm 1: Pseudocode of NSKOA

Step 1:

- Define input power system data (line data b bus data) and identify the control variable limits and number of variables.
- Set **KOA** parameters **N**, Tmax, and μ_0 .

Step 2:

• Initialize objects population with random position, orbital eccentricities, and orbital periods using Equations (43), (44), and (45), respectively.

Step 3:

• Run a power flow algorithm based on the Newton Raphson method to calculate the value of the objective functions for the initial population.

Step 4: Perform non-dominated sorting:

- Calculate ranks (RK) and crowding distance (CD) using the eq() of population using the proposed PFA with the sorting and crowding distance calculation procedure.
- Calculate the best compromise solution (BCS) using Equation (73).

Step 5:

While (t < Tmax):

• Update e_i ... i = 1, 2, ..., N, best(t), worst(t), and $\mu(t)$, using Equations (50), (51), and (52), respectively.

Step 6:

For i = 1: $N P_i = population$

VOLTAGE STABILITY IMPROVEMENT IN PRESENCE OF RENEWABLE ENERGY SOURCES AND FACTS DEVICES

- Calculate the gravitational force between the Sun and the object i using Equation (46).
- Calculate the Euclidian distance between the Sun and the object i using Equation (48).
- Calculate the velocity of the object *Xi* using Equation (53).
- Generate two random numbers r and r1 between 0 and 1.

If r > r1

- Update the position of the planet.
- Update the object position using Equation (66).

Else

- Update the distance between the planet and the Sun.
- Update the object position using Equation (67).

End if

Step 7:

- Run power flow algorithm based on the Newton Raphson algorithm to calculate the objective functions values for the new population (Np_{i)}.
- Combine new population (Npi) with previous population (Pi) to form Upi $Up_i = Np_i U P_i$.

Step 8: Perform non dominated sorting:

• Calculate ranks (RK) and crowding distance (CD) of population using the proposed PFA with the sorting and crowding distance calculation procedure.

Step 8:

• Extract N elitist objects from Upi.

Step 9:

• Generate the Pareto optimal front and extract the best compromise solution.

End for

End while

6.3 Results and Discussion

To address stochastic OPF problems, an analysis was conducted on both the conventional (base case) and the modified IEEE 57-bus network. The base case was simulated using the mono-objective KOA to demonstrate the effects of RES and FACTs on the system. To determine the optimal control variables, sizing, and location of SVC and TCSC, 17 tap changers, as well as the power and voltage of generators, were used as control variables. SVC placement was considered among 50 load buses, and TCSC could be situated across 81 branches, totaling 161 control variables as represented in Table 6-1

Table 6-1: Control Variables Of The Test System

Elements	IEEE 57-Bus Test System		
No of buses	57		
No of branches	81		
No of generators	07		
No of thermal generators	04		
No of RES generators	03		
No of load buses	50		
No of control variables	161		
Initial active and reactive load demand	1250.80 MW; 336.40 Mvar		

The proposed algorithm was implemented using MATLAB software and simulations were conducted on a personal computer with an Intel CoreTM i7-8300H 2.22 GHz processor. To determine the optimal population size for the NSKOA algorithm, empirical tests were conducted with different population sizes, taking into account the search space complexity and the number of control variables. Population sizes of 100, 200, and 300 were tested. Although specific test results are not provided here, the best outcomes were achieved with a population size of 200 individuals, which was then used for all simulation cases. For equitable comparison, the control variables of the test system were treated as continuous variables.

6.3.1 Test-System: Conventional and Modified IEEE 57 BUS Network

The IEEE 57-bus test system consists of seven power plants installed at buses 1, 2, 3, 6, 8, 9, and 12; eighty transmission lines of which 17 are equipped with tap changer transformers, and three parallel compensators are installed at buses 18, 25, and 53, respectively. The complete data are available in [23]. The modified IEEE-57 bus system consists of a combined production of a solar–hydro power generator replacing a thermal power plant at bus 6 and a solar PV generator at bus 9, as well as wind generators at bus 12. The parameters of the probability density function (PDF) and the cost coefficients of the RES are detailed in Table 6-2 [61].

The study was conducted using three scenarios:

- **Base Case Scenario:** In this case, the conventional IEEE 57 bus was simulated in order to show the impact of RESs and FACTs devices on the four optimization cases (cost, power losses, voltage deviation, and voltage stability index) in the next two scenarios.
- Scenario number 1: This study was conducted on the modified IEEE 57 system after the integration of RES sources.
- Scenario number 2: This study was conducted on the modified IEEE 57 system after the integration of RES sources and FACTs devices.

The findings of the case studies are presented in a tabulated format. Figures 5–8 exhibit the characteristics of the probabilities of RESs, while Figures 9–12 represent the available real power at the RES units.

Table 6-2:PDF parameters of renewable generators

	Wind-power unit								
No. of turbines	Rated power, F	Pwr (MW)	Weibull PDF parameters						
25	75	5	1 = 9; p = 2						
	Phot	ovoltaic plan	nt						
Rated power,	P_{sr} (MW)	Lognormal PDF parameters							
50		$\mu = 5.2 \ \sigma = 0.6$							
	Combined solar	and small h	ydro power						
Photovoltaic rated p	power P _{sr} (MW)	Lognormal PDF parameters							
45		$\mu = 5.0 \ \sigma = 0.6$							
Small hydro rated p	oower P _{hr} (MW)	Gumbel PDF parameters							
5		$\lambda = 15 \ \gamma = 1.2$							

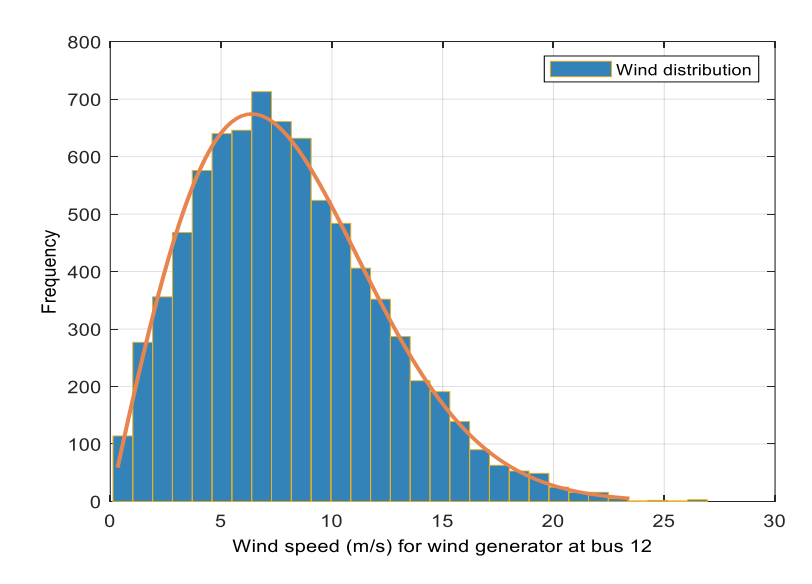


Figure 6-4: Distribution of wind speed at bus 12

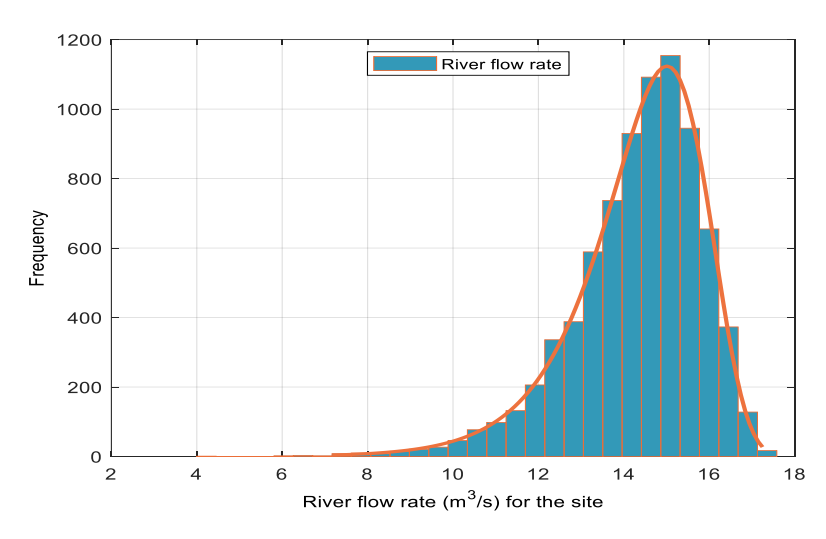


Figure 6-5: The Rate Of River Flow For The Site

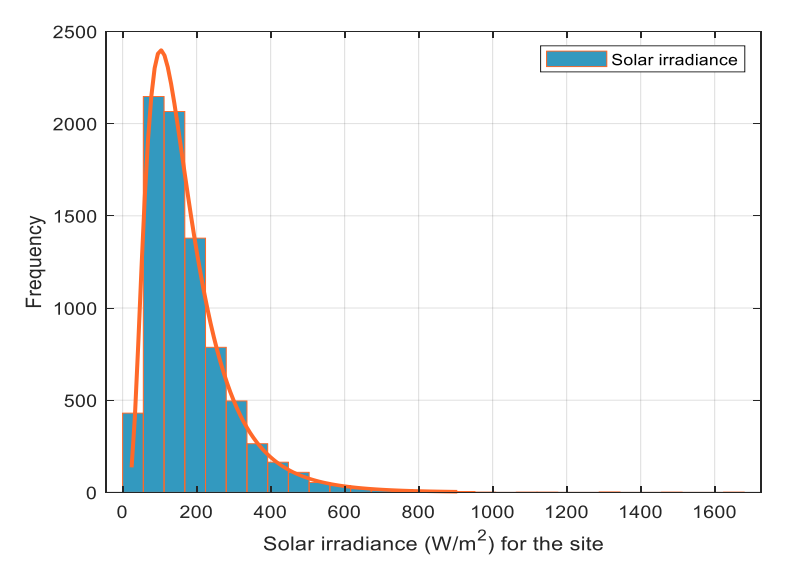


Figure 6-6: Solar Irradiance For The Site

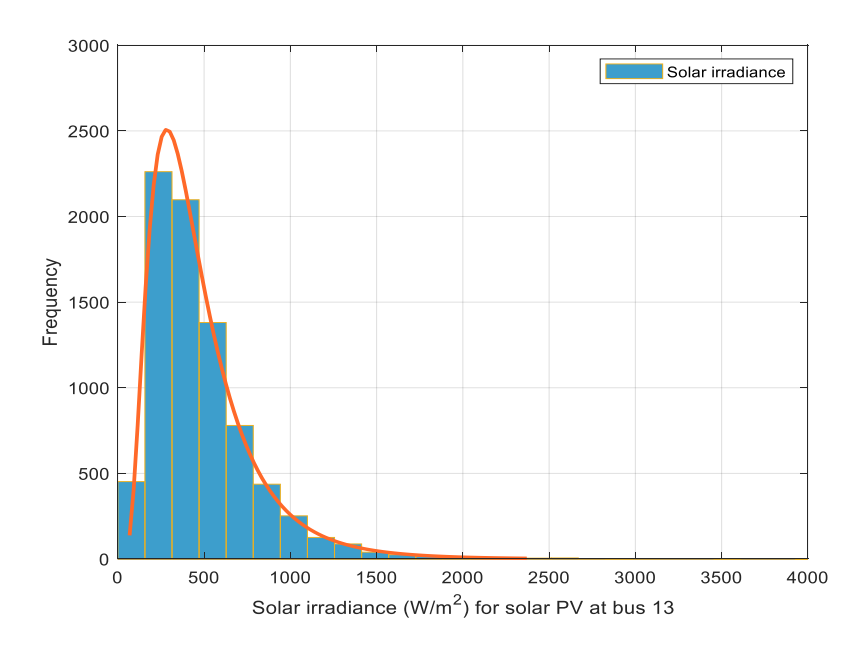


Figure 6-7: Solar Irradiance For Solar PV Generator

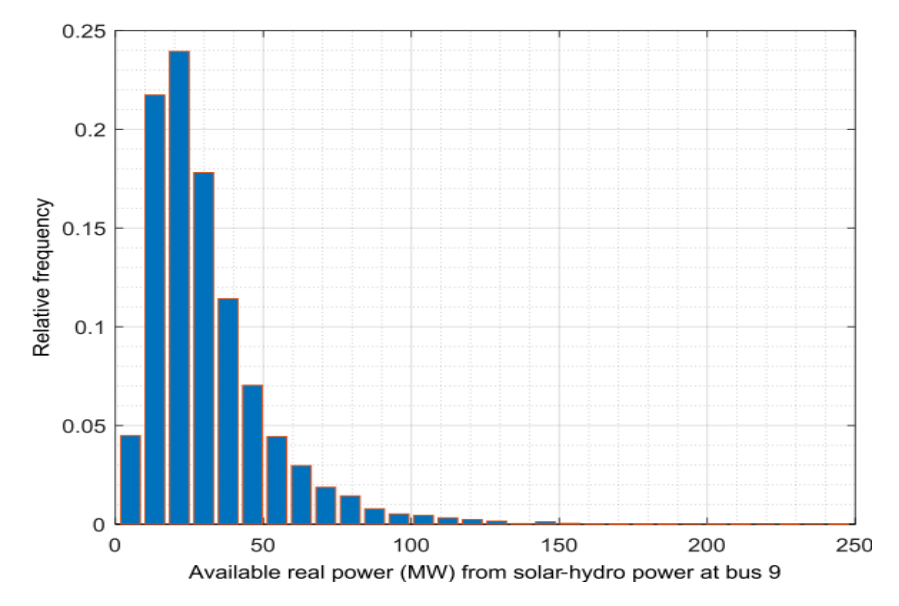


Figure 6-8: Available Real Power At Bus 9

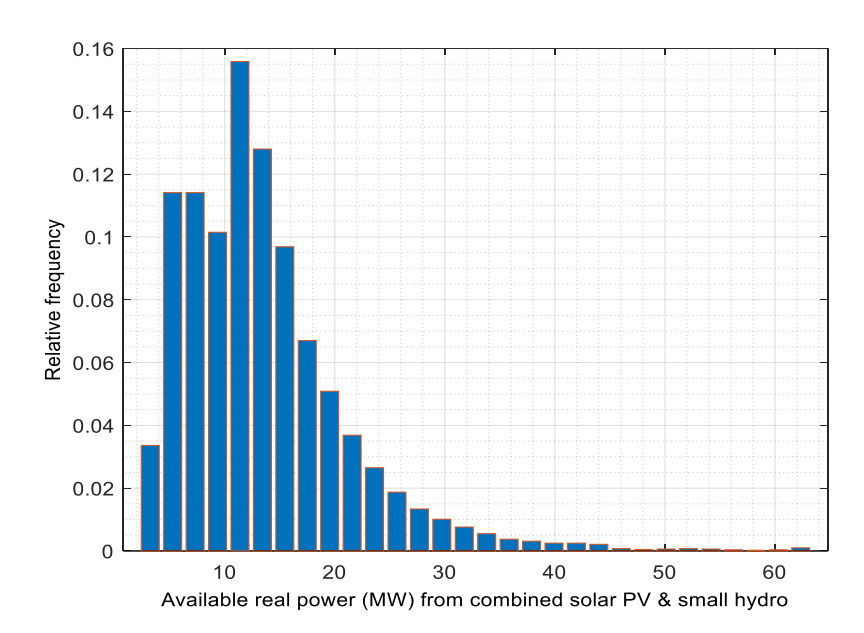


Figure 6-9: Available Real Power For Combined Solar–Hydro Power

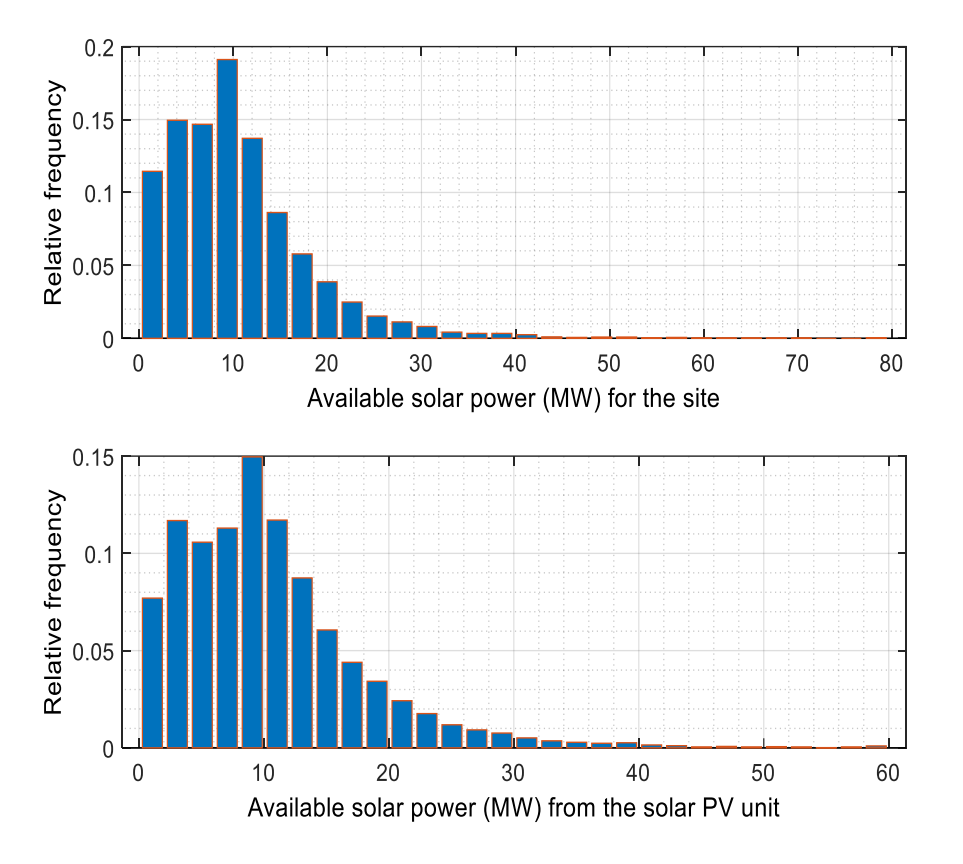


Figure 6-10: Available Real Power For Solar PV Unit

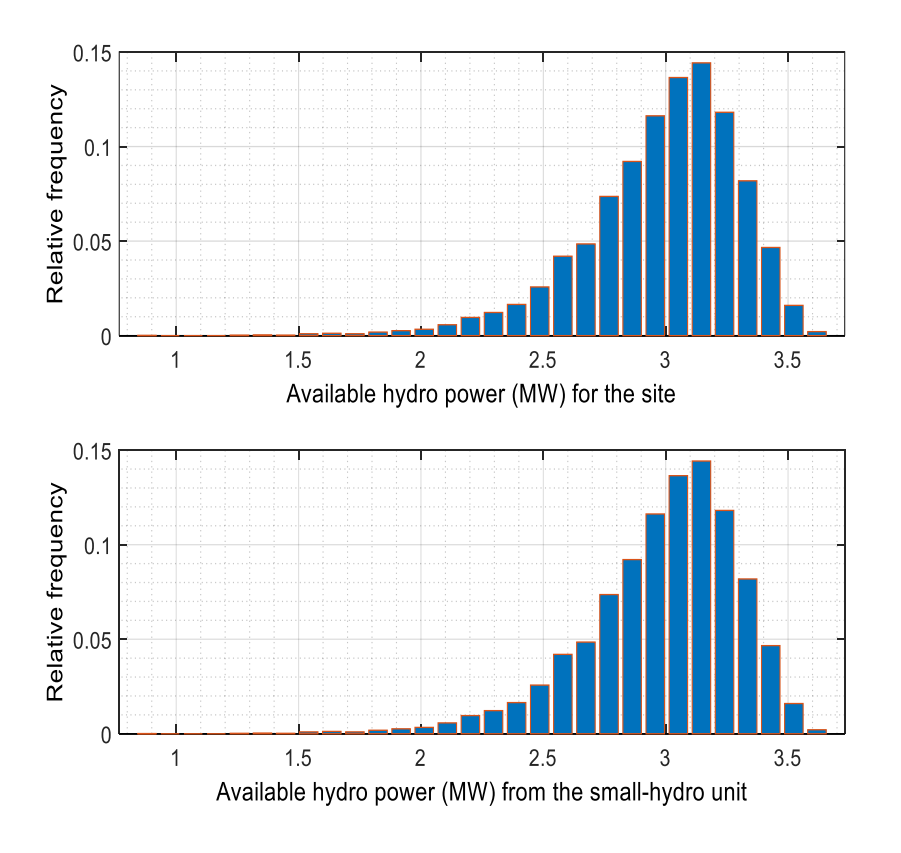


Figure 6-11: Available Real Power For Hydro Unit

6.3.1.1 Case 1: Total Generation Cost and the Investment Cost of FACTS Optimization

A comprehensive investigation into the OPF for the IEEE 57-bus system was undertaken, examining three distinct scenarios. Initially, the conventional configuration of the system was analyzed, followed by two additional cases: one integrating (RESs) and the other involving RES integration alongside Flexible Alternating Current Transmission System (FACTS) devices. The primary objective was to minimize the cost of power production in the conventional IEEE 57 system designed as the base case scenario, and then with the integration of RES designated as scenario 1, while simultaneously considering the investment cost associated with FACTS devices, defined as scenario 2.

In the base case scenario, the production cost was recorded at 5570.956 (USD/h), with an emission rate of 234.75 tons/h. Upon the integration of RESs into the system, the production cost decreased to 5217.635 (USD/h) saving 353.32 (USD/h), approximately 6.34% of the power production cost, alongside a reduction in emissions by approximately 22.76%, to 181.294 tons per hour (scenario 1). The subsequent deployment of FACTS devices further reduced the production cost to 5208.97 (USD/h), saving approximately 8.8 (USD /h) representing a marginal saving of approximately 0.17% compared to the RES-integrated scenario. However, this enhancement incurred an additional cost of 288.973 (USD/h) for FACTS deployment, yielding a total cost of 5497.94 (USD/h), but still saving 73 (USD/h) from the total cost compared to the base case.

Notably, the best compromise solution (BCS) yielded a production cost of 5211.722 (USD /h), and a FACTS cost of 82.5115 (USD /h), with a total cost of 5294.231 (USD/h) reflecting savings of approximately 4.98% compared to the base case.

Figure 5-12 shows the Pareto front of case 1, where NSKOA provides a well-distributed front, with the BCS solution positioned almost in the center, while the optimal result and control variables of case 1 are represented in Table 6-3. The results show that the placement of SVC devices at buses 13, 16, 21, 35, 52, and 54 played a significant role in managing reactive power and stabilizing voltage profiles. The addition of SVCs helped improve voltage levels, particularly in buses with high reactive power demand, ensuring more efficient power flow across the network. Similarly, the installation of TCSC devices on transmission lines (21–22), (30–31), (13–49), (29–52), (56–42), and (38–49) optimized power transfer capability by reducing line reactance and enhancing reactive power compensation, leading to more stable voltage regulation and an overall reduction in power losses. The combination of SVCs and TCSCs helped balance reactive power more effectively, improving voltage profiles and reducing strain on power generation units by minimizing unnecessary reactive power generation, thereby contributing to cost optimization. Figures 5-13 and 5-14 illustrate the voltage profile in the load buses and the generated reactive power, respectively, in the same case. All values are within their limits, indicating that the constraints are completely satisfied. Importantly, the combination of RES integration and FACTS deployment not only reduced power production costs and emissions but also enhanced the voltage stability index, significantly mitigating power losses and voltage deviations. This synergy underscores the potential for designing and operating future power systems that ensure a reliable and sustainable electricity supply.

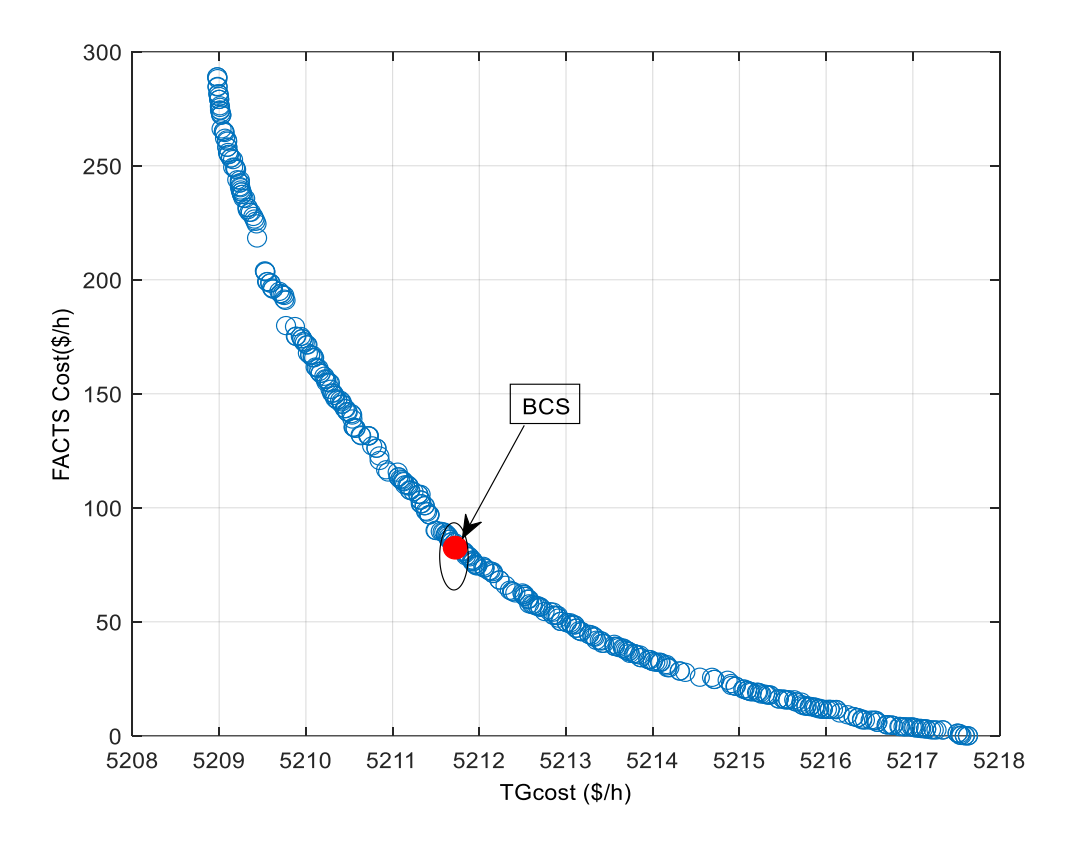


Figure 6-12:Pareto Front Of Case 1

Table 6-3:Optimal Result And Control Variables Of Case 1

Control variable					ues
Base case	Scenario 1	Scenario 2	BCS	Base	<u>case</u>
Pg ₁ 331.516	Pg ₁ 552.331	Pg ₁ 550.564	Pg ₁ 551.9723	Cost (\$/h)	5570.956
Pg ₂ 99.986	Pg ₂ 100.000	Pg ₂ 100.000	Pg ₂ 100.000		
Pg ₃ 76.635	Pg ₃ 76.6229	Pg ₃ 76.6240	Pg ₃ 76.6183	Emission (ton	(h) 234.75
Pg ₆ 99.997	Pg ₆ 100.000	Pg ₆ 100.000	Pg ₆ 99.9995	$RP_L(MW)$	43.958
Pg ₈ 53.916	Pg ₈ 50.5657	Pg ₈ 50.8772	Pg ₈ 50.0453	Ki L (Wi W)	73.730
Pg ₉ 160.173	Pg ₉ 199.9998	Pg ₉ 200.000	Pg ₉ 199.999	TVD(pu)	1.4994
Pg ₁₂ 209.847	Pg ₁₂ 210.000	Pg ₁₂ 209.999	Pg ₁₂ 209.998		
Vg ₁ 1.100000	Vg ₁ 1.09983	Vg ₁ 1.099983	Vg ₁ 1.099990	VSI (pu)	0.2899
Vg ₂ 1.095161	Vg ₂ 1.092973	Vg ₂ 1.093325	Vg ₂ 1.093092	Saana	mia 1
Vg ₃ 1.079965	Vg ₃ 1.070328	Vg ₃ 1.071347	Vg ₃ 1.070841	Scena	<u>110 1</u>
Vg ₆ 1.065115	Vg ₆ 1.04371	Vg ₆ 1.040434	Vg ₆ 1.040998	TGcost (\$/h)	5217.635
Vg ₈ 1.064082	Vg ₈ 1.034728	Vg ₈ 1.029753	Vg ₈ 1.031650		
Vg ₉ 1.050054	Vg ₉ 1.027750	Vg ₉ 1.032134	Vg ₉ 1.028320	Emission (ton	h) 181.294
Vg ₁₂ 1.06068	Vg ₁₂ 1.03707	Vg ₁₂ 1.03637	Vg ₁₂ 1.03660	DD (MW)	20.7202
$T_{(4,18)}$ 1.0539	T _(4,18) 1.0084	T _(4,18) 1.0507	$T_{(4,18)}$ 1.0724	$RP_L(MW)$	38.7203
$T_{(4,18)} = 0.9958$	$T_{(4,18)} = 0.9868$	$T_{(4,18)} = 0.9727$	$T_{(4,18)} = 0.9664$	TVD (pu)	1.5821
$T_{(21,20)}$ 1.0538	$T_{(21,20)}$ 1.0122	$T_{(21,20)}$ 1.0010	$T_{(21,20)}$ 1.0133	1 . 2 (P4)	1.0021
T(24,25) 0.9601	$T_{(24,25)}$ 0.939	T _(24,25) 0.9495	$T_{(24,25)} = 0.9457$	VSI (pu)	0.2757
T _(24,25) 1.0158	$T_{(24,25)}$ 0.9375	$T_{(24,25)} = 0.9622$	$T_{(24,25)} = 0.9585$		
T _(24,26) 1.0020	T _(24,26) 0.9820	T _(24,26) 0.9787	T _(24,26) 0.983	Scena	<u>rio 2</u>
T _(7,29) 1.0006	T _(7,29) 0.9599	T _(7,29) 0.9659	T _(7,29) 0.9634	TGcost (\$/h)	5208.97
$T_{(34,32)}$ 0.9717	T _(34,32) 0.9184	$T_{(34,32)}$ 0.9135	$T_{(34,32)}$ 0.9107	1 GCOSt (\$/11)	3200.77

$T_{(11,41)}$ 0.9220	T _(11,41) 0.9000	T _(11,41) 0.9158	T _(11,41) 0.9123	TFcost (\$/h)	288.973
$T_{(15,45)} 0.9835$	$T_{(15,45)}$ 0.9887	T _(15,45) 1.0014	$T_{(15,45)}$ 0.9959		100 105
$T_{(14,46)}$ 0.9744	T _(14,46) 0.9648	T _(14,46) 0.9800	T _(14,46) 0.9744	Emission(ton/h)	180.125
$T_{(10,51)}$ 0.9978	$T_{(10,51)}$ 0.9723	$T_{(10,51)}$ 0.9782	$T_{(10,51)}$ 0.9775	$RP_L(MW)$	37.263
$T_{(13,49)}$ 0.9503	$T_{(13,49)}$ 0.9331	$T_{(13,49)}$ 0.9784	$T_{(13,49)}$ 0.9771	Ε()	
$T_{(11,43)}$ 0.9997	$T_{(11,43)}$ 0.9591	$T_{(11,43)} 0.9872$	$T_{(11,43)}$ 0.9776	TVD(p.u)	1.9347
$T_{(40,56)}$ 1.0168	$T_{(40,56)}$ 0.9861	$T_{(40,56)}$ 0.9509	$T_{(40,56)}$ 0.9432	NGI()	0.240
$T_{(39,57)}$ 0.9744	$T_{(39,57)}$ 0.9549	$T_{(39,57)}$ 0.9577	$T_{(39,57)}$ 0.9617	VSI(p.u)	0.248
$T_{(9,55)}$ 0.9922	$T_{(9,55)}$ 0.9643	$T_{(9,55)}$ 0.97113	$T_{(9,55)}$ 0.9679	BCS	
Optima	l size and location of	SVC-TCSC		<u> 200</u>	
/	/	svc ₍₁₃₎ 50.000	svc ₍₄₂₎ 0.7796	TGcost (\$/h)	5211.722
/	/	. ,	· /	TE a set (C/la)	02 5115
/	/,	svc ₍₁₆₎ 24.050	svc ₍₄₄₎ 6.5088	TFcost (\$/h)	82.5115
/	/	svc ₍₂₁₎ 7.135	svc ₍₂₁₎ 3.5401	Emission(ton/h)	181.06
/	/	$svc_{(35)}$ 15.038	svc ₍₃₅₎ 12.438	,	,
/	/	$svc_{(52)}$ 5.825	$svc_{(52)}$ 0.6752	$RP_L(MW)$	37.833
/	/	svc ₍₅₄₎ 2.567	svc ₍₅₄₎ 1.5976	TVD()	1 (720
/	/	$Tcsc_{(21,22)}$ 0.0377	/	TVD(p.u)	1.6739
/	/	$Tcsc_{(30,31)}$ 0.3976	$Tcsc_{(30,31)} 0.3588$	VSI(p.u)	0.2533
/	/	Tcsc _(13,49) 0.1260	Tcsc _(13,49) 0.1184	\ \ \ \ \ \ \ \ \ \ \ \ \ \ \ \ \ \ \	
/	/	$Tcsc_{(29,52)}$ 0.1393	Tcsc _(29,52) 0.1430		
/	/	Tcsc _(56,42) 0.1939	Tcsc _(56,42) 0.2421		
/	/	Tcsc _(38,49) 0.0332	Tcsc _(38,49) 0.0138		

 $\overline{P_{Gi}\left(MW\right),\,V_{gi}\left(p.u.\right),\,T_{\left(I,j\right)}\left(p.u.\right),Q\,\,svc_{\left(i\right)}\left(MVAr\right),\,X\,\,Tcsc_{\left(I,j\right)}\left(p.u.\right).}$

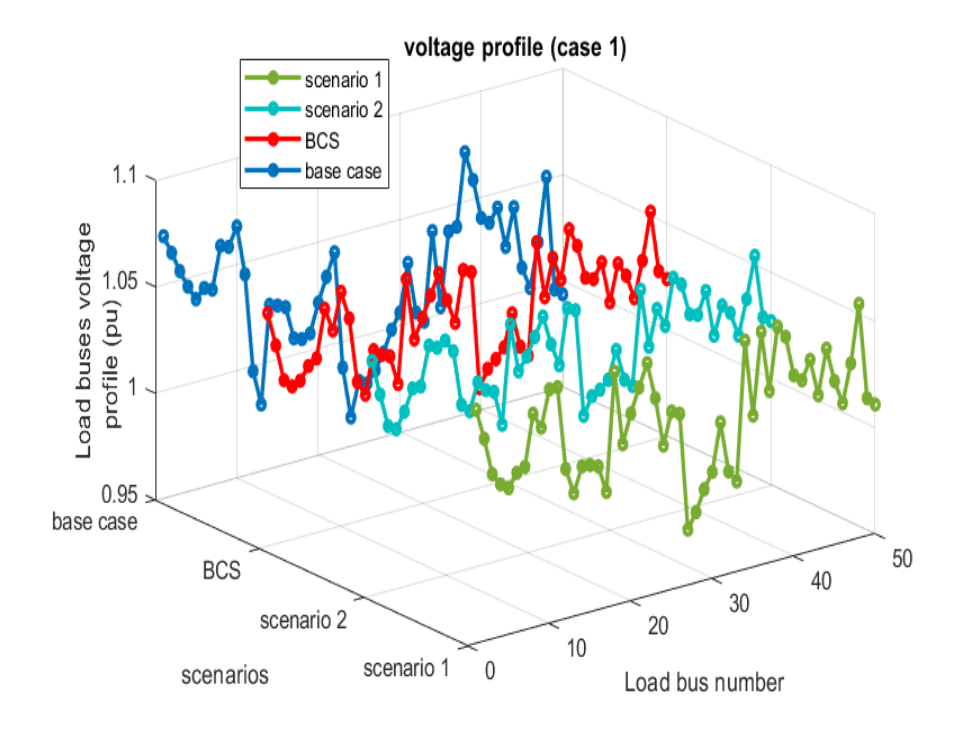


Figure 6-13:Load Bus Voltage Profile For Case 1

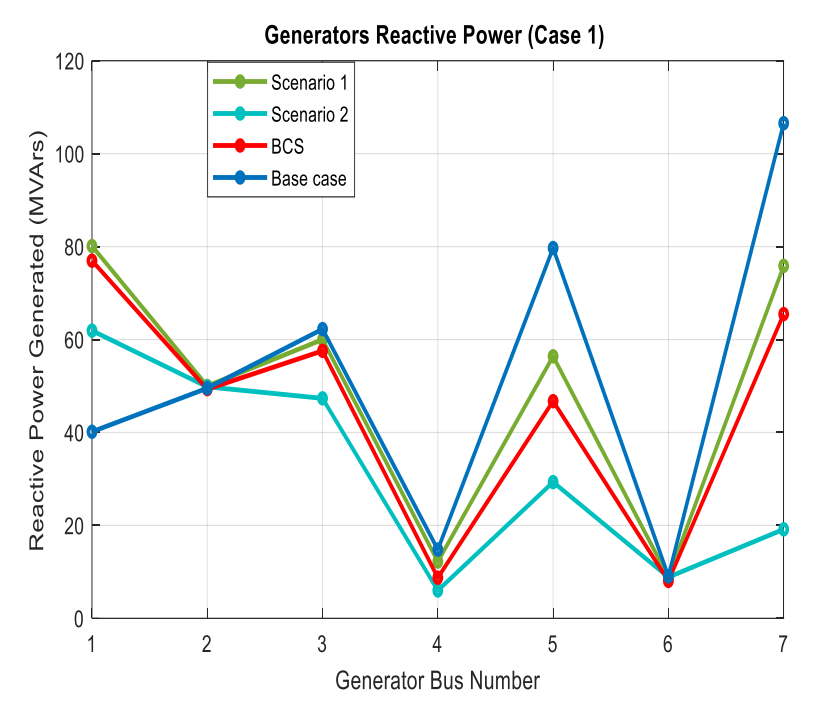


Figure 6-14: Generator's Reactive Power For Case 1

Table 6-4 represents a statistical comparison of the proposed method with six other methods used in case 1 and case 2 for the first scenario, for instance, the barnacles mating optimizer (BMO), moth-flame optimization algorithm (MFO), particle swarm optimization (PSO), efficient optimization algorithm based on weighted mean of vectors optimization (INFO), and artificial ecosystem-based optimization (AEO).

Table 6-4: Statistical Comparison Of Case 1 And Case 2 For The First Scenario

	Case 1	Case 2		
Algorithms	Results (\$/h)	Algorithms	Results (MW)	
BMO [61]	5300.457 (\$/h)	BMO [61]	20.785 (MW)	
MFO [61]	5316.14 (\$/h)	MFO [61]	21.3031 (MW)	
PSO [61]	5417.538 (\$/h)	PSO [61]	21.3621 (MW)	
GTO [63]	5260.0009 (\$/h)	GTO [63]	19.7703 (MW)	
AEO [63]	5260.2497 (\$/h)	AEO [63]	19.7633 (MW)	
INFO [63]	5259.2040 (\$/h)	INFO [63]	19.7040 (MW)	
NS-KOA	5217.635 (\$/h)	NS-KOA	16.836 (MW)	

Bold indicates the best solutions found so far.

6.3.1.2 Case 2: Real Power Loses and the Investment Cost of FACTS Optimization

In a parallel investigation, the optimization of real power losses (RPLs) within the same system configurations was pursued. In the base case scenario, RPL stood at 18.022 MW, which decreased to

17.729 MW following the integration of RESs, achieving a reduction of approximately 1.62% (Objective 1). Subsequent intervention with FACTS devices further diminished RPL to 16.398 MW, demonstrating an additional reduction of approximately 9.05% compared to the base case and 7.45% compared to the RES-integrated scenario. However, this enhancement incurred an additional cost of 227.86 (USD/h) due to FACTS deployment (scenario 2). Conversely, the base case scenario led to an RPL of 16.836 MW, with a FACTS cost of 68.945 (USD/h).

Figure 6-15 shows the Pareto front of case 2, where NSKOA provides a well-distributed front, with the BCS solution positioned almost in the center, as shown in Table 6-5. The strategic placement of SVCs and TCSCs significantly influenced power loss reduction by optimizing reactive power flow. Notably, buses 50 and 53 were equipped with SVCs, highlighting their critical role in reactive power support and reducing power losses. Similarly, the results show that in the IEEE 57 BUS network, the branches (9–12) and (13–49) are the regions that need TCSC device installation to effectively control line impedance and improve power flow efficiency, which reduces power losses in these regions by reducing line reactance. The presence of TCSCs on these repeated branches indicates their importance in minimizing congestion and reducing transmission losses, making them key points for reactive power compensation and power loss mitigation. These findings underscore the efficacy of FACTS deployment in significantly mitigating real power losses within the system, even with an added expense, presenting a nuanced trade-off between loss reduction and investment expenses. Figures 5-16 and 5-17 illustrate the voltage profile in the load buses and the generated reactive power, respectively, in the same case. All values are within their limits, indicating that the constraints are completely satisfied.

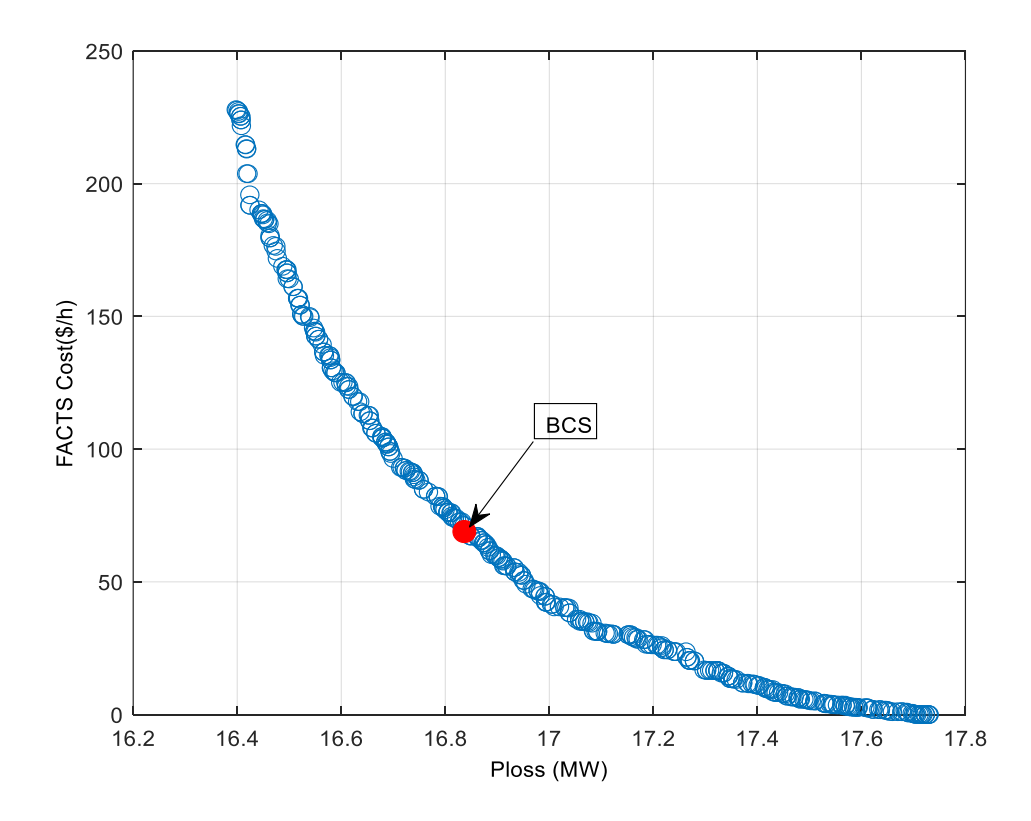


Figure 6-15:Pareto Front of case 2

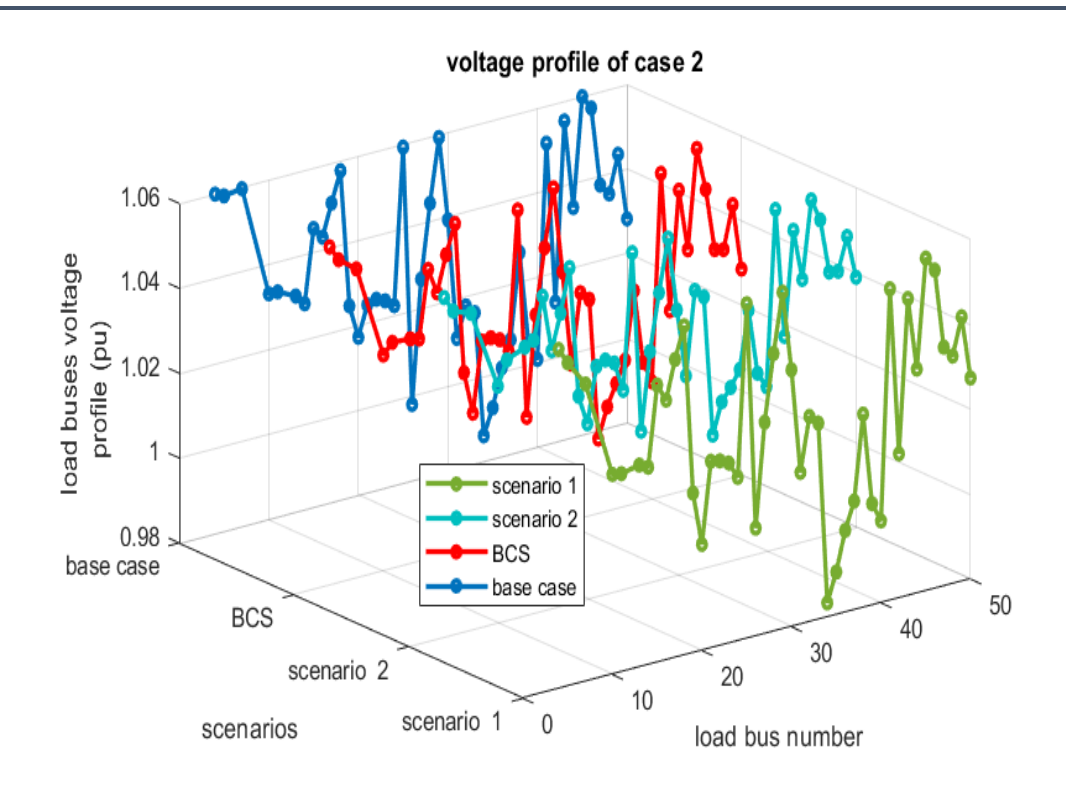


Figure 6-16:Load Bus Voltage Profile For Case 2

Table 6-5:Optimal Result And Control Variables For Case 2

	Fitness values			
Base case	Scenario 1	Scenario 2	BCS	Base case
Pg ₁ 198.3536 Pg ₂ 19.6385 Pg ₃ 136.582 Pg ₆ 94.5306 Pg ₈ 319.912	Pg ₁ 301.5189 Pg ₂ 8.424944 Pg ₃ 140.000 Pg ₆ 99.9969 Pg ₈ 308.590	Pg ₁ 297.4671 Pg ₂ 7.759523 Pg ₃ 139.9811 Pg ₆ 99.9978 Pg ₈ 311.9925	Pg ₁ 299.6088 Pg ₂ 8.143402 Pg ₃ 139.962 Pg ₆ 99.9930 Pg ₈ 309.931	TGcost (\$/h) 10979.12 RP _L (MW) 18.7160 TVD (pu) 1.5782 VSI (pu) 0.2766
Pg ₉ 199.070 Pg ₁₂ 209.994 Vg ₁ 1.074194 Vg ₂ 1.067047 Vg ₃ 1.061879 Vg ₆ 1.063364 Vg ₈ 1.075176	Pg ₉ 199.999 Pg ₁₂ 209.998 Vg ₁ 1.075784 Vg ₂ 1.068157 Vg ₃ 1.064005 Vg ₆ 1.059364 Vg ₈ 1.061550	Pg ₉ 199.999 Pg ₁₂ 210.000 Vg ₁ 1.073172 Vg ₂ 1.066069 Vg ₃ 1.063692 Vg ₆ 1.059340 Vg ₈ 1.064236	Pg ₉ 200.000 Pg ₁₂ 209.997 Vg ₁ 1.075249 Vg ₂ 1.067677 Vg ₃ 1.063580 Vg ₆ 1.059306 Vg ₈ 1.064473	Scenario 1 TGcost (\$/h) 10154.82 RP _L (MW) 17.7299 TVD (pu) 1.5298 VSI (pu) 0.2759
Vg ₉ 1.051757 Vg ₁₂ 1.040481 T _(4,18) 1.042820 T _(4,18) 0.969822 T _(21,20) 1.00078 T _(24,25) 0.946581 T _(24,25) 0.962140 T _(24,26) 1.025195	Vg ₉ 1.043234 Vg ₁₂ 1.037484 T _(4,18) 0.964453 T _(4,18) 1.026266 T _(21,20) 1.019229 T _(24,25) 0.937832 T _(24,25) 0.971551 T _(24,26) 1.013087	Vg ₉ 1.051782 Vg ₁₂ 1.037586 T _(4,18) 0.955661 T _(4,18) 1.035669 T _(21,20) 1.006507 T _(24,25) 0.960908 T _(24,25) 0.975584 T _(24,26) 1.009955	Vg ₉ 1.047636 Vg ₁₂ 1.038832 T _(4,18) 0.950783 T _(4,18) 1.040006 T _(21,20) 1.014671 T _(24,25) 0.954601 T _(24,25) 0.972877 T _(24,26) 1.016856	Scenario 2 TGcost (\$/h) 10269.41 TFcost (\$/h) 227.869 RP _L (MW) 16.3981 TVD(pu) 1.9708 VSI(pu) 0.2468
T _(7,29) 0.991647 T _(34,32) 0.943693 T _(11,41) 0.922844 T _(15,45) 0.982334	T _(7,29) 0.983174 T _(34,32) 0.927002 T _(11,41) 0.900000 T _(15,45) 0.983402	T _(7,29) 0.990604 T _(34,32) 0.929053 T _(11,41) 0.930783 T _(15,45) 0.993976	T _(7,29) 0.986726 T _(34,32) 0.932515 T _(11,41) 0.919565 T _(15,45) 0.984972	<u>BCS</u> TGcost (\$/h) 10198.18

T _(14,46) 0.963354	T _(14,46) 0.963000	T _(14,46) 0.984149	T _(14,46) 0.975964	TFcost (\$/h) 68.945
$T_{(10,51)} 0.975757$	$T_{(10,51)} 0.969271$	$T_{(10,51)}$ 0.986212	$T_{(10,51)}$ 0.977325	RP _L (MW) 16.8366
$T_{(13,49)} \ 0.937087$	T _(13,49) 0.936787	T _(13,49) 0.991151	T _(13,49) 0.980100	TVD (pu) 1.6799
$T_{(11,43)} 0.975505$	T _(11,43) 0.977018	T _(11,43) 0.988254	T _(11,43) 0.982823	VSI (pu) 0.2593
T _(40,56) 1.003564	T _(40,56) 1.006911	T _(40,56) 0.958281	T _(40,56) 0.960962	
$T_{(39,57)} 0.962797$	T _(39,57) 0.968382	T _(39,57) 0.957930	$T_{(39,57)} 0.969004$	
T _(9,55) 0.988405	T _(9,55) 0.986404	T _(9,55) 0.991583	T _(9,55) 0.984642	
	Optimal size and lo	cation of SVC-TCSC	1	
	,	15.000	0.000.4	
/	/	svc ₍₁₃₎ 17.3838	svc ₍₃₅₎ 8.28284	
/	/	svc ₍₁₄₎ 11.2275	svc ₍₃₈₎ 6.5553	
/	/	svc ₍₃₅₎ 12.2902	svc ₍₅₀₎ 2.08968	
/	/	svc ₍₃₈₎ 16.354	svc ₍₅₃₎ 1.7785	
/	/	svc ₍₅₀₎ 11.123	svc ₍₅₄₎ 0.6111	
	/	svc ₍₅₃₎ 6.240	/	
/	/	Tcsc _(9,12) 0.0573	$Tcsc_{(9,12)} 0.0269$	
/	/	Tcsc _(1,16) 0.0308	$Tcsc_{(1,16)} 0.0042$	
/	/	Tcsc _(30,31) 0.3034	Tcsc _(47,48) 0.0039	
/	/	Tcsc _(47,48) 0.0175	Tcsc _(13,49) 0.1356	
/	/	Tcsc _(13,49) 0.1465	Tcsc _(56,42) 0.0228	
/	/	Tcsc _(38,48) 0.0371	Tcsc _(38,48) 0.0347	

 P_{Gi} (MW), V_{gi} (p.u.), $T_{(I,j)}$ (p.u.), Q svc_(i) (MVAr), X Tcsc_(I,j) (p.u.).

6.3.1.3 Case 3: Total Voltage Deviation and the Investment Cost of FACTS Optimization

In a comprehensive analysis encompassing the optimization of total voltage deviation (TVD) within the same system configurations, notable improvements were observed. In the base case scenario, TVD registered at 0.7029 per unit (p.u.), which decreased to 0.6842 p.u. following the integration of RESs, marking a reduction of approximately 2.66% for scenario 1 (Objective 1). Subsequent intervention with FACTS devices yielded a significant improvement, reducing TVD to 0.2138 p.u., reflecting a substantial enhancement of approximately 69.5% compared to the conventional configuration of the IEEE 57 bus and 68.79% compared to the RES-integrated scenario. However, this advancement incurred an additional cost of 237.38 (USD/h) due to FACTS deployment. Conversely, the base case scenario led to TVD of 0.3435 p.u., with a FACTS cost of 73 (USD/h).

Figure 6-18 shows the Pareto front for case 3, where NSKOA provides a well-distributed front, with the best compromise solution (BCS) positioned near the center. Figures 6-19 and 6-20 present the voltage profile at the load buses and the generated reactive power, respectively, for the same case. All values remain within permissible limits, confirming that the constraints are fully satisfied. The numerical results presented in Table 6-6 illustrate that the deployment of SVCs and TCSCs effectively reduced voltage deviation, enhancing voltage stability across the network. SVCs were installed at buses 14, 21, 35, 44, 53, and 54, providing crucial reactive power support to improve voltage profiles at these locations. Notably, in the IEEE 57-bus network, bus 35 required a significant SVC installation, which played a key role in reducing voltage deviation by supplying or absorbing reactive power as needed. This capability helps maintain voltage levels within desired limits, especially during fluctuations in load.

The TCSCs installed on branches (19–20), (21–22), (37–39), and (13–49) facilitated better control of line reactance and optimized the flow of reactive power, which mitigated voltage drops

along transmission lines, contributing to improved voltage levels and further aiding voltage regulation. The consistent presence of SVC at bus 35 and TCSC on branch (13–49) illustrates their pivotal role in mitigating voltage deviations and ensuring stable reactive power management throughout the IEEE 57-bus network. These findings highlight the efficacy of FACTS deployment in reducing total voltage deviation within the system, underscoring the trade-off between improved voltage stability and FACTS deployment cost.

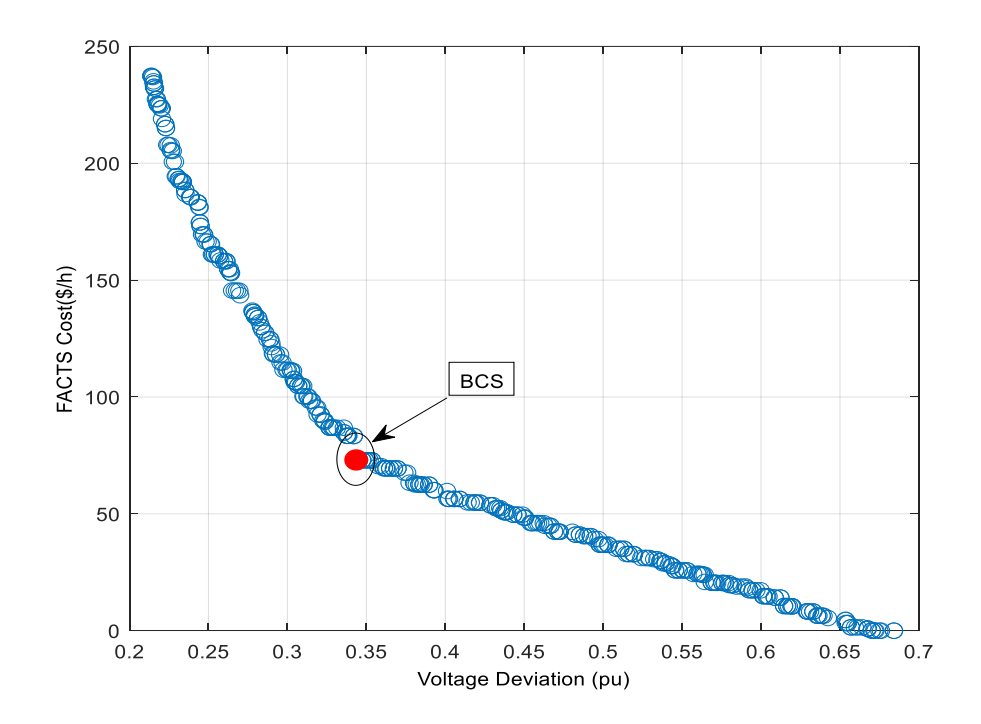


Figure 6-17:Pareto Front Of Case 3

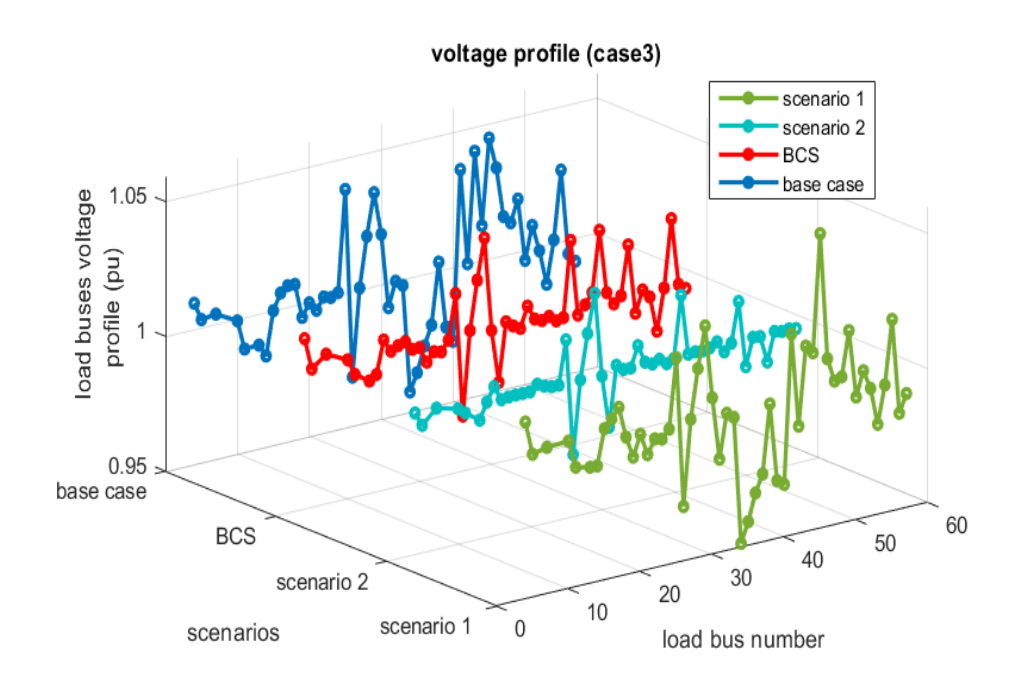


Figure 6-18:Load Bus Voltage Profile For Case 3

Table 6-6:Optimal result and control variables for case 3

Control variables				Fitness values
Base case	Scenario 1	Scenario 2	BCS	
Pg ₁ 198.3536	Pg ₁ 545.1541	Pg ₁ 425.9918	Pg ₁ 519.1516	Base case
Pg ₂ 19.6385 Pg ₃ 136.582	Pg ₂ 42.6645 Pg ₃ 110.9823	Pg ₂ 39.6999 Pg ₃ 118.1849	Pg ₂ 57.4019 Pg ₃ 96.2114	TGcost (\$/h) 10979.12
Pg ₆ 94.5306 Pg ₈ 319.912	Pg ₆ 14.0295 Pg ₈ 239.4711	Pg ₆ 58.4176 Pg ₈ 224.5698	Pg ₆ 0.0000 Pg ₈ 262.5789	RP _L (MW) 17.7160
Pg ₉ 199.070	Pg ₉ 171.4433	Pg ₉ 199.999	Pg ₉ 182.9161	TVD (pu) 1.5782
Pg ₁₂ 209.994 Vg ₁ 1.074194	Pg ₁₂ 164.5253 Vg ₁ 1.04032	Pg ₁₂ 209.999 Vg ₁ 1.02062	Pg ₁₂ 168.6121 Vg ₁ 1.02712	VSI (pu) 0.2766
Vg ₂ 1.067047 Vg ₃ 1.061879	Vg ₂ 1.02816	Vg ₂ 1.01073 Vg ₃ 1.00583	Vg ₂ 1.02244 Vg ₃ 1.02102	
Vg ₆ 1.063364	Vg ₆ 1.00302	Vg ₆ 1.00025	Vg ₆ 1.00153	Scenario 1
Vg ₈ 1.075176 Vg ₉ 1.051757	Vg ₈ 1.02873 Vg ₉ 1.01095	Vg ₈ 1.02203 Vg ₉ 1.01148	Vg ₈ 1.03107 Vg ₉ 1.01119	TGcost (\$/h) 8102.0217
Vg ₁₂ 1.040481 T _(4,18) 1.042820	Vg ₁₂ 1.01479 T _(4,18) 0.97587	Vg ₁₂ 1.00556 T _(4.18) 0.955661	Vg ₁₂ 1.00799 T _(4,18) 0.97037	RP _L (MW) 37.4701
$T_{(4,18)} 0.969822$ $T_{(21,20)} 1.00078$	$T_{(4,18)}$ 1.04991 $T_{(21,20)}$ 0.96580	$T_{(4,18)}$ 1.05236 $T_{(21,20)}$ 0.96297	T _(4,18) 1.04938	TVD (pu) 0.6842
T _(24,25) 0.946581	T _(24,25) 0.96748	T _(24,25) 0.96883	$T_{(21,20)} 0.96335$ $T_{(24,25)} 0.97148$	VSI (pu) 0.29440
$T_{(24,25)} 0.962140$ $T_{(24,26)} 1.025195$	T _(24,25) 0.96013 T _(24,26) 1.03451	T _(24,25) 0.98919 T _(24,26) 1.02960	$T_{(24,25)} 0.98409$ $T_{(24,26)} 1.03335$	
$T_{(7,29)}$ 0.991647 $T_{(34,32)}$ 0.943693	$T_{(7,29)}$ 0.95720 $T_{(34,32)}$ 0.92014	T _(7,29) 0.96383 T _(34,32) 0.95538	T _(7,29) 0.95958 T _(34,32) 0.95523	Scenario 2
T _(11,41) 0.922844	T _(11,41) 0.900000	T _(11,41) 0.92422	T _(11,41) 0.90000	TGcost (\$/h) 7546.581
$T_{(15,45)} 0.982334$ $T_{(14,46)} 0.963354$	$T_{(15,45)} 0.93812$ $T_{(14,46)} 0.98081$	T _(15,45) 1.02301 T _(14,46) 1.00294	T _(15,45) 0.98128 T _(14,46) 0.99451	TFcost (\$/h) 237.380
$T_{(10,51)} 0.975757$ $T_{(13,49)} 0.937087$	$T_{(10,51)}$ 0.99571 $T_{(13,49)}$ 0.90023	T _(10,51) 0.99637 T _(13,49) 0.90764	$T_{(10,51)}$ 0.99666 $T_{(13,49)}$ 0.90000	RP _L (MW) 26.0637
T _(11,43) 0.975505	T _(11,43) 0.97609	T _(11,43) 1.00385	T _(11,43) 1.00178	TVD (pu) 0.2138
T _(40,56) 1.003564 T _(39,57) 0.962797	$T_{(40,56)}$ 1.02057 $T_{(39,57)}$ 0.90000	T _(40,56) 0.92593 T _(39,57) 0.94573	$ \begin{array}{ccc} T_{(40,56)} & 0.94376 \\ T_{(39,57)} & 0.95405 \end{array} $	VSI (pu) 0.2945
T _(9,55) 0.988405	T _(9,55) 0.98505	T _(9,55) 1.01831 ation of SVC-TCSC	T _(9,55) 0.98132	
,	, , , , , , , , , , , , , , , , , , ,	T	, , , , , , , , , , , , , , , , , , ,	BCS
/	/	$\begin{array}{ccc} svc_{(14)} & 21.585 \\ svc_{(21)} & 12.785 \end{array}$	/	TGcost (\$/h) 8671.4377
/	/	svc ₍₃₅₎ 30.907	svc ₍₃₅₎ 28.511	TFcost (\$/h) 73.0604
/	/	svc ₍₄₄₎ 7.757 svc ₍₅₃₎ 5.156	/	RP _L (MW) 36.0721
/	/	svc ₍₅₄₎ 9.580	/	, ,
/	/	Tcsc(19,20) 0.3155	Tcsc _(19,20) 0.3472	TVD (pu) 0.3436
/	/	$Tcsc_{(21,22)} 0.0936$ $Tcsc_{(37,39)} 0.0303$	$Tcsc_{(21,22)} 0.0657$ $Tcsc_{(37,39)} 0.0216$	VSI (pu) 0.29601
/	/	$Tcsc_{(36,40)} 0.0373$	$Tcsc_{(36,40)} 0.0199$	
/	/	Tcsc _(56,42) 0.1961 Tcsc _(38,49) 0.1416	/	
D (MW) W . (a	/	1 CSC(38,49) 0.1410	/	

 $\overline{P_{Gi}\left(MW\right)},\,V_{gi}\left(p.u.\right),\,T_{\left(I,j\right)}\left(p.u.\right),Q\,\,svc_{\left(i\right)}\left(MVAr\right),\,X\,\,Tcsc_{\left(I,j\right)}\left(p.u.\right).$

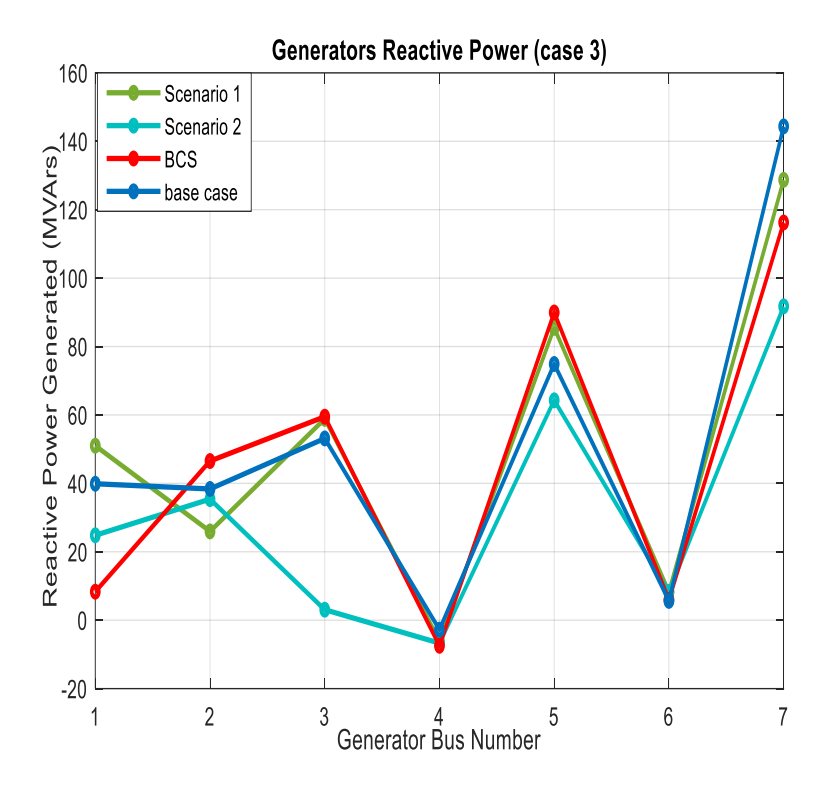


Figure 6-19: Generator's Reactive Power For Case 3

6.3.1.4 Case 4: Voltage Stability Index and the Investment Cost of FACTS Optimization

In this phase, the focus shifted towards optimizing and enhancing the voltage stability index within the examined system configurations. The base case exhibited a voltage stability index of 0.2757 p.u., which notably improved to 0.2018 p.u. following the integration of both RESs and FACTS technologies, representing a significant improvement of approximately 26.80%. However, this improvement came at an additional cost of USD 62.04 per hour due to FACTS deployment. Interestingly, in the BCS, the voltage stability index of 0.2074 p.u. was achieved with a significantly lower FACTS cost of USD 10.38 per hour, showcasing comparable performance with substantial savings of approximately USD 52 per hour, equivalent to approximately 83.78% in investment expenses of FACTS.

Figure 6-21 shows the Pareto front for case 4, where NSKOA provides a well-distributed front, with the best compromise solution (BCS) positioned near the center. Table 6-7 shows that the integration of SVCs and TCSCs significantly influenced the voltage stability index. Notably, the SVCs at buses 16, 21, 28, and 54 provided vital reactive power compensation, especially at bus 28, crucial for keeping the voltage profile at the desired levels. This ability reduces the risk of voltage collapse and improves the voltage stability index as shown in Figures 6-22 and 6-23, which present the voltage profile at the load buses and the generated reactive power where all values remain within permissible limits.

The results indicate that branches (18–19) and (24–25) required larger TCSCs due to high reactive power demand, which directly impacted voltage stability, by enhancing power transfer capability, helping to stabilize voltage levels, and preventing conditions that could lead to instability. The placement of TCSCs on branches (30–31) and (37–38) further emphasizes their crucial role in optimizing voltage stability across the IEEE 57 network. The branches (18–19) and (24–25) demonstrated the need for larger TCSCs as these lines were under significant reactive power demand, directly impacting voltage stability. TCSCs improve the power transfer capability of lines, which can help stabilize voltage levels and prevent conditions leading to voltage instability. The TCSCs on branches (30–31) and (37–38) underscore their critical role in optimizing voltage stability across the IEEE 57 network. These findings underscore the effectiveness of FACTS deployment in enhancing voltage stability while highlighting the importance of cost considerations in optimizing system performance.

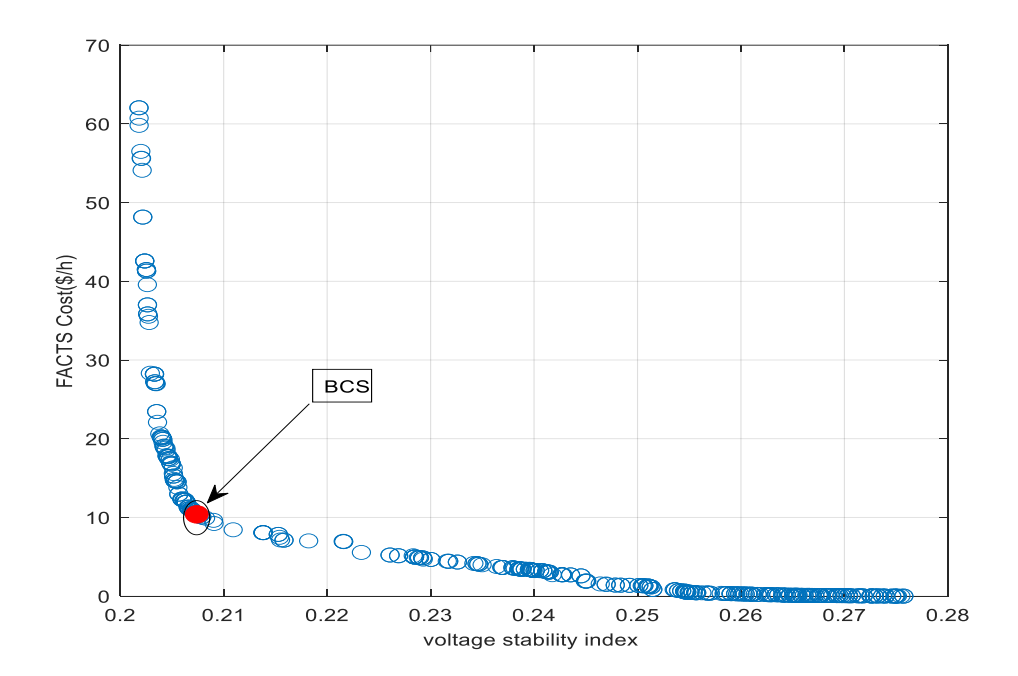


Figure 6-20:Pareto Front Of Case 4

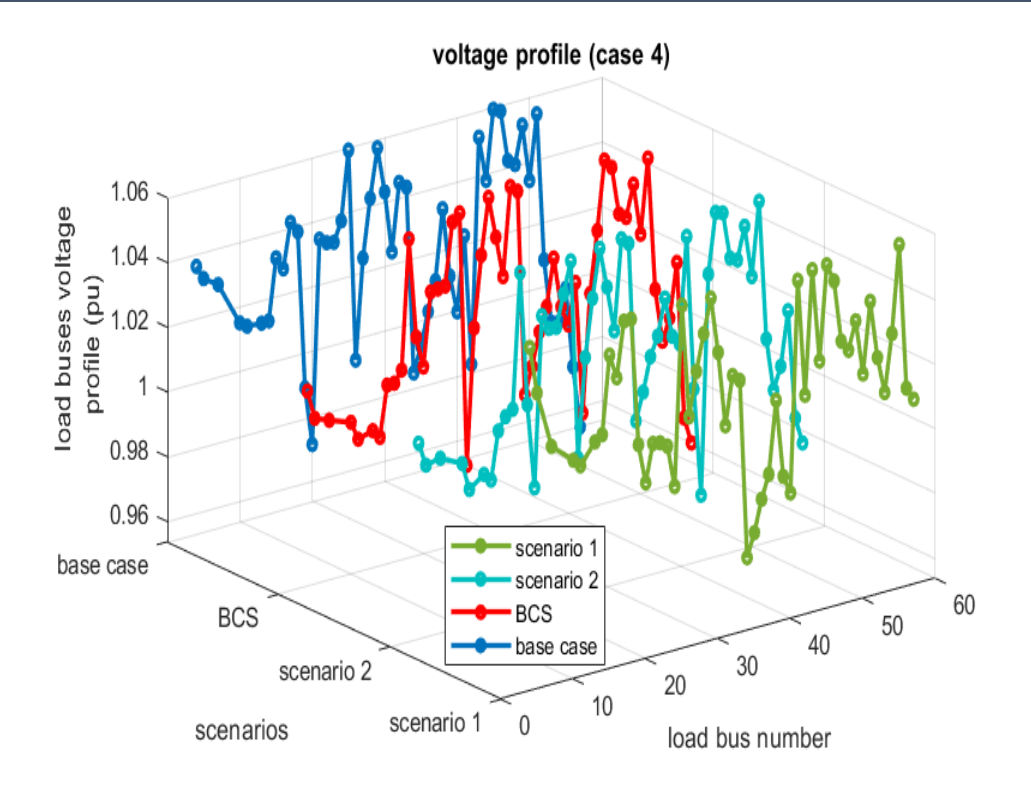


Figure 6-21:Load Bus Voltage Profile For Case 4

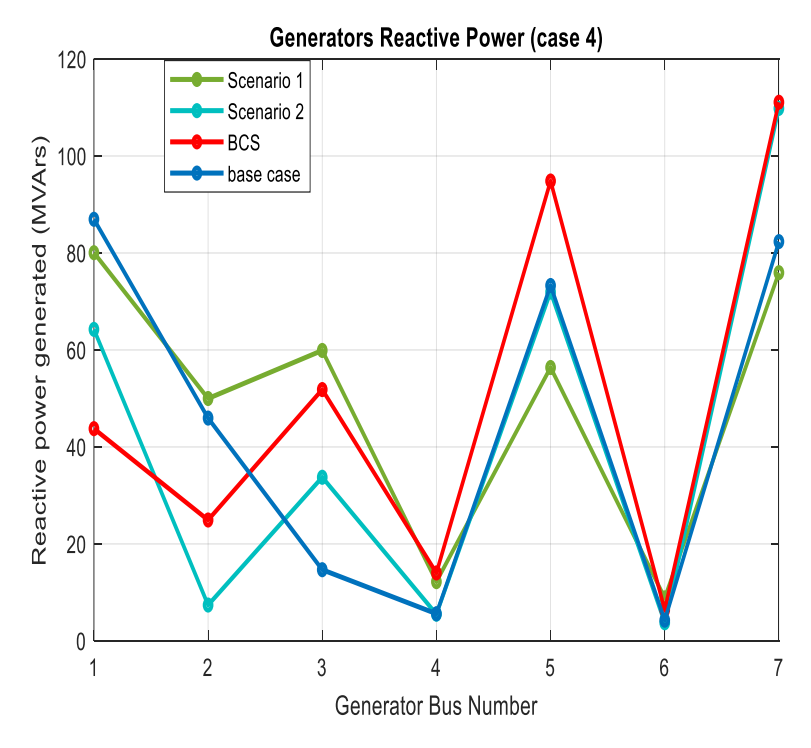


Figure 6-22: Generator's Reactive Power For Case 4

Table 6-7:Optimal Result And Control Variables For Case 4

CONTROLE VARIABLES				Fitness values
Base case	Scenario 1	Scenario 2	BCS	
Pg ₁ 320.9496	Pg ₁ 552.3335	Pg ₁ 402.9396	Pg ₁ 516.5286	-
Pg ₂ 44.2970	Pg ₂ 100.000	Pg ₂ 32.0975	Pg ₂ 93.31830	
Pg ₃ 70.9802	Pg ₃ 76.6229	Pg ₃ 135.201	Pg ₃ 92.04518	
Pg ₆ 49.1657	Pg ₆ 99.9997	Pg ₆ 0.45037	Pg ₆ 0.000000	
Pg ₈ 271.1674	Pg ₈ 50.5656	Pg ₈ 295.800	Pg ₈ 196.9922	
Pg ₉ 197.0577	Pg ₉ 199.998	Pg ₉ 200.000	Pg ₉ 180.3202	
Pg ₁₂ 152.410	Pg ₁₂ 209.999	Pg ₁₂ 208.955	Pg ₁₂ 210.000	Base case
Vg ₁ 1.076947	Vg ₁ 1.099834	Vg ₁ 1.037665	Vg ₁ 1.038911	<u>Dusc cusc</u>
Vg ₂ 1.064682	Vg ₂ 1.092973	Vg ₂ 1.021399	Vg ₂ 1.029121	C _{ost} (\$/h) 9193.49
Vg3 1.040932	Vg3 1.070328	Vg3 1.021756	Vg3 1.021645	$RP_L(MW)$ 29.635
Vg ₆ 1.035024	Vg ₆ 1.043710	Vg ₆ 1.008789	Vg ₆ 1.006930	
Vg ₈ 1.050021	Vg ₈ 1.034728	Vg ₈ 1.031409	Vg ₈ 1.029410	TVD (p.u) 1.4720
Vg ₉ 1.030837	Vg ₉ 1.027750	Vg ₉ 1.014471	Vg ₉ 1.011513	VSI (p.u) 0.2757
Vg ₁₂ 1.023650	Vg ₁₂ 1.037090	Vg ₁₂ 1.018090	Vg ₁₂ 1.014264	Scenario 1
T ₍₄ ,18) 0.9726	$T_{(4,18)}$ 1.008410	$T_{(4,18)}$ 1.022652	$T_{(4,18)}$ 1.017152	
$T_{(21,20)}$ 1.07613	T _(4,18) 0.986867	$T_{(4,18)}$ 0.901523	T _(4,18) 0.922051	TGcost (\$/h) 5217.74
T _(24,25) 0.98528	$T_{(21,20)}$ 1.012262	T _(21,20) 1.069454	$T_{(21,20)}$ 1.017742	
T _(24,25) 0.96546	T _(24,25) 0.939723	T _(24,25) 0.998648	T _(24,25) 1.007304	$RP_L(MW)$ 38.719
T _(24,26) 1.04711	$T_{(24,25)}$ 0.937514	$T_{(24,25)}$ 0.992255	$T_{(24,25)}$ 0.997993	TVD (p.u) 1.5869
T _(7,29) 0.959181	T _(24,26) 0.982061	T _(24,26) 1.054628	T _(24,26) 1.084371	VSI (p.u) 0.2757
T _(34,32) 0.90985	$T_{(7,29)}$ 0.959973	$T_{(7,29)}$ 0.939237	$T_{(7,29)}$ 0.931607	
T _(11,41) 0.95951	T _(34,32) 0.918400	$T_{(34,32)}$ 0.900827	$T_{(34,32)}$ 0.900019	Scenario 2
T _(15,45) 0.97504	$T_{(11,41)}$ 0.900000	$T_{(11,41)}$ 0.900589	$T_{(11,41)}$ 0.900000	
$T_{(14,46)} 0.95079$	T _(15,45) 0.988708	$T_{(15,45)}$ 0.955885	$T_{(15,45)}$ 0.954432	TGcost (\$/h) 9748.93
$T_{(10,51)}$ 0.95684	T _(14,46) 0.964576	$T_{(14,46)}$ 0.935021	$T_{(14,46)}$ 0.934472	TFcost (\$/h) 62.045
T _(13,49) 0.90762	$T_{(10,51)}$ 0.970265	$T_{(10,51)}$ 0.941255	$T_{(10,51)}$ 0.939803	RP _L (MW) 24.645
$T_{(11,43)} 0.95171$	T _(13,49) 0.934064	$T_{(13,49)}$ 0.900053	T _(13,49) 0.900661	TVD (p.u) 1.4312
T _(40,56) 0.98339	$T_{(11,43)}$ 0.95915	$T_{(11,43)}$ 1.053052	$T_{(11,43)}$ 0.975194	VSI (p.u) 0.2018
T _(39,57) 1.09573	T _(40,56) 0.986130	T _(40,56) 1.083148	T _(40,56) 1.058040	(p.u) 0.2010
T _(9,55) 1.032468	$T_{(39,57)}$ 0.954959	T _(39,57) 1.012770	$T_{(39,57)}$ 1.037772	<u>BCS</u>
	T _(9,55) 0.964379	T _(9,55) 0.989115	$T_{(9,55)}$ 0.988271	<u>DCS</u>
	Optimal size and lo	cation of SVC-TCSO	C	TC = = + (\$\frac{1}{2}\) (002.24
/	/	svc ₍₁₆₎ 0.75793	/	TGcost (\$/h) 6993.24
/	/	$svc_{(21)}$ 0.66050	$svc_{(32)}$ 0.39169	TFcost (\$/h) 10.38
/	/	$svc_{(28)}$ 0.01766	$svc_{(28)}$ 0.00171	RP _L (MW) 38.404
/	/	$svc_{(54)}$ 0.0710	$svc_{(54)}$ 0.00202	TVD (p.u) 1.3522
,	,	$Tcsc_{(18.19)} 0.5480$	$Tcsc_{(18,19)} 0.4040$	VSI (p.u) 0.2074
,	,	$Tcsc_{(24,25)} 0.9840$	$Tcsc_{(24,25)} 0.9840$	
,	,	$Tcsc_{(25,30)} 0.1616$	$Tcsc_{(25,30)} 0.1616$	
/	,	$Tcsc_{(30,31)} 0.3952$	$Tcsc_{(30,31)} 0.3964$	
,	,	$Tcsc_{(30,31)} 0.3932$ $Tcsc_{(37,38)} 0.0807$	$Tcsc_{(37,38)} 0.0807$	
/	,	. , ,	* * *	
/	/	$Tcsc_{(11,41)} 0.5992$	$Tcsc_{(11,41)} 0.1752$	

6.4 Conclusion

This chapter presents a comprehensive study on the optimization of power flow through an exploration of a multi-objective optimization strategy that can simultaneously address a range of critical objectives using the non-dominated sorting Kepler optimization algorithm (NSKOA), focusing on the integration of (RESs) and FACTS devices into the electrical network. The proposed NSKOA has demonstrated its effectiveness in achieving significant improvements in several key performance indicators. Notably, the integration of RESs and FACTS devices resulted in a 6.49% reduction in power production costs, a 9.05% reduction in real power losses (RPLs), a 69.5% decrease in voltage deviations (TVDs), and a 26.80% improvement in the voltage stability index (VSI). The approach also achieved a substantial 22.76% reduction in emissions, contributing to environmental sustainability. These results illustrate the robustness of the NSKOA in optimizing power system performance under various operational conditions and its effectiveness in addressing multi-objective problems. It underscores the potential of these approaches in managing the complexities of power systems. It is true that the regulation of control variables, such as generation voltages and transformer tap ratios, ensures the operability of the power system but remains technically insufficient. This highlights the practical implications of RES and FACTS device integration into the design and operation of future power systems, paving the way for a more efficient, reliable, and sustainable electricity supply.

GENERAL CONCLUSION

This thesis has addressed the multifaceted technical, financial, and environmental challenges confronting modern electrical networks both in upgrading aging infrastructure and deploying new systems. While recent advancements in grid technologies and optimization techniques offer significant benefits, they also introduce new operational complexities, particularly with regard to tuning parameters and ensuring system stability. A central focus of this work has been the integration of (RES), which despite their undeniable environmental and economic advantages introduce inherent variability due to fluctuating wind, solar irradiance, and hydrological conditions. These uncertainties complicate reliable system operation, especially under high RES penetration.

To capture the impact of RES variability, this work first identified and characterized key stochastic variables associated with wind, solar, and hydro power generation. Probabilistic modeling techniques, including Monte Carlo simulation and probability density functions, were used to quantify uncertainty and assess the economic implications of generation shortfalls or surpluses. The study then progressed to deterministic power flow and (OPF) models aimed at minimizing generation costs, power losses, and pollutant emissions. However, traditional optimization techniques often fall short when applied to large-scale networks with high renewable integration.

To overcome these limitations, the thesis explored a wide range of metaheuristic optimization techniques including evolutionary, swarm-based, physics-inspired, and human-based algorithms with a particular focus on their ability to balance global exploration and local exploitation. Building on this foundation, the Kepler Optimization Algorithm (KOA) was selected and further enhanced through the development of two key improvements: an exploratory exploitative operator ϕ designed to intensify neighborhood search and accelerate convergence, and a non-dominated sorting scheme tailored for effective multi-objective optimization.

These improvements were applied to the optimal generation dispatch of a 114-bus Algerian power system under RES uncertainty. Results showed that the enhanced KOA achieved a 49% reduction in emissions, significantly lowered generation costs, and reduced carbon tax liabilities. However, despite increased generation diversity and capacity, the system remained vulnerable to power losses and voltage instability. To address this, the study expanded to incorporate Flexible AC Transmission Systems (FACTS) devices, which, though effective in enhancing power flow and voltage profiles, come with high capital costs.

A multi-objective optimization framework was then implemented to jointly minimize investment in FACTS devices while maximizing operational benefits, including cost savings, loss reduction, voltage stability, and emission cuts. The optimized solution yielded a 6.49% reduction in production costs (1.31% net of FACTS investment), a 9.05% drop in real power losses, a 69.5% improvement in voltage deviation, a 26.8% boost in voltage stability index, and a 22.76% reduction in total emissions.

Overall, the enhanced KOA approach demonstrated strong performance and adaptability in managing the complex interplay between renewable uncertainty, grid optimization, and cost-effective

GENERAL CONCLUSION

infrastructure upgrades. The results of this thesis affirm the growing importance of robust, intelligent optimization strategies in guiding the evolution of modern power systems toward more sustainable, resilient, and economically efficient operation.

FUTURE WORK

In future work, we will extend our stochastic optimization framework to capitalize on surplus renewable energy that arises under under-estimation scenarios by diverting excess generation into green hydrogen production rather than incurring penalty fees. Specifically, we will integrate an electrolyzer model into the dispatch algorithm so that any power exceeding forecasted demand is automatically allocated to hydrogen synthesis. By co-optimizing generation scheduling and hydrogen production, the system can transform what would have been a curtailment penalty into a revenue-generating process, effectively doubling the economic value of surplus energy. We will quantify this benefit by comparing baseline penalty costs against combined revenues from avoided fees and hydrogen sales, while also tracking the volume of green hydrogen produced. This approach promises not only to reduce operational risk and improve system profitability, but also to contribute to decarbonization by creating a low-carbon fuel stream from otherwise wasted renewable output.

BIBLIOGRAPHY

- [1] O. Ellabban, H. Abu-Rub, and F. Blaabjerg, "Renewable energy resources: Current status, future prospects and their enabling technology," *Renew. Sustain. Energy Rev.*, vol. 39, pp. 748–764, 2014, doi: 10.1016/j.rser.2014.07.113.
- [2] J. M. Morales, A. J. Conejo, H. Madsen, P. Pinson, and M. Zugno, "Integrating renewables in electricity markets Operational problems," *Springer*, vol. 205, p. 429, 2014, doi: 10.1007/978-1-4614-9411-9.
- [3] I. Marouani *et al.*, "Optimized FACTS Devices for Power System Enhancement: Applications and Solving Methods," *Sustain.*, vol. 15, no. 12, 2023, doi: 10.3390/su15129348.
- [4] C. H. N. Kumari and K. C. Sekhar, "Power flow control using FACTS device in modern power system," *IEEE Int. Conf. Circuits Syst. ICCS 2017*, vol. 2018-Janua, no. 1, pp. 372–376, 2017, doi: 10.1109/ICCS1.2017.8326024.
- [5] B. H. Alajrash, M. Salem, M. Swadi, T. Senjyu, M. Kamarol, and S. Motahhir, "A comprehensive review of FACTS devices in modern power systems: Addressing power quality, optimal placement, and stability with renewable energy penetration," *Energy Reports*, vol. 11, no. April, pp. 5350–5371, 2024, doi: 10.1016/j.egyr.2024.05.011.
- [6] A. Castillo and D. F. Gayme, "Grid-scale energy storage applications in renewable energy integration: A survey," *Energy Convers. Manag.*, vol. 87, pp. 885–894, 2014, doi: 10.1016/j.enconman.2014.07.063.
- [7] D. Mehta, D. K. Molzahn, and K. Turitsyn, "Recent advances in computational methods for the power flow equations," *Proc. Am. Control Conf.*, vol. 2016-July, pp. 1753–1765, 2016, doi: 10.1109/ACC.2016.7525170.
- [8] M. E. Khodayar, L. Wu, and M. Shahidehpour, "Hourly coordination of electric vehicle operation and volatile wind power generation in SCUC," *IEEE Trans. Smart Grid*, vol. 3, no. 3, pp. 1271–1279, 2012, doi: 10.1109/TSG.2012.2186642.
- [9] F. G. Montoya, R. Baños, A. Alcayde, and F. Manzano-Agugliaro, *Optimization methods applied to power systems*, vol. 12, no. 12. 2019. doi: 10.3390/en12122302.
- [10] T. Van Luong, N. Melab, and E. G. Talbi, "GPU computing for parallel local search metaheuristic algorithms," *IEEE Trans. Comput.*, vol. 62, no. 1, pp. 173–185, 2013, doi: 10.1109/TC.2011.206.
- [11] K. N. Hasan, R. Preece, and J. V. Milanović, "Existing approaches and trends in uncertainty modelling and probabilistic stability analysis of power systems with renewable generation," *Renew. Sustain. Energy Rev.*, vol. 101, no. December 2017, pp. 168–180, 2019, doi: 10.1016/j.rser.2018.10.027.
- [12] K. K. Nandini, N. S. Jayalakshmi, and V. K. Jadoun, "A probabilistic approach on uncertainty modelling and their effect on the optimal operation of charging stations," *IET Gener. Transm. Distrib.*, vol. 18, no. 13, pp. 2325–2338, 2024, doi: 10.1049/gtd2.13194.
- [13] W. Fendzi Mbasso *et al.*, "Reliability analysis of a grid-connected hybrid renewable energy system using hybrid Monte-Carlo and Newton Raphson methods," *Front. Energy Res.*, vol. 12, no. August, pp. 1–28, 2024, doi: 10.3389/fenrg.2024.1435221.
- [14] A. M. Hakami, K. N. Hasan, M. Alzubaidi, and M. Datta, "A Review of Uncertainty Modelling Techniques for Probabilistic Stability Analysis of Renewable-Rich Power Systems," *Energies*, vol. 16, no. 1, 2023, doi: 10.3390/en16010112.
- [15] M. Aien, A. Hajebrahimi, and M. Fotuhi-Firuzabad, "A comprehensive review on uncertainty

- modeling techniques in power system studies," *Renew. Sustain. Energy Rev.*, vol. 57, pp. 1077–1089, 2016, doi: 10.1016/j.rser.2015.12.070.
- [16] D. Martin, W. Zhang, J. Chan, and J. Lindley, "A comparison of Gumbel and Weibull statistical models to estimate wind speed for wind power generation," 2014 Australas. Univ. Power Eng. Conf. AUPEC 2014 Proc., no. October, 2014, doi: 10.1109/AUPEC.2014.6966499.
- [17] D. Nugent and B. K. Sovacool, "Assessing the lifecycle greenhouse gas emissions from solar PV and wind energy: A critical meta-survey," *Energy Policy*, vol. 65, pp. 229–244, 2014, doi: 10.1016/j.enpol.2013.10.048.
- [18] IRENA, "Renewable energy: A key climate solution," Int. Renew. Energy Agency, p. 8, 2017.
- [19] B. Patrick and N. Foster, "Life Cycle Emissions of Renewable Energy Systems," no. May, 2025.
- [20] S. D. Ahmed, F. S. M. Al-Ismail, M. Shafiullah, F. A. Al-Sulaiman, and I. M. El-Amin, "Grid Integration Challenges of Wind Energy: A Review," *IEEE Access*, vol. 8, pp. 10857–10878, 2020, doi: 10.1109/ACCESS.2020.2964896.
- [21] H. Ahmed, "Reactive power and voltage control in grid-connected wind farms: an online optimization based fast model predictive control approach," *Electr. Eng.*, vol. 97, no. 1, pp. 35–44, 2015, doi: 10.1007/s00202-014-0314-1.
- [22] M. Abdelateef Mostafa, E. A. El-Hay, and M. M. ELkholy, *Recent Trends in Wind Energy Conversion System with Grid Integration Based on Soft Computing Methods: Comprehensive Review, Comparisons and Insights*, vol. 30, no. 3. Springer Netherlands, 2023. doi: 10.1007/s11831-022-09842-4.
- [23] T. E. K. Zidane *et al.*, "Grid-Connected Solar PV Power Plants Optimization: A Review," *IEEE Access*, vol. 11, no. August, pp. 79588–79608, 2023, doi: 10.1109/ACCESS.2023.3299815.
- [24] M. Premkumar, K. Karthick, and R. Sowmya, "A review on solar PV based grid connected microinverter control schemes and topologies," *Int. J. Renew. Energy Dev.*, vol. 7, no. 2, pp. 171–182, 2018, doi: 10.14710/ijred.7.2.171-182.
- [25] M. Talha, A. Amir, S. R. S. Raihan, and N. Abd Rahim, "Grid-connected photovoltaic inverters with low-voltage ride through for a residential-scale system: A review," *Int. Trans. Electr. Energy Syst.*, vol. 31, no. 10, pp. 1–28, 2021, doi: 10.1002/2050-7038.12630.
- [26] J. Shu, J. J. Qu, R. Motha, J. C. Xu, and D. F. Dong, "Impacts of climate change on hydropower development and sustainability: A review," *IOP Conf. Ser. Earth Environ. Sci.*, vol. 163, no. 1, 2018, doi: 10.1088/1755-1315/163/1/012126.
- [27] A. Fernández-Guillamón, E. Gómez-Lázaro, E. Muljadi, and Á. Molina-García, "Power systems with high renewable energy sources: A review of inertia and frequency control strategies over time," *Renew. Sustain. Energy Rev.*, vol. 115, no. August, p. 109369, 2019, doi: 10.1016/j.rser.2019.109369.
- [28] F. Valdettaro and A. A. Faisal, "Offline Bayesian Aleatoric and Epistemic Uncertainty Quantification and Posterior Value Optimisation in Finite-State MDPs," *Proc. Mach. Learn. Res.*, vol. 244, pp. 3391–3409, 2024.
- [29] H. Emmett and L. Goldman, "Identification of Logical Errors through Monte-Carlo Simulation," *Eur. Spreadsheet Risks Int. Grp.*, pp. 1–8, 2004.
- [30] P. Saracco and M. G. Pia, "An exact framework for uncertainty quantification in Monte Carlo simulation," *J. Phys. Conf. Ser.*, vol. 513, no. TRACK 2, 2014, doi: 10.1088/1742-

- 6596/513/2/022033.
- [31] P. Saracco, M. G. Pia, and M. Batic, "Theoretical grounds for the propagation of uncertainties in monte carlo particle transport," *IEEE Trans. Nucl. Sci.*, vol. 61, no. 2, pp. 877–887, 2014, doi: 10.1109/TNS.2014.2300112.
- [32] A. Srinivasan and N. Takeishi, "An MCMC Method for Uncertainty Set Generation via Operator-Theoretic Metrics," *Proc. IEEE Conf. Decis. Control*, vol. 2020-Decem, pp. 2714–2719, 2020, doi: 10.1109/CDC42340.2020.9304222.
- [33] A. Lye, A. Cicirello, and E. Patelli, "A review of stochastic sampling methods for Bayesian inference problems," *Proc. 29th Eur. Saf. Reliab. Conf. ESREL 2019*, pp. 1866–1873, 2020, doi: 10.3850/978-981-11-2724-3-1087-cd.
- [34] B. O. Ngoko, H. Sugihara, and T. Funaki, "Synthetic generation of high temporal resolution solar radiation data using Markov models," *Sol. Energy*, vol. 103, pp. 160–170, 2014, doi: 10.1016/j.solener.2014.02.026.
- [35] R. J. Sela and C. M. Hurvich, "Computationally E cient Gaussian Maximum Likelihood Methods for Vector ARFIMA Models," *New York*, pp. 1–94, 2008.
- [36] E. Chodakowska, J. Nazarko, Ł. Nazarko, H. S. Rabayah, R. M. Abendeh, and R. Alawneh, "ARIMA Models in Solar Radiation Forecasting in Different Geographic Locations," *Energies*, vol. 16, no. 13, 2023, doi: 10.3390/en16135029.
- [37] I. Tyass, A. Bellat, A. Raihani, K. Mansouri, and T. Khalili, "Wind Speed Prediction Based on Seasonal ARIMA model," *E3S Web Conf.*, vol. 336, pp. 1–6, 2022, doi: 10.1051/e3sconf/202233600034.
- [38] L. Liu *et al.*, "Prediction of short-term PV power output and uncertainty analysis," *Appl. Energy*, vol. 228, no. March, pp. 700–711, 2018, doi: 10.1016/j.apenergy.2018.06.112.
- [39] M. Mohammadi and M. Gentili, "The outcome range problem in interval linear programming," *Comput. Oper. Res.*, vol. 129, 2021, doi: 10.1016/j.cor.2020.105160.
- [40] J. Università and B. Milan, "Sixth International Conference on Sensitivity Analysis of Model Output," *Reliab. Eng.*, no. July, 2010, doi: 10.1016/j.ijpe.2009.12.003.Efron.
- [41] Y. Li, K. Wang, B. Gao, B. Zhang, X. Liu, and C. Chen, "Interval optimization based operational strategy of integrated energy system under renewable energy resources and loads uncertainties," *Int. J. Energy Res.*, vol. 45, no. 2, pp. 3142–3156, 2021, doi: 10.1002/er.6009.
- [42] A. Chassein and M. Goerigk, "Compromise solutions for robust combinatorial optimization with variable-sized uncertainty," *Eur. J. Oper. Res.*, vol. 269, no. 2, pp. 544–555, 2018, doi: 10.1016/j.ejor.2018.01.056.
- [43] T. Tulabandhula and C. Rudin, "Robust optimization using machine learning for uncertainty sets," *Int. Symp. Artif. Intell. Math. ISAIM 2014*, pp. 1–28, 2014.
- [44] B. Xiao, Z. Gao, H. Peng, K. Chen, Y. Li, and K. Liu, "Robust Optimization of Large-Scale Wind-Solar Storage Renewable Energy Systems Considering Hybrid Storage Multi-Energy Synergy," *Sustain.*, vol. 16, no. 1, 2024, doi: 10.3390/su16010243.
- [45] Z. Yang, S. Wang, R. Zhu, J. Cui, J. Su, and L. Chen, "Research on Regulation Method of Energy Storage System Based on Multi-Stage Robust Optimization," *Energy Eng. J. Assoc. Energy Eng.*, vol. 121, no. 3, pp. 807–820, 2024, doi: 10.32604/ee.2023.028167.
- [46] S. Shah, "Monte Carlo Simulation in Renewable Energy Planning: A Comprehensive Review and Novel Framework for Uncertainty Quantification," *Am. J. Eng. Technol.*, vol. 07, no. 06, pp. 24–45, 2025, doi: 10.37547/tajet/volume07issue06-04.
- [47] P. Richter, J. Wolters, and M. Frank, "Uncertainty quantification of offshore wind farms using

- Monte Carlo and sparse grid," *Energy Sources, Part B Econ. Plan. Policy*, vol. 17, no. 1, pp. 1–27, 2022, doi: 10.1080/15567249.2021.2000520.
- [48] K. Zheng *et al.*, "Stochastic Scenario Generation Methods for Uncertainty in Wind and Photovoltaic Power Outputs: A Comprehensive Review," *Energies*, vol. 18, no. 3, 2025, doi: 10.3390/en18030503.
- [49] M. S. Hashish *et al.*, "Monte Carlo Simulation and a Clustering Technique for Solving the Probabilistic Optimal Power Flow Problem for Hybrid Renewable Energy Systems," *Sustain.*, vol. 15, no. 1, 2023, doi: 10.3390/su15010783.
- [50] H. Shi, Z. Dong, N. Xiao, and Q. Huang, "Wind Speed Distributions Used in Wind Energy Assessment: A Review," *Front. Energy Res.*, vol. 9, no. November, pp. 1–14, 2021, doi: 10.3389/fenrg.2021.769920.
- [51] P. P. Biswas, P. N. Suganthan, and G. A. J. Amaratunga, "Optimal power flow solutions incorporating stochastic wind and solar power," *Energy Convers. Manag.*, vol. 148, pp. 1194–1207, 2017, doi: 10.1016/j.enconman.2017.06.071.
- [52] S. Mouassa, A. Althobaiti, F. Jurado, and S. S. M. Ghoneim, "Novel Design of Slim Mould Optimizer for the Solution of Optimal Power Flow Problems Incorporating Intermittent Sources: A Case Study of Algerian Electricity Grid," *IEEE Access*, vol. 10, pp. 22646–22661, 2022, doi: 10.1109/ACCESS.2022.3152557.
- [53] S. Surender Reddy, P. R. Bijwe, and A. R. Abhyankar, "Real-Time Economic Dispatch Considering Renewable Power Generation Variability and Uncertainty over Scheduling Period," *IEEE Syst. J.*, vol. 9, no. 4, pp. 1440–1451, 2015, doi: 10.1109/JSYST.2014.2325967.
- [54] H. M. Dubey, M. Pandit, and B. K. Panigrahi, "Hybrid flower pollination algorithm with time-varying fuzzy selection mechanism for wind integrated multi-objective dynamic economic dispatch," *Renew. Energy*, vol. 83, pp. 188–202, 2015, doi: 10.1016/j.renene.2015.04.034.
- [55] M. H. Sulaiman, Z. Mustaffa, and M. I. Mohd Rashid, "An application of teaching—learning-based optimization for solving the optimal power flow problem with stochastic wind and solar power generators," *Results Control Optim.*, vol. 10, no. November 2022, p. 100187, 2023, doi: 10.1016/j.rico.2022.100187.
- M. H. Sulaiman and Z. Mustaffa, "An application of improved salp swarm algorithm for [56] optimal power flow solution considering stochastic solar power generation," e-Prime - Adv. Electr. Eng. Electron. Energy, vol. 5, no. June, p. 100195, 2023, doi: 10.1016/j.prime.2023.100195.
- [57] A. Wijesinghe and L. L. Lai, "Small hydro power plant analysis and development," *DRPT* 2011 2011 4th Int. Conf. Electr. Util. Deregul. Restruct. Power Technol., pp. 25–30, 2011, doi: 10.1109/DRPT.2011.5993857.
- [58] P. P. Biswas, P. N. Suganthan, B. Y. Qu, and G. A. J. Amaratunga, "Multiobjective economic-environmental power dispatch with stochastic wind-solar-small hydro power," *Energy*, vol. 150, pp. 1039–1057, 2018, doi: 10.1016/j.energy.2018.03.002.
- [59] P. Cabus, "River flow prediction through rainfall-runoff modelling with a probability-distributed model (PDM) in Flanders, Belgium," *Agric. Water Manag.*, vol. 95, no. 7, pp. 859–868, 2008, doi: 10.1016/j.agwat.2008.02.013.
- [60] S. Mouassa, S. Makhloufi, C. Djabali, and F. Jurado, "Optimal power flow solution based on gorilla troops optimization technique considering uncertainty of renewable energy sources: A case study of Adrar's isolated power network," *Wind Eng.*, 2023, doi: 10.1177/0309524X231163826.

- [61] M. H. Sulaiman and Z. Mustaffa, "Solving optimal power flow problem with stochastic wind—solar—small hydro power using barnacles mating optimizer," *Control Eng. Pract.*, vol. 106, no. October 2020, p. 104672, 2021, doi: 10.1016/j.conengprac.2020.104672.
- [62] M. Abid, M. Belazzoug, S. Mouassa, A. Chanane, and F. Jurado, "Optimal power flow of thermal-wind- solar power system using enhanced Kepler optimization algorithm: Case study of a large-scale practical power system," 2024, doi: 10.1177/0309524X241229206.
- [63] E. ayache Belagra, S. Mouassa, S. Chettih, and F. Jurado, "Optimal power flow calculation in hybrid power system involving solar, wind, and hydropower plant using weighted mean of vectors algorithm," *Wind Eng.*, 2023, doi: 10.1177/0309524X231212639.
- [64] M. H. Sulaiman and Z. Mustaffa, "Optimal power flow incorporating stochastic wind and solar generation by metaheuristic optimizers," *Microsyst. Technol.*, vol. 7, no. 2004, 2020, doi: 10.1007/s00542-020-05046-7.
- [65] K. Vaisakh, L. R. Srinivas, and K. Meah, "Genetic evolving ant direction particle swarm optimization algorithm for optimal power flow with non-smooth cost functions and statistical analysis," *Appl. Soft Comput. J.*, vol. 13, no. 12, pp. 4579–4593, 2013, doi: 10.1016/j.asoc.2013.07.002.
- [66] G. Pingen and K. Maute, "Optimal design for non-Newtonian flows using a topology optimization approach," *Comput. Math. with Appl.*, vol. 59, no. 7, pp. 2340–2350, 2010, doi: 10.1016/j.camwa.2009.08.044.
- [67] S. Frank, I. Steponavice, and S. Rebennack, "Optimal power flow: A bibliographic survey I Formulations and deterministic methods," *Energy Syst.*, vol. 3, no. 3, pp. 221–258, 2012, doi: 10.1007/s12667-012-0056-y.
- [68] H. Abdi, S. D. Beigvand, and M. La Scala, "A review of optimal power flow studies applied to smart grids and microgrids," *Renew. Sustain. Energy Rev.*, vol. 71, no. May 2015, pp. 742–766, 2017, doi: 10.1016/j.rser.2016.12.102.
- [69] E. Mezura-Montes and C. A. Coello Coello, "Constraint-handling in nature-inspired numerical optimization: Past, present and future," *Swarm Evol. Comput.*, vol. 1, no. 4, pp. 173–194, 2011, doi: 10.1016/j.swevo.2011.10.001.
- [70] C. A. Coello Coello, "Theoretical and numerical constraint-handling techniques used with evolutionary algorithms: A survey of the state of the art," *Comput. Methods Appl. Mech. Eng.*, vol. 191, no. 11–12, pp. 1245–1287, 2002, doi: 10.1016/S0045-7825(01)00323-1.
- [71] T. P. Runarsson and X. Yao, "Stochastic ranking for constrained evolutionary optimization," *IEEE Trans. Evol. Comput.*, vol. 4, no. 3, pp. 284–294, 2000, doi: 10.1109/4235.873238.
- [72] T. E. Aalberts, "Interdisciplinarity on the move: Reading Kratochwil as counter-disciplinarity proper," *Millenn. J. Int. Stud.*, vol. 44, no. 2, pp. 242–249, 2016, doi: 10.1177/0305829815620047.
- [73] J. K. Skolfield and A. R. Escobedo, "Operations research in optimal power flow: A guide to recent and emerging methodologies and applications," *Eur. J. Oper. Res.*, vol. 300, no. 2, pp. 387–404, 2022, doi: 10.1016/j.ejor.2021.10.003.
- [74] C. Yang *et al.*, "Optimal Power Flow in Distribution Network: A Review on Problem Formulation and Optimization Methods †," *Energies*, vol. 16, no. 16, pp. 1–42, 2023, doi: 10.3390/en16165974.
- [75] S. Frank and S. Rebennack, "An introduction to optimal power flow: Theory, formulation, and examples," *IIE Trans.* (*Institute Ind. Eng.*, vol. 48, no. 12, pp. 1172–1197, 2016, doi: 10.1080/0740817X.2016.1189626.

- [76] B. A. Al-Himyari, H. Al-khafaji, and N. F. Hussain, "Exploration-Exploitation Tradeoffs in Metaheuristics: A Review," *Asian J. Appl. Sci.*, vol. 12, no. 1, 2025, doi: 10.24203/98kbmk88.
- [77] T. Dokeroglu, D. Canturk, and T. Kucukyilmaz, "A survey on pioneering metaheuristic algorithms between 2019 and 2024," 2024, [Online]. Available: http://arxiv.org/abs/2501.14769
- [78] A. M. Andrew, *Introduction to Evolutionary Computing*, vol. 33, no. May. 2004. doi: 10.1108/03684920410699216.
- [79] S. Katoch, S. S. Chauhan, and V. Kumar, A review on genetic algorithm: past, present, and future Content courtesy of Springer Nature, terms of use apply. Rights reserved. Content courtesy of Springer Nature, terms of use apply. Rights reserved. Multimedia Tools and Applications, 2021.
- [80] X. S. Yang, S. Deb, Y. X. Zhao, S. Fong, and X. He, "Swarm intelligence: past, present and future," *Soft Comput.*, vol. 22, no. 18, pp. 5923–5933, 2018, doi: 10.1007/s00500-017-2810-5.
- [81] T. M. Shami, A. A. El-Saleh, M. Alswaitti, Q. Al-Tashi, M. A. Summakieh, and S. Mirjalili, "Particle Swarm Optimization: A Comprehensive Survey," *IEEE Access*, vol. 10, no. January, pp. 10031–10061, 2022, doi: 10.1109/ACCESS.2022.3142859.
- [82] S. Chattopadhyay, A. Marik, and R. Pramanik, "A Brief Overview of Physics-inspired Metaheuristic Optimization Techniques," 2022, [Online]. Available: http://arxiv.org/abs/2201.12810
- [83] E. Rashedi, H. Nezamabadi-pour, and S. Saryazdi, "GSA: A Gravitational Search Algorithm," *Inf. Sci. (Ny).*, vol. 179, no. 13, pp. 2232–2248, 2009, doi: 10.1016/j.ins.2009.03.004.
- [84] M. M. Saber, M. A.Elsayed, A. Meshref, and M. A Elsisy, "Human-Based Optimization Algorithms and Their Applications," *Benha J. Appl. Sci.*, vol. 9, no. 5, pp. 289–320, 2024, doi: 10.21608/bjas.2025.280508.1389.
- [85] R. V. Rao, V. J. Savsani, and D. P. Vakharia, "Teaching-Learning-Based Optimization: An optimization method for continuous non-linear large scale problems," *Inf. Sci. (Ny).*, vol. 183, no. 1, pp. 1–15, 2012, doi: 10.1016/j.ins.2011.08.006.
- [86] M. Abdel-basset, R. Mohamed, and S. A. A. Azeem, "Jou 1P," 2023.
- [87] J. T. Katsikadelis, "Derivation of Newton's law of motion from Kepler's laws of planetary motion," *Arch. Appl. Mech.*, vol. 88, no. 1–2, pp. 27–38, 2018, doi: 10.1007/s00419-017-1245-x.
- [88] J. L. Russell, "Kepler's laws of planetary motion: 1609–1666," *Br. J. Hist. Sci.*, vol. 2, no. 1, pp. 1–24, 1964, doi: 10.1017/S0007087400001813.
- [89] R. Malhotra, M. Holman, and T. Ito, "Chaos and stability of the solar system," *Proc. Natl. Acad. Sci. U. S. A.*, vol. 98, no. 22, pp. 12342–12343, 2001, doi: 10.1073/pnas.231384098.
- [90] M. Abid, M. Belazzoug, S. Mouassa, A. Chanane, and F. Jurado, "Multi-Objective Optimal Power Flow Analysis Incorporating Renewable Energy Sources and FACTS Devices Using Non-Dominated Sorting Kepler Optimization Algorithm," *Sustain.*, vol. 16, no. 21, 2024, doi: 10.3390/su16219599.
- [91] K. Deb, A. Pratap, S. Agarwal, and T. Meyarivan, "A fast and elitist multiobjective genetic algorithm: NSGA-II," *IEEE Trans. Evol. Comput.*, vol. 6, no. 2, pp. 182–197, 2002, doi: 10.1109/4235.996017.
- [92] R. Jin, K. Cho, C. Hyun, and M. Son, "MRA-based revised CBR model for cost prediction in the early stage of construction projects," *Expert Syst. Appl.*, vol. 39, no. 5, pp. 5214–5222,

- 2012, doi: 10.1016/j.eswa.2011.11.018.
- [93] Z. Chen, "Optimal Power Flow in Renewable-Integrated Power Systems: A Comprehensive Review," pp. 1–22, 2024, [Online]. Available: https://arxiv.org/pdf/2408.05254
- [94] E. E. Elattar and S. K. ElSayed, "Modified JAYA algorithm for optimal power flow incorporating renewable energy sources considering the cost, emission, power loss and voltage profile improvement," *Energy*, vol. 178, pp. 598–609, 2019, doi: 10.1016/j.energy.2019.04.159.
- [95] R. P. Singh, V. Mukherjee, and S. P. Ghoshal, "Particle swarm optimization with an aging leader and challengers algorithm for the solution of optimal power flow problem," *Appl. Soft Comput. J.*, vol. 40, pp. 161–177, 2016, doi: 10.1016/j.asoc.2015.11.027.
- [96] S. Duman, J. Li, and L. Wu, "AC optimal power flow with thermal—wind—solar—tidal systems using the symbiotic organisms search algorithm," *IET Renew. Power Gener.*, vol. 15, no. 2, pp. 278–296, 2021, doi: 10.1049/rpg2.12023.
- [97] M. H. Hassan, S. Kamel, M. A. El-Dabah, T. Khurshaid, and J. L. Dominguez-Garcia, "Optimal Reactive Power Dispatch with Time-Varying Demand and Renewable Energy Uncertainty Using Rao-3 Algorithm," *IEEE Access*, vol. 9, pp. 23264–23283, 2021, doi: 10.1109/ACCESS.2021.3056423.
- [98] S. P. Dash, K. R. Subhashini, and P. Chinta, "Development of a Boundary Assigned Animal Migration Optimization algorithm and its application to optimal power flow study," *Expert Syst. Appl.*, vol. 200, no. March, p. 116776, 2022, doi: 10.1016/j.eswa.2022.116776.
- [99] M. Farhat, S. Kamel, A. M. Atallah, and B. Khan, "Optimal power flow solution based on jellyfish search optimization considering uncertainty of renewable energy sources," *IEEE Access*, vol. 9, pp. 100911–100933, 2021, doi: 10.1109/ACCESS.2021.3097006.
- [100] M. Ghasemi, P. Trojovský, E. Trojovská, and M. Zare, "Gaussian bare-bones Levy circulatory system-based optimization for power flow in the presence of renewable units," *Eng. Sci. Technol. an Int. J.*, vol. 47, no. September, 2023, doi: 10.1016/j.jestch.2023.101551.
- [101] H. C. Chin, "Fault section diagnosis of power system using fuzzy logic," *IEEE Trans. Power Syst.*, vol. 18, no. 1, pp. 245–250, 2003, doi: 10.1109/TPWRS.2002.807095.